UCRL-LR-105358

Lecture Notes on Nonlinear Inversion and Tomography

James G. Berryman

November 1990

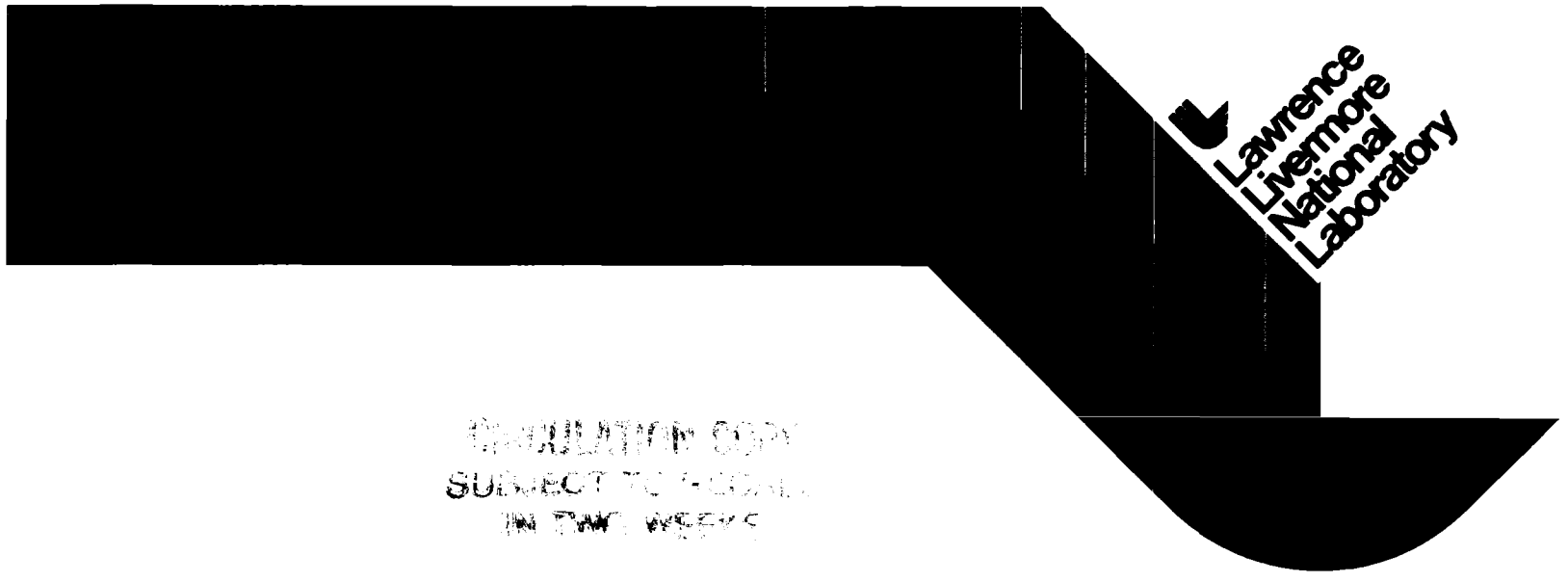

DISCLAIMER

Work performed under the auspices of the U.S. Department of Energy by Lawrence Livermore National Laboratory under Contract W-7405-Eng-48.

UCRL-LR-105358
Distribution Category UC-703

Lecture Notes on Nonlinear Inversion and Tomography

James G. Berryman

Manuscript date: November 1990

From a Series of Lectures by

James G. Berryman
University of California
Lawrence Livermore National Laboratory
Livermore, CA 94550

Presented at

Earth Resources Laboratory
Massachusetts Institute of Technology
July 9–30, 1990

Compiled and Edited by

William L. Rodi
Earth Resources Laboratory
42 Carleton Street
Cambridge, MA 02142

LAWRENCE LIVERMORE NATIONAL LABORATORY
University of California • Livermore, California • 94551

Available to DOE and DOE contractors from the Office of Scientific and Technical Information
P.O. Box 62, Oak Ridge, TN 37831 Prices available from (615) 576-8601, FTS 626-8401

Available from: National Technical Information Service • U.S. Department of Commerce
5285 Port Royal Road • Springfield, VA 22161 • A04 • (Microfiche A01)

Acknowledgments

It is my pleasure to thank Nafi Toksöz for inviting me to present this series of lectures at MIT/ERL during July, 1990 and for his warm hospitality during my stay. My sincere thanks go to Bill Rodi for his efforts to help produce these lecture notes. I also want to thank my many colleagues both at Lawrence Livermore and elsewhere who have shared their insights into tomography with me through the years. It is often difficult to remember who taught me what, but it is not difficult to remember that I have learned much of what I know from the following people: J. A. Beatty, N. R. Burkhard, M. Cheney, W. D. Daily, A. J. Degroot, A. J. Devaney, K. A. Dines, D. M. Goodman, F. A. Grünbaum, P. E. Harben, D. Isaacson, J. S. Kallman, P. W. Kasameyer, R. V. Kohn, S.-Y. Lu, R. J. Lytle, G. J. F. MacDonald, J. R. McLaughlin, Ch. Y. Pichot, A. L. Ramirez, F. Santosa, W. W. Symes, J. E. Vidale, M. Vogelius, T. J. Yorkey, G. Zandt, and J. J. Zucca.

This work was performed under the auspices of the U. S. Department of Energy by the Lawrence Livermore National Laboratory under contract No. W-7405-ENG-48 and supported specifically by the DOE Office of Basic Energy Sciences, Division of Engineering and Geosciences.

Preface

The idea of using variational/feasibility constraints in inverse problems and tomography is new and relatively unexplored. This approach has far-reaching consequences with both theoretical and practical import, including rigorous results on convexity properties of the solution sets and stability of nonlinear reconstruction algorithms. The idea arose at Lawrence Livermore National Laboratory about four years ago and the extent to which it has been understood and applied at present was discussed in my lectures at MIT/ERL in July, 1990. These Lecture Notes attempt to supply both a summary of the lectures for those who were not able to attend and also an expansion on some of the details that were left out for lack of time. I want to emphasize that these were *research lectures*, on topics that were still developing then and are continuing to develop.

One major difference between the Notes and the lectures is that I have decided not to include any color reproductions in the Notes. That decision has in turn led me to leave out discussion of any actual reconstructions on synthetic or real data obtained using these methods, some of which can be found in the published or to-be-published references. In any case, the excitement of seeing these reconstructions performed in real time on color graphics workstations (as we did at MIT to supplement the lectures) is not likely to be captured on paper, so I have not tried. If there is sufficient demand, I will expand these Notes in the the future to include a variety of sample reconstructions to illustrate the various conclusions in the analysis.

James G. Berryman

November, 1990

Contents

Lecture Notes on Nonlinear Inversion and Tomography

1 Introduction to the Traveltime Tomography Problem

The main topic of these lectures is seismic traveltime tomography in 2-D and 3-D heterogeneous media. Our main problem is to infer the (isotropic) P-wave slowness (reciprocal velocity) distribution of a medium, given a set of observed first-arrival traveltimes between sources and receivers of known location within the medium. This problem is typical of borehole-to-borehole seismic tomography in oil field applications. We will also consider the problem of inverting for wave slowness when the absolute traveltimes are not known, as is expected to be the case in earthquake seismology.

1.1 Slowness Models

We will consider three kinds of slowness models. Sometimes we will allow the slowness to be a general function of position, $s(\vec{x})$. However, we will often make one of two more restrictive assumptions that (*i*) the model comprises homogeneous blocks, or cells, with s_j then denoting the slowness value of the jth cell, or (*ii*) the model is composed of a grid with values of slowness assigned at the grid points with some interpolation scheme to assign the values between grid points. Of course, we can think of blocks of constant slowness as a special case of continuous models, or continuous models as a limiting case of blocks as the blocks become infinitesimal.

When it is not important which type of slowness model is involved, we will refer to the model abstractly as a vector $\mathbf{s}$ in a vector space $\mathcal{S}$. For a block model with n blocks we have $\mathcal{S} = \mathbf{R}^n$, the n-dimensional Euclidean vector space. ($\mathbf{R}$ denotes the set of real numbers.) A continuous slowness model, on the other hand, is an element of a function space, e.g., $\mathcal{S} = C(\mathbf{R}^3)$, the set of continuous functions of three real variables.

1.2 Fermat's Principle and Traveltime Functionals

The traveltime of a seismic wave is the integral of slowness along a ray path connecting the source and receiver. To make this more precise, we will define two functionals[1] for traveltime.

Let P denote an arbitrary path connecting a given source and receiver in a slowness model $\mathbf{s}$. We will refer to P as a *trial ray path*. We define a functional τ^P which yields the traveltime along P. Letting $\mathbf{s}$ be the continuous slowness distribution $s(\vec{x})$, we have

$$\tau^P(\mathbf{s}) = \int_P s(\vec{x})\, dl^P, \tag{1}$$

[1] A *functional* is a function which maps a function space or a vector space to the set of real numbers.

where dl^P denotes the infinitesimal distance along the path P.

Fermat's principle states that the correct ray path between two points is the one of least overall traveltime, *i.e.*, it minimizes[2] $\tau^P(\mathbf{s})$ with respect to P.

Let us define τ^* to be the functional that yields the traveltime along the Fermat (least-time) ray path. Fermat's principle then states

$$\tau^*(\mathbf{s}) = \min_{P \in Paths} \tau^P(\mathbf{s}), \tag{2}$$

where *Paths* denotes the set of all continuous paths connecting the given source and receiver.[3] The particular path that produces the minimum in (2) is denoted P^*. If more than one path produces the same minimum traveltime value, then P^* denotes any particular member in this set of minimizing paths.

To summarize, we have

$$\tau^P(\mathbf{s}) = \int_P s(\vec{x})\, dl^P, \tag{3}$$

$$\tau^*(\mathbf{s}) = \int_{P^*} s(\vec{x})\, dl^{P^*} = \min_P \int_P s(\vec{x})\, dl^P. \tag{4}$$

The traveltime functional $\tau^*(\mathbf{s})$ is stationary with respect to small variations in the path $P^*(s)$.

1.3 Snell's Law

Snell's law is a consequence of Fermat's principle. This can be seen from a simple geometric argument based on stationarity of the traveltime functional, illustrated in Figure 1.

We consider a medium with two regions of constant slowness s_1, s_2 separated by a plane boundary, and the ray path connecting two points, A and B, located on either side of the boundary. Referring to Figure 1, we let the solid lines denote the ray path having stationary traveltime and let the dashed line be a perturbed ray path. Each path is assumed to comprise straight lines bent at the boundary. We let θ_1 and θ_2 denote the angles of the stationary path from the normal to the boundary in the two regions, respectively. A simple geometrical argument can be used to infer the difference in length between the two paths to first order in h, the distance between the points where the paths intersect the boundary. We find that the segment of the perturbed path in region 1 is $h \sin(\theta_1 + \delta\theta)$ units longer than the stationary path, while in region 2 the perturbed path is $h \sin\theta_2$ units shorter. Therefore, the traveltime along the perturbed ray differs from that along the stationary ray by Δt, given by

$$\Delta t = s_1 h \sin\theta_1 - s_2 h \sin\theta_2, \tag{5}$$

neglecting the second order effects due to finite $\delta\theta$ and due to the slight differences in the remainders of these two paths. Since the traveltime is stationary, we set $\Delta t = 0$ and find

[2]Fermat's principle is actually the weaker condition that the traveltime integral is *stationary* with respect to variations in the ray path, but for traveltime tomography using measured first arrivals it follows that the traveltimes must be *minima*.

[3]The notation $P \in Paths$ means that P is a *member* of the set *Paths*.

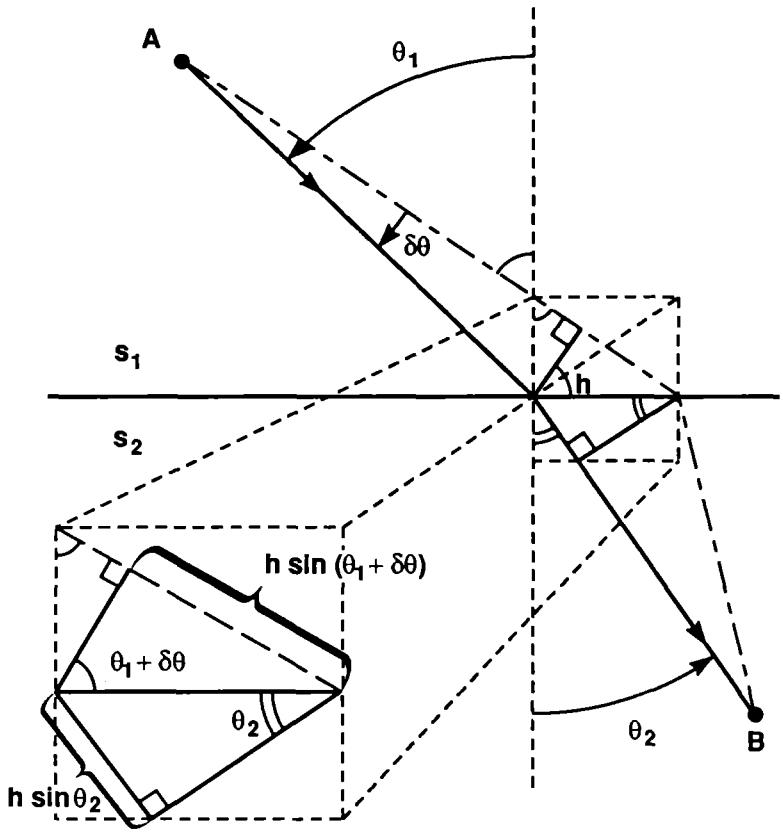

Figure 1: Snell's law is a consequence of the stationarity of the traveltime functional.

that

$$s_1 \sin\theta_1 = s_2 \sin\theta_2 \quad \text{(Snell's law)}. \tag{6}$$

A thorough discussion of the physical significance of Fermat's principle and its relation to Snell's law may be found in *The Feynman Lectures* [Feynman, Leighton, and Sands, 1963].

1.4 Seismic Inversion

Suppose we have a set of observed traveltimes, $t_1, \ldots, t_m$, from m source-receiver pairs in a slowness medium $s(\vec{x})$. Let P_i be the Fermat ray path connecting the ith source-receiver pair. In the absence of observational errors, we can write

$$\int_{P_i} s(\vec{x})\, dl^{P_i} = t_i, \quad i = 1, \ldots, m. \tag{7}$$

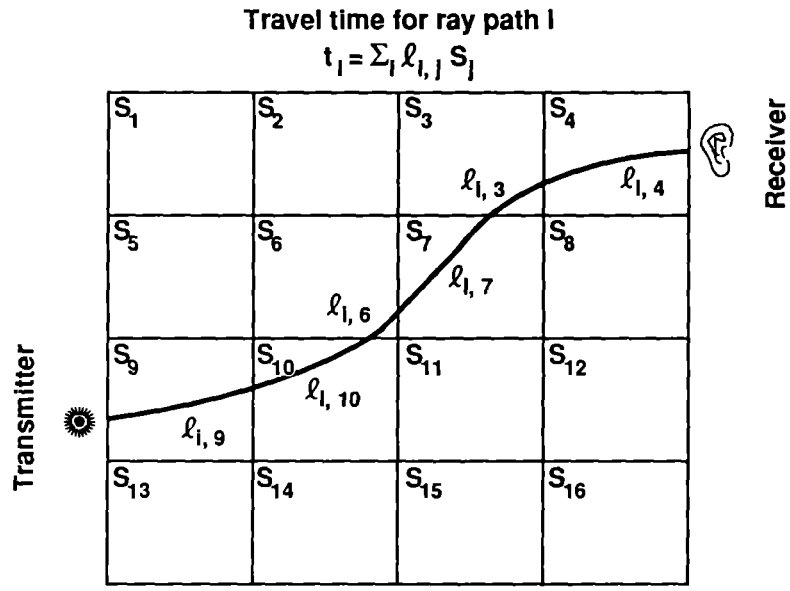

Figure 2: Schematic illustration of ray paths through a block velocity model.

Given a block model of slowness, let l_{ij} be the length of the ith ray path through the jth cell:

$$l_{ij} = \int_{P_i \cap \text{cell}_j} dl^{P_i}. \tag{8}$$

Given a model with n cells, Eq. (7) can then be written

$$\sum_{j=1}^{n} l_{ij} s_j = t_i, \quad i = 1, \ldots, m. \tag{9}$$

Note that for any given i, the ray path lengths l_{ij} are zero for most cells j, as a given ray path will in general intersect only a few of the cells in the model. Figure 2 illustrates the ray path intersections for a 2-D block model.

We can rewrite (9) in matrix notation by defining the column vectors $\mathbf{s}$ and $\mathbf{t}$ and the matrix $\mathbf{M}$ as follows:

$$\mathbf{s} = \begin{pmatrix} s_1 \\ s_2 \\ \vdots \\ s_n \end{pmatrix}, \qquad \mathbf{t} = \begin{pmatrix} t_1 \\ t_2 \\ \vdots \\ t_m \end{pmatrix}, \qquad \mathbf{M} = \begin{pmatrix} l_{11} & l_{12} & \cdots & l_{1n} \\ l_{21} & l_{22} & \cdots & l_{2n} \\ \vdots & \vdots & \ddots & \vdots \\ l_{m1} & l_{m2} & \cdots & l_{mn} \end{pmatrix}. \tag{10}$$

Equation (9) then becomes

$$\mathbf{M}\mathbf{s} = \mathbf{t}. \tag{11}$$

1.5 Linear vs Nonlinear Tomography

We now define three problems in the context of Eq. (11).

In the *forward* problem, we are given $\mathbf{s}$; the goal is to determine $\mathbf{M}$ and $\mathbf{t}$. This entails computing the ray path between each source and receiver (using a ray tracing algorithm) and then computing the traveltime integral along each path.

In the *linear tomography* problem, we are given $\mathbf{M}$ and $\mathbf{t}$; the objective is to determine $\mathbf{s}$. The assumption here is that the ray paths are known *a priori*, which is justified under a linear approximation that ignores the dependence of the ray paths on the slowness distribution. Typically, the ray paths are assumed to be straight lines connecting sources and receivers, adding a second connotation to the term "linear." Linear tomography is commonly practiced in medical imaging and in many geophysical situations as well.

In *nonlinear tomography*, we are given only $\mathbf{t}$ (and, of course, the source and receiver locations); the goal is to infer $\mathbf{M}$ and $\mathbf{s}$. In this problem, the dependence of the ray paths on the slowness distribution is acknowledged. Nonlinear tomography is necessary in problems in which the slowness varies significantly across the medium of interest, which includes many seismic tomography problems. The ray paths in such media will show significant curvature (i.e., be nonlinear) in a way that cannot be known *a priori*.

The linear tomography problem can be solved with a variety of optimization techniques. In the least-squares method, for example, the normal solution for $\mathbf{s}$ is expressed analytically as

$$\hat{\mathbf{s}} = (\mathbf{M}^T\mathbf{M})^{-1}\mathbf{M}^T\mathbf{t}, \tag{12}$$

assuming this inverse exists. If the inverse does not exist, then (12) must be "regularized." Typically, regularization is accomplished by adding a positive matrix to $\mathbf{M}^T\mathbf{M}$ and replacing the singular inverse in (12) by the inverse of the modified matrix.

In nonlinear tomography, an iterative algorithm is generally needed to find an approximate solution $\hat{\mathbf{s}}$. The basic structure of such an algorithm is as follows:

1. Set $\hat{\mathbf{s}}$ to a given initial model (a constant or the previously best-known geological model).
2. Compute the ray path matrix $\mathbf{M}$ and traveltimes $\hat{\mathbf{t}}$ for $\hat{\mathbf{s}}$ and set $\Delta\mathbf{t} = \mathbf{t} - \hat{\mathbf{t}}$.
3. If $\Delta\mathbf{t}$ is sufficiently small, stop.
4. Find a model correction $\widehat{\Delta\mathbf{s}}$ as the solution to the linear tomography problem: $\mathbf{M}\widehat{\Delta\mathbf{s}} = \Delta\mathbf{t}$.
5. Update $\hat{\mathbf{s}}$ to the new model obtained by adding the model correction $\widehat{\Delta\mathbf{s}}$ to the previous model $\hat{\mathbf{s}}$.
6. Go to Step 2.

This algorithm looks very reasonable and in fact it actually works in some cases! But not always. For models with low slowness contrasts, the algorithm will converge to a sensible result. When the method fails, the failure mode is usually a divergence to a highly oscillatory

model. *Ad hoc* procedures to reduce the possible range of slowness values and to guarantee a high degree of smoothness have commonly been introduced to deal with this instability. But a really satisfactory method of stabilizing the iteration scheme has been lacking.

Analyzing the algorithm, we see that there are really only two significant calculations contained in it. Step 2 is just the solution of the *forward problem* for $\hat{\mathbf{s}}$. This step should not introduce any instability, since it can be performed essentially as accurately as we like, and are willing to pay for. Step 4, on the other hand, is a *linear tomography* step imbedded in a nonlinear algorithm. We should be skeptical of this step. Linear inversion implicitly assumes that the updated model (after adding the model correction) is not so different from the previous model that the ray path matrix $\mathbf{M}$ should change significantly from one iteration to the next. If this implicit assumption is violated, then this step is not justified, and steps 4 and/or 5 in the algorithm must be modified.

In the remainder of these lectures, these problems will be analyzed in some detail, and several methods of stabilizing the nonlinear inversion problem will be developed.

1.6 Diffraction Tomography

Geophysical diffraction tomography [Devaney, 1983; Wu and Toksöz, 1987; Lo, Duckworth, and Toksöz, 1990] consists of a collection of methods including Born and Rytov inversion that make use of full waveform information in seismic data. Successful inversion of real data has also been performed using both microwave and ultrasonic diffraction tomography [Tabbara, Duchêne, Pichot, Lesslier, Chommeloux, and Joachimowicz, 1988]. Instead of using only the first arrival traveltimes as the data in the inversion, wave amplitude and phase in the waveform following the first arrival are used. It is necessary to use full waveform information whenever the wavelengths of the probing waves are comparable in size to the anomalies present in the region to be imaged. The ray approximation is strictly valid only for very high frequencies or equivalently for wavelengths "small" compared with the size of the anomalies (there will be a discussion of the eikonal equation in a later lecture). The term "small" is subject to interpretation, but extensive experience with the asymptotic analysis of wave propagation problems has shown that if the largest wavelength found in bandlimited data is $\lambda_{\max}$, then the ray approximation is valid when the anomalies are of size $\simeq 3\lambda_{\max}$ or larger. If this relationship is violated by the tomographic experiment, then diffraction tomography should play an important role in the reconstruction.

Diffraction tomography is both more and less ambitious than traveltime tomography. As it exists today, diffraction tomography is a strictly linear tomography method. A starting model is required. The usual starting model is a constant, because this method requires a comparison between predicted wave fields (planewaves for a constant background) and the measured wave fields. If a nonconstant starting model is used, then "distorted wave" diffraction tomography may be applied to the differences between the computed complex wave field and the measured wave field. In either case, it is possible to prove convergence of diffraction tomography to a solution of the inversion problem if the comparison wave field differs by a small enough amount from the measured wave field. Thus, diffraction tomography is another version of *linear tomography* — although in this case the "rays" may not be straight, it is still linear in the mathematical sense that the perturbations from the

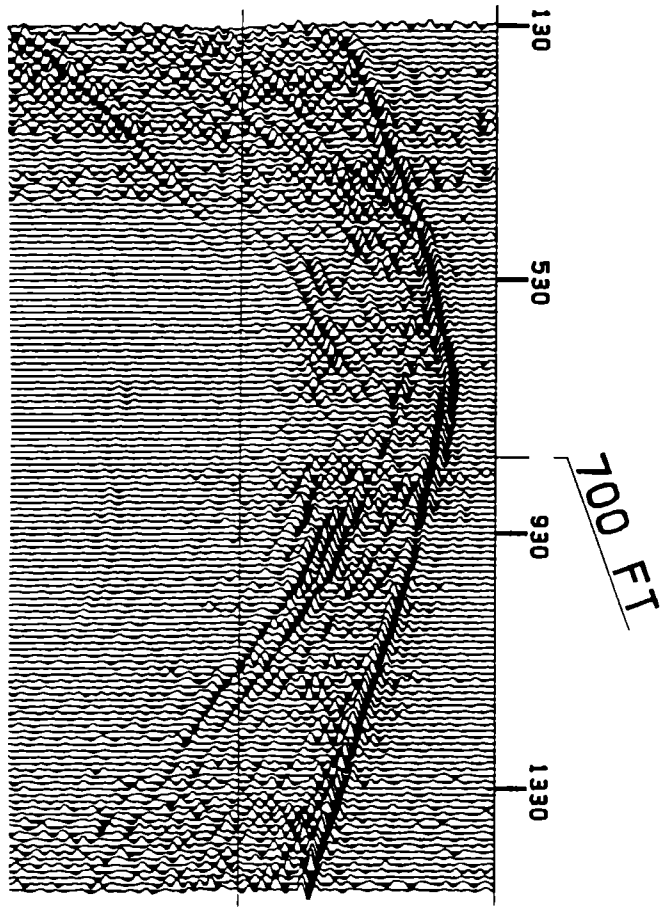

Figure 3: Example of real data for crosshole seismic tomography showing the result of a single fan beam with a source at 700 feet in one borehole and receivers spaced 10 feet apart in the other hole. (Courtesy of CONOCO Inc.)

starting model are very small. So diffraction tomography is less ambitious than traveltime tomography in the sense that it is inherently limited to be *linear tomography.*[4]

On the other hand, diffraction tomography is more ambitious than traveltime tomography, because it tries to make use of more of the information contained in the measured seismic waveforms. There are serious problems involved with this process, because amplitude information can be ambiguous. It is well known that wave attenuation, three-dimensional geometrical spreading, scattering, and reflection/transmission effects can all mimic each other — producing similar effects in the waveform. Thus, to be successful, diffraction tomography must meet the ambitious goal of solving all of these problems simultaneously for real data. To date, most of the work in diffraction tomography has been limited to two-dimensional inversions and the most successful applications have used ultrasound for medical imaging or microwaves for imaging metallic reinforcements in concrete.

I view diffraction tomography as an interesting long-term goal. The results obtained from traveltime tomography may be used as the required starting model for "distorted wave" diffraction tomography.

2 Feasibility Analysis for Tomography

The idea of using feasibility constraints in nonlinear programming problems is well established [Fiacco and McCormick, 1990]. However, it has only recently been realized that physical principles such as Fermat's principle actually lead to rigorous feasibility constraints for nonlinear inversion problems [Berryman, 1991]. The main practical difference between the standard analysis in nonlinear programming and the new analysis in nonlinear inversion is that, whereas the functions involved in nonlinear programming are often continuous, differentiable, and relatively easy to compute, the functionals in nonlinear inversion (*e.g.*, the traveltime functional) need not be continuous or differentiable and furthermore are very often comparatively difficult to compute.

We present the rigorous analysis here in a general setting, because it is actually quite easy to follow once we have understood the concepts of convex function and convex set. This analysis is important because it will help us to characterize the solution set for the inversion problem, and it will help to clarify the questions about local and global minima of the inverson problem.

2.1 Feasibility Constraints

Equation (7) assumed that P_i is a Fermat (least-time) path. Now let us suppose that P_i is a trial ray path which may or may not be the least-time path. Fermat's principle allows us to write

$$\int_{P_i} s(\vec{x}) dl^{P_i} \geq t_i. \tag{13}$$

When we discretize (13) for block models, it becomes

$$\mathbf{Ms} \geq \mathbf{t}. \tag{14}$$

[4] An iterative method for diffraction tomography has been proposed recently by Ladas and Devaney [1991]. Such methods are "nonlinear" in the sense used here.

Equations (13) and (14) can be interpreted as a set of inequality constraints on the slowness model $\mathbf{s}$. When $\mathbf{s}$ obeys these m constraints, we say that $\mathbf{s}$ is *feasible*. When any of the constraints is violated, we say $\mathbf{s}$ is *infeasible*. The set of inequalities collectively will be called the *feasibility constraints*.

2.2 Review of Convexity

Here we define some mathematical concepts [Hardy, Littlewood, and Pólya, 1934] which will facilitate the discussion and analysis of feasible models. In the following, we let S denote a linear vector space.

Definition 2.1 (convex set) *A set $\mathcal{A} \subseteq S$ is convex if, for every $\mathbf{s}_1, \mathbf{s}_2 \in \mathcal{A}$ and every number $\lambda \in [0,1]$, we have $\lambda\mathbf{s}_1 + (1-\lambda)\mathbf{s}_2 \in \mathcal{A}$.*[5]

Examples of convex sets are

1. $\mathbf{R}$ (the real numbers).
2. $\mathbf{R}_+$ (the positive real numbers).
3. The positive n-tant $\mathbf{R}_+^n$; *i.e.*, the set of n-dimensional vectors whose components are all positive.
4. $C_+(\mathbf{R}^3)$ (the set of positive, continuous functions, $s(\vec{x}) > 0$, where $\vec{x} \in \mathbf{R}^3$).
5. A closed interval $[a,b]$ in $\mathbf{R}$.[6]
6. A hyperplane in $\mathbf{R}^n$; *i.e.*, vectors $\mathbf{s}$ obeying $\mathbf{c}^T\mathbf{s} = \gamma$ where $\mathbf{c}$ is a vector and γ is a scalar.[7]
7. The interior of a circular disk in 2-space; *i.e.*, points (x,y) obeying
$$(x-a)^2 + (y-b)^2 < c^2$$
for real a, b and c.

We note that $\mathbf{R}_+^n$ (example 3) defines the set of n-dimensional block slowness models such that the slowness of each cell is a positive number. $C_+(\mathbf{R}^3)$ (example 4) is the space of positive, continuous 3-D slowness distributions.

Lemma 2.1 *If $\mathcal{A}_1$ and $\mathcal{A}_2$ are convex sets, then $\mathcal{A}_1 \cap \mathcal{A}_2$ is a convex set.*[8]

Proof. If $\mathcal{A}_1 \cap \mathcal{A}_2$ is empty, it is convex by default (one cannot find $\mathbf{s}_1$, $\mathbf{s}_2$ and λ which disobey the definition).

Assume the intersection is not empty and let $\mathbf{s} = \lambda\mathbf{s}_1 + (1-\lambda)\mathbf{s}_2$ for some $0 \le \lambda \le 1$ and $\mathbf{s}_1, \mathbf{s}_2 \in \mathcal{A}_1 \cap \mathcal{A}_2$. Since $\mathcal{A}_1$ and $\mathcal{A}_2$ are each convex, we must have $\mathbf{s} \in \mathcal{A}_1$ and $\mathbf{s} \in \mathcal{A}_2$. Consequently, $\mathbf{s} \in \mathcal{A}_1 \cap \mathcal{A}_2$. ∎

[5] $\mathcal{A} \subseteq S$ should be read here as: $\mathcal{A}$, which is a *subset* of S.
[6] $[a,b]$ means the set of numbers x such that $a \le x \le b$.
[7] T used in a superscript means to take the transpose of a vector or a matrix.
[8] $\mathcal{A}_1 \cap \mathcal{A}_2$ denotes the *intersection* of sets $\mathcal{A}_1$ and $\mathcal{A}_2$ (i.e., the set of elements common to both sets).

Definition 2.2 (cone) *A set $\mathcal{A} \subseteq \mathcal{S}$ is a cone if, for every $\mathbf{s} \in \mathcal{A}$ and every number $\gamma > 0$, we have $\gamma\mathbf{s} \in \mathcal{A}$.*

Examples 1–4 of convex sets given above are also examples of cones. We infer that the set of positive slowness models (block or continuous) is convex and conical (a *convex cone*).

Definition 2.3 (linear functional) *The functional $f: \mathcal{S} \to \mathbf{R}$ is linear if, for all $\mathbf{s}_1, \mathbf{s}_2 \in \mathcal{S}$ and real numbers λ_1, λ_2, we have*[9]

$$f(\lambda_1\mathbf{s}_1 + \lambda_2\mathbf{s}_2) = \lambda_1 f(\mathbf{s}_1) + \lambda_2 f(\mathbf{s}_2). \tag{15}$$

Note that a linear functional vanishes at the origin. We will also need to consider the broader class of functionals that are linear except for a shift at the origin.

Definition 2.4 (shifted linear functional) *The functional $f: \mathcal{S} \to \mathbf{R}$ is shifted linear if the functional*

$$g(\mathbf{s}) \equiv f(\mathbf{s}) - f(0) \tag{16}$$

is linear.

Definition 2.5 (convex functional) *Let $\mathcal{A}$ be a convex set in $\mathcal{S}$. A functional $f: \mathcal{A} \to \mathbf{R}$ is convex if, for every $\mathbf{s}_1, \mathbf{s}_2 \in \mathcal{A}$ and number $\lambda \in [0, 1]$, we have*

$$f(\lambda\mathbf{s}_1 + (1-\lambda)\mathbf{s}_2) \leq \lambda f(\mathbf{s}_1) + (1-\lambda) f(\mathbf{s}_2). \tag{17}$$

Definition 2.6 (concave functional) *A functional f is concave if $(-f)$ is convex.*

Definition 2.7 (homogeneous functional) *Let $\mathcal{A}$ be a cone in $\mathcal{S}$. A functional $f: \mathcal{A} \to \mathbf{R}$ is homogeneous if, for every $\mathbf{s} \in \mathcal{A}$ and $\gamma > 0$, we have*

$$f(\gamma\mathbf{s}) = \gamma f(\mathbf{s}). \tag{18}$$

It should be clear that every linear functional is also convex, concave and homogeneous.

2.3 Properties of Traveltime Functionals

Lemma 2.2 *τ^P is a linear functional.*

The proof of this stems from the fact that integration is a linear functional of the integrand.

Since it is linear, it follows that τ^P is also convex, concave, and homogeneous.

Lemma 2.3 *τ^* is a homogeneous functional.*

[9] $f: \mathcal{S} \to \mathbf{R}$ means: the function f which maps each element of the set $\mathcal{S}$ to an element of the set $\mathbf{R}$.

Proof. Given $\gamma > 0$ we have

$$\tau^*(\gamma \mathbf{s}) = \min_P \tau^P(\gamma \mathbf{s}). \tag{19}$$

Using the linearity of τ^P,

$$\tau^*(\gamma \mathbf{s}) = \min_P \gamma \tau^P(\mathbf{s}) = \gamma \min_P \tau^P(\mathbf{s}) = \gamma \tau^*(\mathbf{s}). \quad \blacksquare \tag{20}$$

Lemma 2.4 *τ^* is a concave functional.*

Proof. Given slowness models $\mathbf{s}_1$ and $\mathbf{s}_2$ and $\lambda \in [0,1]$, let $\mathbf{s} = \lambda \mathbf{s}_1 + (1-\lambda)\mathbf{s}_2$. Letting $P^*(\mathbf{s})$ be the Fermat ray path for $\mathbf{s}$, we have

$$\tau^*(\mathbf{s}) = \tau^{P^*(\mathbf{s})}(\mathbf{s}). \tag{21}$$

The linearity of τ^P then implies

$$\tau^*(\mathbf{s}) = \lambda \tau^{P^*(\mathbf{s})}(\mathbf{s}_1) + (1-\lambda)\tau^{P^*(\mathbf{s})}(\mathbf{s}_2). \tag{22}$$

Since τ^* minimizes τ^P for any fixed model, it must be the case that $\tau^{P^*(\mathbf{s})}(\mathbf{s}_1) \geq \tau^*(\mathbf{s}_1)$ and similarly for $\mathbf{s}_2$. Further, λ and $(1-\lambda)$ are non-negative. Therefore, (22) implies

$$\tau^*(\mathbf{s}) \geq \lambda \tau^*(\mathbf{s}_1) + (1-\lambda)\tau^*(\mathbf{s}_2). \quad \blacksquare \tag{23}$$

2.4 Feasibility Sets

Given the set of observed traveltimes, t_i for $i = 1, \ldots, m$, we define two sets of models.

Definition 2.8 (local feasibility set) *The local feasibility set with respect to a set of trial ray paths $\mathcal{P} = \{P_1, \ldots, P_m\}$ and observed traveltimes $t_1, \ldots, t_m$ is*

$$\mathcal{F}^{\mathcal{P}} = \{\mathbf{s} \mid \tau_i^P(\mathbf{s}) \geq t_i, \quad \textit{for all} \quad i = 1, \ldots, m\}. \tag{24}$$

Definition 2.9 (global feasibility set) *The global feasibility set with respect to the observed traveltimes $t_1, \ldots, t_m$ is*

$$\mathcal{F}^* = \{\mathbf{s} \mid \tau_i^*(\mathbf{s}) \geq t_i, \quad \textit{for all} \quad i = 1, \ldots, m\}. \tag{25}$$

Now we show that the concavity of τ_i^P and τ_i^* implies the convexity of $\mathcal{F}^{\mathcal{P}}$ and $\mathcal{F}^*$.

Theorem 2.1 *$\mathcal{F}^{\mathcal{P}}$ is a convex set.*

Proof. Suppose $\mathbf{s}_1, \mathbf{s}_2 \in \mathcal{F}^{\mathcal{P}}$ and let $\mathbf{s} = \lambda \mathbf{s}_1 + (1-\lambda)\mathbf{s}_2$ where $0 \leq \lambda \leq 1$. Since, for each i, τ_i^P is a concave (actually linear) functional, we have

$$\tau_i^P(\mathbf{s}) \geq \lambda \tau_i^P(\mathbf{s}_1) + (1-\lambda)\tau_i^P(\mathbf{s}_2). \tag{26}$$

(Although equality applies in the present case, the "greater than or equal to" is important in the next proof.) But $\tau_i^P(\mathbf{s}_1), \tau_i^P(\mathbf{s}_2) \geq t_i$ and λ and $(1-\lambda)$ are non-negative. Therefore,

$$\tau_i^P(\mathbf{s}) \geq \lambda t_i + (1-\lambda)t_i = t_i. \tag{27}$$

Thus, $\mathbf{s} \in \mathcal{F}^{\mathcal{P}}$. $\blacksquare$

Theorem 2.2 *$\mathcal{F}^*$ is a convex set.*

The proof proceeds in analogy with the previous proof, with τ_i^* replacing τ_i^P, but the inequalities come into play this time.

Theorem 2.3 *Given any model* $\mathbf{s}$*, there exists* $\gamma > 0$ *such that* $\gamma\mathbf{s} \in \mathcal{F}^*$.

Proof. Let

$$\gamma = \max_{k \in \{1,\ldots,m\}} \frac{t_k}{\tau_k^*(\mathbf{s})}. \tag{28}$$

For any i, τ_i^* is homogeneous, implying

$$\tau_i^*(\gamma\mathbf{s}) = \gamma\tau_i^*(\mathbf{s}) = \tau_i^*(\mathbf{s}) \max_k \frac{t_k}{\tau_k^*(\mathbf{s})} \geq \tau_i^*(\mathbf{s}) \frac{t_i}{\tau_i^*(\mathbf{s})} = t_i. \tag{29}$$

We see that $\gamma\mathbf{s}$ satisfies all the feasibility constraints, so it is in $\mathcal{F}^*$.

We can decompose $\mathcal{F}^*$ into two parts: its *boundary* and its *interior*. The boundary of $\mathcal{F}^*$, denoted Bdy $\mathcal{F}^*$, comprises feasible models $\mathbf{s}$ which satisfy some feasibility constraint with equality, *i.e.*,

$$\text{Bdy } \mathcal{F}^* = \{\mathbf{s} \in \mathcal{F}^* \mid \tau_i^*(\mathbf{s}) = t_i, \text{ for some } i\}. \tag{30}$$

Models in the interior of $\mathcal{F}^*$, denoted Int $\mathcal{F}^*$, satisfy all constraints with inequality:

$$\text{Int } \mathcal{F}^* = \{\mathbf{s} \in \mathcal{F}^* \mid \tau_i^*(\mathbf{s}) > t_i, \text{ for all } i\}. \tag{31}$$

2.5 Convex Programming for Inversion

We will first define convex programming for first arrival traveltime inversion. Then we present some basic theorems about convex programming in this context.

Definition 2.10 *Let $\phi(\mathbf{s})$ be any convex function of $\mathbf{s}$. Then the convex nonlinear programming problem associated with ϕ is to minimize $\phi(\mathbf{s})$ subject to the global feasibility constraints $\tau_i^*(\mathbf{s}) \geq t_i$, for $i = 1, \ldots, m$.*

Definition 2.11 *Let $\Psi^P(\mathbf{s}) = \sum_{i=1}^m w_i[\tau_i^P(\mathbf{s}) - t_i]^2$ for some positive weights w_i and some set of ray paths $P = \{P_1, \ldots, P_m\}$. Then, the convex linear programming problem associated with Ψ^P is to minimize $\Psi^P(\mathbf{s})$ subject to the local feasibility constraints $\tau_i^P(\mathbf{s}) \geq t_i$ for $i = 1, \ldots, m$.*

Theorem 2.4 *Every local minimum $\mathbf{s}^*$ of the convex nonlinear programming problem associated with $\phi(\mathbf{s})$ is a global minimum.*

Theorem 2.5 *Every local minimum $\mathbf{s}^*$ of the convex linear programming problem associated with $\Psi^P(\mathbf{s})$ is a global minimum.*

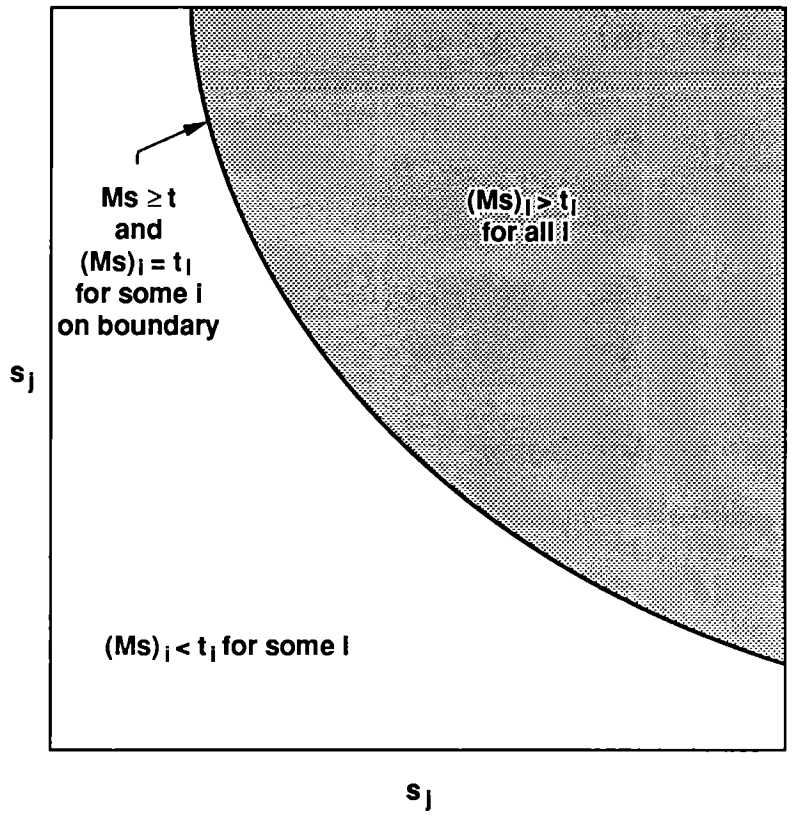

Figure 4: The defining conditions for the feasible and infeasible parts of the model space and the boundary separating them.

Proof. This proof follows one given in Fiacco and McCormick [1990]. Let $\mathbf{s}^*$ be a local minimum. Then, by definition, there is a compact set $\mathcal{C}$ such that $\mathbf{s}^*$ is in the interior of $\mathcal{C} \cap \mathcal{F}^*$ and

$$\phi(\mathbf{s}^*) = \min_{\mathcal{C} \cap \mathcal{F}^*} \phi(\mathbf{s}). \tag{32}$$

If $\mathbf{s}$ is any point in the feasible set $\mathcal{F}^*$ and $0 \leq \lambda \leq 1$ such that $\mathbf{s}^*_\lambda \equiv \lambda \mathbf{s}^* + (1-\lambda)\mathbf{s}$ is in $\mathcal{C} \cap \mathcal{F}^*$, then

$$\phi(\mathbf{s}) \geq \frac{\phi(\mathbf{s}^*_\lambda) - \lambda\phi(\mathbf{s}^*)}{1-\lambda} \geq \frac{\phi(\mathbf{s}^*) - \lambda\phi(\mathbf{s}^*)}{1-\lambda} = \phi(\mathbf{s}^*). \tag{33}$$

The first step of (33) follows from the convexity of ϕ and the second from the fact that $\mathbf{s}^*$ is a minimum in $\mathcal{C} \cap \mathcal{F}^*$. Convexity of $\mathcal{F}^*$ guarantees that the convex combination $\mathbf{s}^*_\lambda$ lies in the feasible set. This completes the proof of the first theorem.

The proof of the second theorem follows that of the first once we have shown that the function Ψ^P is convex. Consider a term of Ψ^P

$$\begin{aligned}[\tau_i^P(\lambda \mathbf{s}_1 + (1-\lambda)\mathbf{s}_2) - t_i]^2 &= [\lambda\tau_i^P(\mathbf{s}_1) + (1-\lambda)\tau_i^P(\mathbf{s}_2) - t_i]^2 \\ &= \lambda[\tau_i^P(\mathbf{s}_1) - t_i]^2 + (1-\lambda)[\tau_i^P(\mathbf{s}_2) - t_i]^2 \\ &\quad -\lambda(1-\lambda)[\tau_i^P(\mathbf{s}_1) - \tau_i^P(\mathbf{s}_2)]^2 \\ &\leq \lambda[\tau_i^P(\mathbf{s}_1) - t_i]^2 + (1-\lambda)[\tau_i^P(\mathbf{s}_2) - t_i]^2.\end{aligned}$$

Then, if $\mathbf{s}_\lambda = \lambda\mathbf{s}_1 + (1-\lambda)\mathbf{s}_2$,

$$\Psi^P(\mathbf{s}_\lambda) \leq \lambda\Psi^P(\mathbf{s}_1) + (1-\lambda)\Psi^P(\mathbf{s}_2), \tag{34}$$

so Ψ^P is a convex function. ∎

3 Least-Squares Methods

We will consider solutions to the tomography problem for the case of block models. Given a set of weights $w_i > 0$, $i = 1, \ldots, m$, we define the functional Ψ: $\mathcal{S} \rightarrow \mathbf{R}$ by

$$\Psi(\mathbf{s}) = \sum_{i=1}^{m} w_i[\tau_i^*(\mathbf{s}) - t_i]^2. \tag{35}$$

$\Psi(\mathbf{s})$ measures the degree of "misfit" between the observed data and traveltimes predicted by the model $\mathbf{s}$.

3.1 Scaled Least-Squares Model

Definition 3.1 (scaled least-squares model) *The scaled least-squares model with respect to a given model* $\mathbf{s}_0$, *and set of weights* w_i, *is the model* $\hat{\mathbf{s}}_{\mathrm{LS}[\mathbf{s}_0]}$ *minimizing* Ψ *subject to the constraint that* $\mathbf{s} = \gamma\mathbf{s}_0$ *for* $\gamma > 0$. *Thus*

$$\Psi(\hat{\mathbf{s}}_{\mathrm{LS}[\mathbf{s}_0]}) = \min_{\gamma} \Psi(\gamma\mathbf{s}_0). \tag{36}$$

The scaled least-squares model associated with $\mathbf{s}_0$ is unique.

To solve for the scaled least-squares model, we expand $\Psi(\gamma\mathbf{s}_0)$ as

$$\Psi(\gamma\mathbf{s}_0) = \sum_i w_i[\tau_i^*(\gamma\mathbf{s}_0) - t_i]^2 \tag{37}$$

$$= \sum_i w_i\tau_i^*(\gamma\mathbf{s}_0)^2 - 2\sum_i w_i t_i \tau_i^*(\gamma\mathbf{s}_0) + \sum_i w_i t_i^2. \tag{38}$$

Using the homogeneity of τ_i^*, we can write

$$\Psi(\gamma\mathbf{s}_0) = \gamma^2 \sum_i w_i\tau_i^*(\mathbf{s}_0)^2 - 2\gamma\sum_i w_i t_i \tau_i^*(\mathbf{s}_0) + \sum_i w_i t_i^2. \tag{39}$$

This is simply a second-order polynomial in γ and achieves its minimum at $\gamma = \gamma_{\mathrm{LS}[\mathbf{s}_0]}$, where

$$\gamma_{\mathrm{LS}[\mathbf{s}_0]} = \frac{\sum_i w_i t_i \tau_i^*(\mathbf{s}_0)}{\sum_i w_i \tau_i^*(\mathbf{s}_0)^2}. \tag{40}$$

Thus

$$\hat{\mathbf{s}}_{\mathrm{LS}[\mathbf{s}_0]} = \mathbf{s}_0 \frac{\sum_i w_i t_i \tau_i^*(\mathbf{s}_0)}{\sum_i w_i \tau_i^*(\mathbf{s}_0)^2}. \tag{41}$$

Theorem 3.1 *For any* $\mathbf{s}_0$, $\hat{\mathbf{s}}_{\mathrm{LS}[\mathbf{s}_0]} \notin \mathrm{Int}\, \mathcal{T}^*$.

Proof. We have from (40)

$$\gamma_{\mathrm{LS}[\mathbf{s}_0]} \sum_{i=1}^{m} w_i \tau_i^*(\mathbf{s}_0)^2 = \sum_{i=1}^{m} w_i t_i \tau_i^*(\mathbf{s}_0), \tag{42}$$

or, given the homogeneity of τ_i^*,

$$\sum_{i=1}^{m} w_i \tau_i^*(\mathbf{s}_0)[\tau_i^*(\hat{\mathbf{s}}_{\mathrm{LS}[\mathbf{s}_0]}) - t_i] = 0. \tag{43}$$

Since the w_i and values of τ_i^* are positive, this can only be true if either $\tau_i^*(\hat{\mathbf{s}}_{\mathrm{LS}[\mathbf{s}_0]}) = t_i$ for all i (i.e., $\hat{\mathbf{s}}_{\mathrm{LS}[\mathbf{s}_0]} \in \mathrm{Bdy}\, \mathcal{T}^*$ and is an exact solution to the inversion problem) or if $\tau_i^*(\hat{\mathbf{s}}_{\mathrm{LS}[\mathbf{s}_0]}) < t_i$ for at least one i (*i.e.*, $\hat{\mathbf{s}}_{\mathrm{LS}[\mathbf{s}_0]} \notin \mathcal{T}^*$). Thus, the scaled least-squares model cannot be in $\mathrm{Int}\, \mathcal{T}^*$. ∎

We can write the scaled least-squares model in matrix notation as follows. Let $\mathbf{W}$ be the diagonal matrix formed from the positive weights w_i:

$$\mathbf{W} = \begin{pmatrix} w_1 & & & \\ & w_2 & & \\ & & \ddots & \\ & & & w_m \end{pmatrix}. \tag{44}$$

Further, let $\mathbf{M}_0$ be the ray-path matrix computed from $\mathbf{s}_0$. Thus, $\tau_i^*(\mathbf{s}_0) = [\mathbf{M}_0\mathbf{s}_0]_i$. In matrix notation, (40) becomes

$$\gamma_{\mathrm{LS}[\mathbf{s}_0]} = \frac{\mathbf{s}_0^T \mathbf{M}_0^T \mathbf{W} \mathbf{t}}{\mathbf{s}_0^T \mathbf{M}_0^T \mathbf{W} \mathbf{M}_0 \mathbf{s}_0}, \tag{45}$$

implying

$$\hat{\mathbf{s}}_{\mathrm{LS}[\mathbf{s}_0]} = \mathbf{s}_0 \frac{\mathbf{s}_0^T \mathbf{M}_0^T \mathbf{W} \mathbf{t}}{\mathbf{s}_0^T \mathbf{M}_0^T \mathbf{W} \mathbf{M}_0 \mathbf{s}_0}. \tag{46}$$

3.2 Least-Squares Models

Definition 3.2 (least-squares model) *A least-squares model, with respect to weights w_i, is a vector $\hat{\mathbf{s}}_{\mathrm{LS}}$ which minimizes Ψ, i.e.,*

$$\Psi(\hat{\mathbf{s}}_{\mathrm{LS}}) = \min_{\mathbf{s}} \Psi(\mathbf{s}). \tag{47}$$

The least-squares model may be nonunique. Nonuniqueness is expected when $m < n$, *i.e.*, there are fewer traveltime data than model cells, or when $m > n$ and the ray-path matrix has a right null space containing ghosts $\mathbf{g}$. The most common method of picking the "best" least-squares solution [Penrose, 1955b] is to choose the one of minimum Euclidean norm. This "best" solution has some nice properties as we shall see when we discuss ghosts in tomography, but it may not represent the "best" solution to the inversion problem.

Corollary 3.1 $\hat{\mathbf{s}}_{\mathrm{LS}} \notin \mathrm{Int}\, \mathcal{F}^*$.

Proof. This corollary follows from the fact that $\hat{\mathbf{s}}_{\mathrm{LS}} = \hat{\mathbf{s}}_{\mathrm{LS}[\hat{\mathbf{s}}_{\mathrm{LS}}]}$, *i.e.*, a least-squares model is the scaled least-squares model with respect to itself (or otherwise there would be a model yielding smaller Ψ). ∎

The preceding proof is entirely adequate to establish the infeasibility of the least-squares point. However, it may be enlightening to present a second proof based on stationarity of the ray paths.

Consider the deviation of the least-squares functional induced by a small change in the model:

$$\delta\Psi = \Psi(s + \delta s) - \Psi(s) = \sum_i w_i [\tau_i^*(s + \delta s) - t_i]^2 - \sum_i w_i [\tau_i^*(s) - t_i]^2. \tag{48}$$

This equation may be rearranged without approximation into the form

$$\delta\Psi = 2 \sum_i w_i [\tau_i^*(s + \delta s) - \tau_i^*(s)][(\tau_i^*(s + \delta s) + \tau_i^*(s))/2 - t_i]. \tag{49}$$

For small slowness perturbations δs, the first bracket in the sum of (49) is clearly of order δs, while any contributions of order δs in the second bracket are therefore of second order and may be neglected. If $dl_i^*[s]$ is the infinitesimal increment of the (or a) least-time ray along path i for s, then

$$\tau_i^*(s + \delta s) - \tau_i^*(s) = \int (s + \delta s)\, dl_i^*[s + \delta s] - \int s\, dl_i^*[s]. \tag{50}$$

Recall that stationarity of the ray paths near the one of least time implies that

$$\int s\, dl_i^*[s + \delta s] = \int s\, \{dl_i^*[s] + d\delta l_i^*\} \simeq \int s\, dl_i^*[s], \tag{51}$$

where $d\delta l_i^*$ is the perturbation in the infinitesimal increment $dl_i^*[s]$ of the ray path induced by the fact that $dl_i^*[s + \delta s]$ is the one for the perturbed model and therefore generally only slightly different from that for s. (Note: There are pathological cases where a small change

in the model s can induce a large change in the ray path, but we will ignore this possibility for the present argument.)

Using (51) in (50), we find that

$$\tau_i^*(s+\delta s) - \tau_i^*(s) \simeq \int \delta s \, dl_i^*[s+\delta s] \simeq \int \delta s \, dl_i^*[s] \tag{52}$$

to lowest order in δs. Thus, (49) becomes

$$\delta\Psi = 2\sum_i w_i \Big(\int \delta s \, dl_i^*[s] \Big) [\tau_i^*(s) - t_i]. \tag{53}$$

Equation (53) is the expression needed to construct the functional (Frechét) derivative of Ψ. If s produces the minimum of $\Psi(s)$, then the functional derivative should vanish. We see that the weights w_i are positive, the coefficient of δs is the integral of the increment of the ray path itself in the regions of change which is strictly positive, and if the the traveltime function $\tau_i^*(s) - t_i \geq 0$ as is required for all i in order for the model s to be feasible, then the derivative cannot vanish and therefore s is not the minimum. This contradiction shows again that either the minimum of the traveltime function must be infeasible, or it must solve the inversion problem.

3.3 Damped Least-Squares Model

Let $\mathbf{C}$ be a diagonal (coverage) matrix formed from the positive weights c_j:

$$\mathbf{C} = \begin{pmatrix} c_1 & & & \\ & c_2 & & \\ & & \ddots & \\ & & & c_n \end{pmatrix}. \tag{54}$$

The c_js may be treated here as arbitrary positive weights, but a definite choice of the c_js will be found later.

Definition 3.3 (damped least-squares model) *The damped least-squares model with respect to a given model* $\mathbf{s}_0$*, and set of weights* w_i, c_j*, is the model* $\hat{\mathbf{s}}_{\mathrm{LS}[\mathbf{s}_0,\mu]}$ *minimizing*

$$\Psi(\mathbf{s}) + \mu(\mathbf{s}-\mathbf{s}_0)^T\mathbf{C}(\mathbf{s}-\mathbf{s}_0). \tag{55}$$

Like the scaled least-squares model, the damped least-squares model is unique.

We can solve for the damped least-squares model based on a linear approximation to the traveltime functionals. Given the model $\mathbf{s}_0$, let P_i^0 denote the least-time ray paths through $\mathbf{s}_0$. Then, to first order in $\mathbf{s}-\mathbf{s}_0$ we have

$$\tau_i^*(\mathbf{s}) \simeq \tau_i^{P_i^0}(\mathbf{s}). \tag{56}$$

This approximation yields

$$\Psi(\mathbf{s}) = (\mathbf{t} - \mathbf{M}_0\mathbf{s})^T\mathbf{W}(\mathbf{t} - \mathbf{M}_0\mathbf{s}), \tag{57}$$

where $\mathbf{M}_0$ is the ray-path matrix obtained from the ray paths P_i^0.

Using the first-order approximation, the damped least-squares model becomes

$$\hat{\mathbf{s}}_{\mathrm{LS}[\mathbf{s}_0,\mu]} = \mathbf{s}_0 + (\mathbf{M}_0^T\mathbf{W}\mathbf{M}_0 + \mu\mathbf{C})^{-1}\mathbf{M}_0^T\mathbf{W}(\mathbf{t} - \mathbf{M}_0\mathbf{s}_0). \tag{58}$$

This equation can be rearranged to show that

$$\mu\mathbf{C}(\hat{\mathbf{s}}_{\mathrm{LS}[\mathbf{s}_0,\mu]} - \mathbf{s}_0) = \mathbf{M}_0^T\mathbf{W}(\mathbf{t} - \mathbf{M}_0\hat{\mathbf{s}}_{\mathrm{LS}[\mathbf{s}_0,\mu]}). \tag{59}$$

Then, we obtain the following two theorems:

Theorem 3.2 *If* $\mathbf{s}_0 \notin \mathcal{F}^{P_0}$, *then* $\hat{\mathbf{s}}_{\mathrm{LS}[\mathbf{s}_0,\mu]}$ *does not solve the inversion problem for any* $\mu > 0$.

Theorem 3.3 *If* $\mathbf{s}_0 \notin \mathcal{F}^{P_0}$, *then* $\hat{\mathbf{s}}_{\mathrm{LS}[\mathbf{s}_0,\mu]} \notin \mathcal{F}^{P_0}$.

Proof. The proofs are by contradiction.

First, suppose that $\hat{\mathbf{s}}_{\mathrm{LS}[\mathbf{s}_0,\mu]}$ solves the inversion problem so $\mathbf{M}_0\hat{\mathbf{s}}_{\mathrm{LS}[\mathbf{s}_0,\mu]} \equiv \mathbf{t}$. Then, (59) shows that $\hat{\mathbf{s}}_{\mathrm{LS}[\mathbf{s}_0,\mu]} = \mathbf{s}_0$ (if $\mu > 0$) so $\mathbf{M}_0\mathbf{s}_0 \equiv \mathbf{t}$. But this result contradicts the assumption that $\mathbf{s}_0 \notin \mathcal{F}^{P_0}$ so $\hat{\mathbf{s}}_{\mathrm{LS}[\mathbf{s}_0,\mu]}$ does not solve the inversion problem if $\mathbf{s}_0$ is infeasible.

Second, suppose that $\hat{\mathbf{s}}_{\mathrm{LS}[\mathbf{s}_0,\mu]}$ is feasible (*i.e.*, $\mathbf{M}_0\hat{\mathbf{s}}_{\mathrm{LS}[\mathbf{s}_0,\mu]} \geq \mathbf{t}$ and, making use of the previous theorem, we may exclude the possibility that it solves the inversion problem), then it follows from the positivity of all the matrix elements in (59) that $\hat{\mathbf{s}}_{\mathrm{LS}[\mathbf{s}_0,\mu]} \leq \mathbf{s}_0$. But, if $\mathbf{s}_0$ is infeasible so $(\mathbf{M}_0\mathbf{s}_0)_i < t_i$ for some i, then it also follows that $(\mathbf{M}_0\hat{\mathbf{s}}_{\mathrm{LS}[\mathbf{s}_0,\mu]})_i < t_i$ for the same i so $\hat{\mathbf{s}}_{\mathrm{LS}[\mathbf{s}_0,\mu]}$ is infeasible, which contradicts the original feasibility supposition on $\hat{\mathbf{s}}_{\mathrm{LS}[\mathbf{s}_0,\mu]}$. ∎

These results are strong because the infeasibility of $\hat{\mathbf{s}}_{\mathrm{LS}[\mathbf{s}_0,\mu]}$ holds for any value of the damping parameter $\mu > 0$.

3.4 Physical Basis for Weighted Least-Squares

So far we have treated the weights w_i as if they are arbitrary positive constants. But are they arbitrary? If they are not arbitrary, then what physical or mathematical feature of the inversion problem determines the weights?

Our goal in these lectures is ultimately to solve (if possible) the nonlinear inversion problem. So we must keep in mind that the arguments often given for determining the weights in weighted least-squares schemes in other contexts may not be relevant to our problem. In particular, these weights are very often chosen on the basis of statistical (uncorrelated) errors in the data. The assumption behind these choices may be very good indeed in some cases, but generally not in the nonlinear inversion problem. Our working hypothesis for this analysis is that the major source of error in nonlinear inversion is not the measurement error, but the error due to the erroneous choices of ray paths currently in use in the algorithm. The statistical errors in the data become a significant issue only after we have constructed a reliable set of ray paths so that the errors due to wrong ray paths are smaller than the errors in the traveltime data. In fact, for high contrast reconstructions, it may be the case that the errors in the traveltime data are only a small fraction of one percent while the errors introduced by erroneous choices of ray paths are on the order of several percent, or even more in pathological cases.

We envision a two step process. First, we solve the inversion problem iteratively to find a good set of ray paths. This step requires the weighting scheme described here. Second, once we have a reliable set of paths, the weighting scheme can be changed to take proper account of the statistical errors in the data.

Now we will try to use physical arguments to help us construct a proper set of weights. Suppose that the traveltime data in our reconstruction actually come from a model that is homogeneous, *i.e.*, with constant slowness σ_0. What will be the characteristics of such data? Clearly, the rays will in fact be straight and the average wave slowness along each ray will be the same constant

$$\sigma_0 = \frac{t_1}{L_1} = \frac{t_2}{L_2} = \cdots = \frac{t_m}{L_m}, \tag{60}$$

where

$$L_i = \sum_{j=1}^{n} l_{ij}. \tag{61}$$

Furthermore, it follows that the constant value of slowness is also given by the formula

$$\sigma_0 = \frac{\sum_{i=1}^{m} t_i}{\sum_{i=1}^{m} L_i}. \tag{62}$$

This problem is an ideal use for the scaled least-squares approach presented earlier. We know the ray paths are straight, so we know the ray-path matrix $\mathbf{M}$. We know that the slowness has the form $\mathbf{s} = \gamma\mathbf{v}$, where $\mathbf{v}^T = (1, \ldots, 1)$ is an n-vector of ones. We want to minimize the least-squares error

$$\Psi(\gamma\mathbf{v}) = (\mathbf{t} - \mathbf{M}\gamma\mathbf{v})^T\mathbf{W}(\mathbf{t} - \mathbf{M}\gamma\mathbf{v}) \tag{63}$$

with respect to the coefficient γ. The minimum of (63) occurs for

$$\mathbf{v}^T\mathbf{M}^T\mathbf{W}(\mathbf{t} - \mathbf{M}\gamma\mathbf{v}) = 0. \tag{64}$$

Solving for γ gives

$$\sigma_0 = \gamma = \frac{\mathbf{v}^T\mathbf{M}^T\mathbf{W}\mathbf{t}}{\mathbf{v}^T\mathbf{M}^T\mathbf{W}\mathbf{M}\mathbf{v}}. \tag{65}$$

To make it easier to compare (65) and (62), we will now introduce some more notation. Define the m-vector of ones $\mathbf{u}^T = (1, \ldots, 1)$. Then,

$$\mathbf{M}\mathbf{v} = \mathbf{L}\mathbf{u} \tag{66}$$

and

$$\mathbf{M}^T\mathbf{u} = \mathbf{C}\mathbf{v}, \tag{67}$$

where $\mathbf{L}$ is a diagonal $m \times m$ matrix whose diagonal elements are the row sums of $\mathbf{M}$ given by (61) and $\mathbf{C}$ is a diagonal $n \times n$ matrix whose diagonal elements are the column sums of $\mathbf{M}$ given by

$$C_{jj} = \sum_{i=1}^{m} l_{ij}. \tag{68}$$

In our later analysis, we will see that the matrix $\mathbf{C}$ (which we will call the coverage matrix) is a good choice for the second weight matrix in damped least-squares (54).

Now we see that (65) can be rewritten in this notation as

$$\sigma_0 = \frac{\mathbf{u}^T\mathbf{LWt}}{\mathbf{u}^T\mathbf{LWLu}}, \tag{69}$$

while (62) becomes

$$\sigma_0 = \frac{\mathbf{u}^T\mathbf{t}}{\mathbf{u}^T\mathbf{Lu}}. \tag{70}$$

Comparing (69) to (70), we see that these two equations would be identical if

$$\mathbf{WLu} = \mathbf{u}. \tag{71}$$

Equation (71) states that $\mathbf{u}$ is an eigenvector of the matrix $\mathbf{WL}$ with eigenvalue unity. Two choices for the product $\mathbf{WL}$ are

$$\mathbf{WL} = \mathbf{I}, \tag{72}$$

where $\mathbf{I}$ is the identity matrix and

$$\mathbf{WL} = \mathbf{L}^{-1}\mathbf{M}\mathbf{C}^{-1}\mathbf{M}^T. \tag{73}$$

The choice (73) is undesirable because it leads to a weight matrix that is not positive definite. The choice (72) leads to

$$\mathbf{W} = \mathbf{L}^{-1}, \tag{74}$$

which is both positive definite and diagonal.

The true significance of this result becomes more apparent when we consider that the traveltime data $\mathbf{t} = \bar{\mathbf{t}} + \Delta\mathbf{t}$ will generally include some experimental error $\Delta\mathbf{t}$. If we assume the data are unbiased and the number of source/receiver pairs is sufficiently large, then to a good approximation we should have $\mathbf{u}^T\Delta\mathbf{t} = 0$. The result (69) can be rewritten as

$$\gamma = \frac{\mathbf{a}^T\mathbf{L}^{-1}\mathbf{t}}{\mathbf{a}^T\mathbf{u}}, \tag{75}$$

where $\mathbf{a} = \mathbf{LWLu}$ may be treated for these purposes as an arbitrary weighting vector. For γ to be unbiased, we must have

$$\mathbf{a}^T\mathbf{L}^{-1}\Delta\mathbf{t} = \mathbf{u}^T\Delta\mathbf{t} = 0. \tag{76}$$

Since the Δts are otherwise arbitrary, we must have

$$\mathbf{u} = \mathbf{L}^{-1}\mathbf{a} = \mathbf{WLu}, \tag{77}$$

which is the same condition as that found in (71). Thus, the choice (74) produces the simplest weight matrix giving a linear unbiased estimator of the scale factor for a constant slowness model. In a later lecture, we derive weights producing unbiased estimates for arbitrary slowness.

Weighting inversely with respect to the lengths of the ray paths can be justified on physical grounds using several different arguments [Frank and Balanis, 1989]. Signal-to-noise ratio is expected to be better on shorter paths than longer ones, since the overall attenuation will typically be smaller and the likelihood of missing the true first arrival therefore smaller. Shorter trial paths are more likely to correspond to real paths that remain completely in the image plane for two-dimensional reconstruction problems.

A disadvantage of using this weighting scheme is that sometimes the ray path is long because the source and receiver are far apart (*e.g.*, from the top of one borehole to the bottom of the other). Yet the information contained in the ray is important because such diagonal rays may help to determine the horizontal extent of some feature of interest, especially when the experimental view angles are severely limited as in crosshole tomography. Weighting inversely with respect to the ray-path length tends to reduce the possibly significant improvement in horizontal resolution that can come from inclusion of these rays. This disadvantage can be circumvented to some extent by using more of these diagonal rays, *i.e.*, using more closely spaced sources and receivers for the diagonal rays. Then, the weights of the individual rays are smaller, but their overall influence on the reconstruction can still be significant.

In a later lecture, we will show that mathematical arguments based on stability lead to the same choice of weight matrices.

4 Algorithms for Linear Tomography

In the previous lecture, we spent a considerable amount of our time showing that least-squares methods generally produce infeasible models in traveltime tomography. Having thus ruined the reputation of least-squares methods, we will try to recover and arrive at a new understanding of the true significance of least-squares methods in the present lecture. We will find that there are two main points to be stressed: (1) The least-squares methods and generalized inverses are intimately related and lead to the same results. (2) Iterative methods based on least-squares criteria fall into the class of "exterior" methods for tomography, *i.e.*, at each step of the iteration sequence the "best estimate" of the solution is infeasible so we are trying to approach the solution from outside the set of feasible models.

In linear tomography with block models, we must solve the linear system of equations given by

$$\mathbf{Ms} = \mathbf{t}, \tag{78}$$

where we recall that $\mathbf{M}$ is an $m \times n$ matrix, $\mathbf{s}$ is an n-vector and $\mathbf{t}$ is an m-vector. There are a number of numerical algorithms for solving this system. These include

1. Tomographic reconstruction methods (e.g., ART and SIRT).
2. Iterative matrix methods (e.g., Gauss-Seidel and Jacobi's method).
3. Simple iteration.
4. Conjugate direction/gradient methods.
5. "Neural network" method.

Two difficulties arise in solving (78):

1. $\mathbf{M}$ is *not* a square matrix.
2. $\mathbf{M}$ is rank deficient.

The rank of a matrix is the dimension of the subspace spanned by its columns (or rows) and cannot exceed the smaller of the two dimensions of the matrix. Letting r be the rank of our m by n matrix $\mathbf{M}$, if $r = \min(m, n)$ we say $\mathbf{M}$ has *full rank*. If $r < m, n$ then $\mathbf{M}$ is *rank deficient*.

Because of these two difficulties, we cannot simply solve (78) in terms of an inverse matrix of $\mathbf{M}$, because such an inverse does not exist.

Two techniques for handling the first difficulty ($\mathbf{M}$ is not square) are *completing the square* and *Moore-Penrose pseudoinverses*. Two techniques for handling the second difficulty (rank deficiency) are *regularization* and *pseudoinverses*. Thus, the Moore-Penrose pseudoinverse is a common solution to both.

4.1 Moore-Penrose Pseudoinverse and SVD

Any nonsymmetric (and/or nonsquare) matrix $\mathbf{M}$ of real numbers can be decomposed in terms of a set of positive eigenvalues and two sets of orthonormal eigenvectors. Let r be the rank of $\mathbf{M}$. There exist r solutions to the eigenvalue problem

$$\mathbf{M}\mathbf{v} = \lambda\mathbf{u}, \tag{79}$$

$$\mathbf{M}^T\mathbf{u} = \lambda\mathbf{v}, \tag{80}$$

such that $\lambda > 0$ and $\mathbf{u}^T\mathbf{u} = \mathbf{v}^T\mathbf{v} = 1$. Letting λ_i, $\mathbf{u}_i$, $\mathbf{v}_i$, $i = 1, \ldots, r$, denote the solutions, then

$$\mathbf{u}_i^T\mathbf{M}\mathbf{M}^T\mathbf{u}_j = (\lambda_i^2\mathbf{u}_i^T)\mathbf{u}_j = \mathbf{u}_i^T(\lambda_j^2\mathbf{u}_j), \tag{81}$$

and

$$\mathbf{v}_i^T\mathbf{M}^T\mathbf{M}\mathbf{v}_j = (\lambda_i^2\mathbf{v}_i^T)\mathbf{v}_j = \mathbf{v}_i^T(\lambda_j^T\mathbf{v}_j), \tag{82}$$

so that

$$(\lambda_j^2 - \lambda_i^2)\mathbf{u}_i^T\mathbf{u}_j = 0 = (\lambda_j^2 - \lambda_i^2)\mathbf{v}_i^T\mathbf{v}_j. \tag{83}$$

Then, after normalizing the eigenvectors, it follows from (83) that

$$\mathbf{u}_i^T \mathbf{u}_j = \mathbf{v}_i^T \mathbf{v}_j = \delta_{ij}. \tag{84}$$

The vectors $\mathbf{u}_i$ and $\mathbf{v}_i$, respectively, are left- and right-hand eigenvectors of $\mathbf{M}$ corresponding to the eigenvalue λ_i. Multiple eigenvectors associated with the same eigenvalue are not necessarily orthogonal to each other, but they do form a subspace that is orthogonal to all other eigenvectors with different eigenvalues.

4.1.1 Completing the square

These results are most easily derived and understood by using a technique of Lanczos [1961] for completing the square. We define a real symmetric square $(m+n) \times (m+n)$ matrix

$$\mathbf{H} = \begin{pmatrix} 0 & \mathbf{M} \\ \mathbf{M}^T & 0 \end{pmatrix}. \tag{85}$$

Then, (79)–(80) becomes

$$\mathbf{H} \begin{pmatrix} \mathbf{u}_i \\ \mathbf{v}_i \end{pmatrix} = \lambda_i \begin{pmatrix} \mathbf{u}_i \\ \mathbf{v}_i \end{pmatrix}. \tag{86}$$

Clearly, for each positive eigenvalue λ_i with eigenvector $(\mathbf{u}_i^T, \mathbf{v}_i^T)^T$, there is a corresponding negative eigenvalue $-\lambda_i$ with eigenvector $(\mathbf{u}_i^T, -\mathbf{v}_i^T)^T$.

4.1.2 Generalized inverse

The *singular value decomposition* (SVD) of $\mathbf{M}$ is given by

$$\mathbf{M} = \sum_{i=1}^{r} \lambda_i \mathbf{u}_i \mathbf{v}_i^T. \tag{87}$$

The Moore-Penrose pseudoinverse of $\mathbf{M}$ can be expressed as

$$\mathbf{M}^\dagger = \sum_{i=1}^{r} \lambda_i^{-1} \mathbf{v}_i \mathbf{u}_i^T. \tag{88}$$

Completing the square also permits us to find a simple derivation of the uniqueness conditions required for a meaningful generalized inverse that gives rise to the formula (88).

Let $\mathbf{A} = \mathbf{M}^T\mathbf{M}$ so that

$$\mathbf{A} = \sum_{i=1}^{r} \lambda_i^2 \mathbf{v}_i \mathbf{v}_i^T. \tag{89}$$

Then, $\mathbf{A}$ is real symmetric and therefore has real eigenvalues. A generalized inverse for $\mathbf{A}$ can be written in the form

$$\mathbf{A}^\dagger = \sum_{ij}^{r} \alpha_{ij} \mathbf{v}_i \mathbf{v}_j^T, \tag{90}$$

and must satisfy the consistency conditions

$$\mathbf{A}\mathbf{A}^\dagger = \mathbf{A}^\dagger\mathbf{A} = \mathbf{I}_r = \sum_{i=1}^{r} \mathbf{v}_i\mathbf{v}_i^T. \tag{91}$$

The final expression in (91) is just the completeness relation within the subspace orthogonal to the null space. Equaation (91) implies that $\mathbf{A}^\dagger$ is the unique matrix that satisfies the conditions

$$\mathbf{A}\mathbf{A}^\dagger\mathbf{A} = \mathbf{A}, \tag{92}$$

$$\mathbf{A}^\dagger\mathbf{A}\mathbf{A}^\dagger = \mathbf{A}^\dagger. \tag{93}$$

It follows easily from (91) that

$$\alpha_{ij} = \delta_{ij}/\lambda_i^2. \tag{94}$$

Thus, the generalized inverse of this symmetric square matrix is just

$$\mathbf{A}^\dagger = \sum_{i=1}^{r} \mathbf{v}_i\mathbf{v}_i^T/\lambda_i^2. \tag{95}$$

To find the needed relation for the nonsymmetric/nonsquare matrix $\mathbf{M}$, again consider the square matrix $\mathbf{H}$. We find easily that

$$\mathbf{H}^2 = \begin{pmatrix} \mathbf{M}\mathbf{M}^T & 0 \\ 0 & \mathbf{M}^T\mathbf{M} \end{pmatrix}. \tag{96}$$

Then, to be consistent we must have

$$\mathbf{H}^\dagger = \mathbf{H}(\mathbf{H}^2)^\dagger = (\mathbf{H}^2)^\dagger\mathbf{H}, \tag{97}$$

from which it follows that

$$\mathbf{H}^\dagger = \begin{pmatrix} 0 & \mathbf{M}(\mathbf{M}^T\mathbf{M})^\dagger \\ \mathbf{M}^T(\mathbf{M}\mathbf{M}^T)^\dagger & 0 \end{pmatrix} = \begin{pmatrix} 0 & (\mathbf{M}\mathbf{M}^T)^\dagger\mathbf{M} \\ (\mathbf{M}^T\mathbf{M})^\dagger\mathbf{M}^T & 0 \end{pmatrix}. \tag{98}$$

Equation (98) implies that

$$\mathbf{M}^\dagger = \mathbf{M}^T(\mathbf{M}\mathbf{M}^T)^\dagger = (\mathbf{M}^T\mathbf{M})^\dagger\mathbf{M}^T. \tag{99}$$

Using (95) in (99) then finally yields (88).

A more direct derivation comes from (95) by writing down the equivalent expansion fo $\mathbf{H}^\dagger$. First, expand $\mathbf{H}$ in terms of the eigenvectors as

$$\mathbf{H} = \frac{1}{2}\sum_{i=1}^{r} \lambda_i \left[\begin{pmatrix} \mathbf{u}_i \\ \mathbf{v}_i \end{pmatrix} \begin{pmatrix} \mathbf{u}_i^T & \mathbf{v}_i^T \end{pmatrix} - \begin{pmatrix} \mathbf{u}_i \\ -\mathbf{v}_i \end{pmatrix} \begin{pmatrix} \mathbf{u}_i^T & -\mathbf{v}_i^T \end{pmatrix} \right] \tag{100}$$

$$= \sum_{i=1}^{r} \lambda_i \left[\begin{pmatrix} 0 \\ \mathbf{v}_i \end{pmatrix} \begin{pmatrix} \mathbf{u}_i^T & 0 \end{pmatrix} + \begin{pmatrix} \mathbf{u}_i \\ 0 \end{pmatrix} \begin{pmatrix} 0 & \mathbf{v}_i^T \end{pmatrix} \right]. \tag{101}$$

The factor of one-half in (100) arises from the fact that the norm of the eigenvectors of H (as defined here) is 2. Then, from (100) and (95), we obtain

$$\mathbf{H}^\dagger = \sum_{i=1}^{r} \lambda_i^{-1} \left[\begin{pmatrix} 0 \\ \mathbf{v}_i \end{pmatrix} \begin{pmatrix} \mathbf{u}_i^T & 0 \end{pmatrix} + \begin{pmatrix} \mathbf{u}_i \\ 0 \end{pmatrix} \begin{pmatrix} 0 & \mathbf{v}_i^T \end{pmatrix} \right] = \begin{pmatrix} 0 & (\mathbf{M}^T)^\dagger \\ \mathbf{M}^\dagger & 0 \end{pmatrix}, \tag{102}$$

and (88) again follows.

4.1.3 Relation to least-squares

Now we can solve the least-squares problem using the SVD of $\mathbf{M}$. To see this, we will let $w_i = 1$ for simplicity. To begin, we recognize that we can expand $\hat{\mathbf{s}}$ and $\mathbf{t}$ in terms of the left- and right-eigenvectors:

$$\mathbf{t} = \sum_{i=1}^{r} \tau_i \mathbf{u}_i + \mathbf{t}_0, \tag{103}$$

$$\hat{\mathbf{s}} = \sum_{i=1}^{r} \sigma_i \mathbf{v}_i + \mathbf{s}_0, \tag{104}$$

where

$$\mathbf{v}_i^T \mathbf{s}_0 = \mathbf{u}_i^T \mathbf{t}_0 = 0, \tag{105}$$

and

$$\tau_i = \mathbf{u}_i^T \mathbf{t}, \tag{106}$$

$$\sigma_i = \mathbf{v}_i^T \hat{\mathbf{s}}. \tag{107}$$

In terms of the expansion coefficients and unit weights, we have

$$\Psi(\hat{\mathbf{s}}) = (\mathbf{M}\hat{\mathbf{s}} - \mathbf{t})^T (\mathbf{M}\hat{\mathbf{s}} - \mathbf{t}) \tag{108}$$

$$= \mathbf{t}_0^T \mathbf{t}_0 + \sum_{i=1}^{r} (\lambda_i \sigma_i - \tau_i)^2. \tag{109}$$

For the nonzero eigenvalues, setting

$$\lambda_i \sigma_i = \tau_i \tag{110}$$

minimizes Ψ by eliminating the sum in (109). Then,

$$\hat{\mathbf{s}} = \mathbf{s}_0 + \sum_{i=1}^{r} \lambda_i^{-1} \tau_i \mathbf{v}_i. \tag{111}$$

The vector $\mathbf{s}_0$ is an arbitrary vector from the right null space of $\mathbf{M}$. We can minimize $\hat{\mathbf{s}}^T \hat{\mathbf{s}}$ by setting $\mathbf{s}_0 = 0$. Thus, we obtain the minimum-norm least-squares model:

$$\hat{\mathbf{s}}_{\mathrm{LS}} = \sum_{i=1}^{r} \lambda_i^{-1} \tau_i \mathbf{v}_i. \tag{112}$$

The reader can easily verify that

$$\hat{\mathbf{s}}_{\mathrm{LS}} = \mathbf{M}^{\dagger} \mathbf{t}. \tag{113}$$

It is a general result that the Moore-Penrose pseudoinverse solves the least-squares problem. We will make use of this fact later when we attempt to construct methods of solving the inversion problem that are both fast and easy to implement.

We observe two special cases in which $\mathbf{M}$ is full rank. If $r = n \leq m$, then $\mathbf{s}_0$ is necessarily zero. Further, we can write

$$\mathbf{M}^\dagger = (\mathbf{M}^T\mathbf{M})^{-1}\mathbf{M}^T. \tag{114}$$

Second, if $r = m \leq n$, then $\mathbf{t}_0 = 0$ and

$$\mathbf{M}^\dagger = \mathbf{M}^T(\mathbf{M}\mathbf{M}^T)^{-1}. \tag{115}$$

A subcase of both cases is $r = m = n$. $\mathbf{M}$ is then square and full rank, and we have

$$\mathbf{M}^\dagger = \mathbf{M}^{-1}. \tag{116}$$

4.2 Sequential and Iterative Methods

We will first consider the case where $r = n$. The least-squares solution is then given by

$$\hat{\mathbf{s}}_{\mathrm{LS}} = (\mathbf{M}^T\mathbf{M})^{-1}\mathbf{M}^T\mathbf{t}. \tag{117}$$

We will begin by summarizing the main ideas behind two matrix inversion methods that work if $\mathbf{M}^T\mathbf{M}$ is invertible. Then, we discuss other methods applicable to more realistic problems.

4.2.1 Series expansion method

Again letting $\mathbf{A} = \mathbf{M}^T\mathbf{M}$, we observe that $\mathbf{A}$ is square and we suppose that it is of full rank. In terms of the SVD of $\mathbf{M}$,

$$\mathbf{A} = \sum_{i=1}^{n} \lambda_i^2 \mathbf{v}_i \mathbf{v}_i^T. \tag{118}$$

Let $\rho_i = \lambda_i^2$. Then, since $\mathbf{A}$ satisfies its own characteristic polynomial, we have the following matrix identity:

$$(\mathbf{A} - \rho_1\mathbf{I})(\mathbf{A} - \rho_2\mathbf{I}) \ldots (\mathbf{A} - \rho_n\mathbf{I}) = 0. \tag{119}$$

The left-hand side of this equation is simply an nth order matrix polynomial in $\mathbf{A}$, which we can rewrite as

$$\mathbf{A}^n - (\rho_1 + \cdots + \rho_n)\mathbf{A}^{n-1} + \cdots + (-1)^n \rho_1 \cdots \rho_n \mathbf{I} = 0. \tag{120}$$

Multiplying through by $\mathbf{A}^{-1}$

$$\mathbf{A}^{n-1} - (\rho_1 + \cdots + \rho_n)\mathbf{A}^{n-2} + \cdots + (-1)^n \rho_1 \cdots \rho_n \mathbf{A}^{-1} = 0, \tag{121}$$

or

$$\mathbf{A}^{-1} = \frac{(-1)^{n+1}}{\rho_1 \cdots \rho_n}(\mathbf{A}^{n-1} - (\rho_1 + \cdots + \rho_n)\mathbf{A}^{n-2} + \cdots + \mathbf{I}). \tag{122}$$

This gives a series expansion for $\mathbf{A}^{-1}$ in powers of $\mathbf{A}$ itself. Based on this series we could compute $\mathbf{A}^{-1}\mathbf{M}^T\mathbf{t}$ recursively if we knew the eigenvalues of $\mathbf{A}$, or at least knew the symmetric functions of the eigenvalues that appear in the formulas.

This approach clearly fails if $\mathbf{A}$ is not of full rank, since the final division by the product of the eigenvalues cannot be performed.

4.2.2 Conjugate directions

In conjugate directions [Hestenes and Stiefel, 1952], we expand $\mathbf{A}^{-1}$ differently. Let $\mathbf{p}_1, \ldots, \mathbf{p}_n$ be a set of vectors such that

$$\mathbf{p}_i^T \mathbf{A} \mathbf{p}_j = \delta_{ij} \mathbf{p}_i^T \mathbf{A} \mathbf{p}_i. \tag{123}$$

The vectors $\mathbf{p}_i$ are not necessarily orthogonal with respect to the usual vector dot product, but they are orthogonal relative to the matrix $\mathbf{A}$. The vectors $\mathbf{p}_i$ are then said to be conjugate relative to $\mathbf{A}$. Then suppose that

$$\mathbf{A}^{-1} = \mathbf{A}' \equiv \sum_{i=1}^{n} \frac{\mathbf{p}_i \mathbf{p}_i^T}{\mathbf{p}_i^T \mathbf{A} \mathbf{p}_i}. \tag{124}$$

It follows from (123) and (124) that

$$\mathbf{A}'(\mathbf{A}\mathbf{p}_j) = \sum_{i=1}^{n} \mathbf{p}_i \delta_{ij} = \mathbf{p}_j, \tag{125}$$

so

$$\mathbf{A}'\mathbf{A} = \mathbf{I} = \mathbf{A}\mathbf{A}', \tag{126}$$

if the $\mathbf{p}_j$s span the entire vector space, so the completeness relation in terms of the $\mathbf{p}_j$s is

$$\mathbf{I} = \sum_{j=1}^{n} \frac{\mathbf{p}_j \mathbf{p}_j^T \mathbf{A}}{\mathbf{p}_j^T \mathbf{A} \mathbf{p}_j}. \tag{127}$$

This approach therefore produces a valid and simple formula (124) for $\mathbf{A}^{-1}$ when $\mathbf{A}$ is of full rank, and furthermore it is guaranteed to converge in a finite number of steps. But, when $\mathbf{A}$ is rank deficient, it must happen that $\mathbf{p}_i^T \mathbf{A} \mathbf{p}_i = 0$ for some $\mathbf{p}_i$ and, therefore, this method fails also in the cases of most interest to tomography.

Conjugate directions may still be of interest however if care is taken to choose only $\mathbf{p}_i$s orthogonal to the null space of $\mathbf{A}$. Then, this approach may be used to generate the generalized inverse of $\mathbf{A}$.

4.2.3 Simple iteration

In simple iteration, we start with an initial model $\mathbf{s}^{(0)}$ and iteratively generate a sequence $\mathbf{s}^{(k)}$, $k = 1, 2, \ldots$ using

$$\mathbf{s}^{(k+1)} = \mathbf{s}^{(k)} + \mathbf{M}^T(\mathbf{t} - \mathbf{M}\mathbf{s}^{(k)}). \tag{128}$$

In terms of eigenvector expansion coefficients, the iteration sequence becomes

$$\sigma_i^{(k+1)} = \sigma_i^{(k)} + \lambda_i(\tau_i - \lambda_i \sigma_i^{(k)}). \tag{129}$$

To solve this equation, we note that it can be rewritten as

$$\sigma_i^{(k+1)} = \lambda_i \tau_i + (1 - \lambda_i^2)\sigma_i^{(k)} = \lambda_i \tau_i + (1 - \lambda_i^2)[\lambda_i \tau_i + (1 - \lambda_i^2)\sigma_i^{(k-1)}]. \tag{130}$$

Rearranging the resulting series, we find

$$\sigma_i^{(k+1)} = [1 + (1-\lambda^2) + (1-\lambda^2)^2 + \ldots + (1-\lambda^2)^k]\lambda_i\tau_i + (1-\lambda^2)^{k+1}\sigma_i^{(0)}. \quad (131)$$

The series multiplying τ_i can be summed exactly for any value of $\lambda_i \neq 0$ as

$$[1 + (1-\lambda_i^2) + (1-\lambda_i^2)^2 + \ldots + (1-\lambda_i^2)^k] = \frac{1-(1-\lambda_i^2)^{k+1}}{1-(1-\lambda_i^2)} \quad (132)$$

from which it follows that

$$\sigma_i^{(k+1)} = \left[\frac{1-(1-\lambda_i^2)^{k+1}}{\lambda_i}\right]\tau_i + (1-\lambda_i^2)^{k+1}\sigma_i^{(0)}. \quad (133)$$

If $\lambda_i = 0$, (129) shows that $\sigma_i^{(k+1)} = \sigma_i^{(0)}$. If we assume that the eigenvalues, λ_i, are all between -2 and 2, the iteration sequence converges. The condition $-2 < \lambda_i < 2$ thus implies that $\sigma_i^{(k)} \to \tau_i/\lambda_i$ as $k \to \infty$. That is, the iteration converges to a least-squares model.

We will see later that the stronger condition $-1 \leq \lambda_i \leq 1$ can be guaranteed with an appropriate preconditioning (prescaling) of the matrix $\mathbf{M}$.

Simple iteration is a good method for solving linear tomography problems, and is much simpler to implement than other methods such as conjugate directions or conjugate gradients. This method has significant computational advantages when the dimensions of $\mathbf{M}$ are large.

4.2.4 Neural network method

In this approach we consider a sequence of models as a function of a continuous index variable, $\mathbf{s}(\eta)$. The data misfit functional, Ψ, applied to this sequence then is also a function of η. We have

$$\frac{d\Psi}{d\eta} = 2\frac{d\mathbf{s}^T}{d\eta}\nabla_{\mathbf{s}^T}\Psi, \quad (134)$$

where

$$\nabla_{\mathbf{s}^T}\Psi = \mathbf{M}^T(\mathbf{M}\mathbf{s} - \mathbf{t}). \quad (135)$$

We would like $d\Psi/d\eta < 0$ so that $\mathbf{s}(\eta)$ converges to a model that minimizes Ψ as $\eta \to \infty$. It is easy to verify that we achieve a negative derivative by requiring, for some scalar $\gamma > 0$,

$$\frac{d\mathbf{s}}{d\eta} = -\gamma\mathbf{M}^T(\mathbf{M}\mathbf{s} - \mathbf{t}). \quad (136)$$

We thus have a first-order differential equation for $\mathbf{s}(\eta)$. In terms of the expansion coefficients, σ_i, this becomes

$$\frac{d\sigma_i}{d\eta} = \gamma\lambda_i(\tau_i - \lambda_i\sigma_i). \quad (137)$$

Using $\sigma_i = 0$ as an initial condition, the solution to (137) is given by

$$\sigma_i(\eta) = \lambda_i^{-1} r_i \left[1 - e^{-\gamma \lambda_i^2 \eta}\right]. \tag{138}$$

We see that $\mathbf{s}(\eta)$ does indeed converge to $\hat{\mathbf{s}}_{\mathrm{LS}}$, with its exponential convergence rate controlled by γ.

Further discussion of this approach together with comparisons to other methods may found in Jeffrey and Rosner [1986a,b] and Lu and Berryman [1991].

4.3 Scaling Methods

Given $\mathbf{M}$ we define two diagonal matrices based on row and column sums of its elements, l_{ij}. Let $\mathbf{L}$ and $\mathbf{C}$ be diagonal matrices such that

$$L_{ii} = \sum_{j=1}^{n} l_{ij}, \quad i = 1, \ldots m, \tag{139}$$

$$C_{jj} = \sum_{i=1}^{m} l_{ij}, \quad j = 1, \ldots, n. \tag{140}$$

L_{ii} is the length of the ith ray path, obtained by summing the lengths of its intersection with all cells. C_{jj}, on the other hand, is the total length of ray segments intersecting the jth cell. C_{jj} is known variously as the *illumination*, *hit parameter*, or *coverage* of cell j.

Let $\mathbf{1}_n$ be the n-vector whose components are each 1:

$$\mathbf{1}_n = \begin{pmatrix} 1 \\ 1 \\ \vdots \\ 1 \end{pmatrix}. \tag{141}$$

Similarly, let $\mathbf{1}_m$ be the analogous m-vector. Then $\mathbf{M}\mathbf{1}_n$ is the m-vector containing the ray lengths. We can also infer that $\mathbf{L}\mathbf{1}_m$ is the same vector. Analogously, $\mathbf{M}^T\mathbf{1}_m$ and $\mathbf{C}\mathbf{1}_n$ are both the n-vector containing the cell coverages. That is,

$$\mathbf{M}\mathbf{1}_n = \mathbf{L}\mathbf{1}_m, \tag{142}$$

$$\mathbf{M}^T\mathbf{1}_m = \mathbf{C}\mathbf{1}_n. \tag{143}$$

This implies that $\lambda = 1$, $\mathbf{u} = \mathbf{1}_m$, $\mathbf{v} = \mathbf{1}_n$ is a solution to the eigenvalue problem

$$\mathbf{M}\mathbf{v} = \lambda \mathbf{L}\mathbf{u}, \tag{144}$$

$$\mathbf{M}^T\mathbf{u} = \lambda \mathbf{C}\mathbf{v}. \tag{145}$$

This problem is a generalization of our earlier eigenvalue problem (79)–(80) in that it incorporates positive definite weighting matrices $\mathbf{L}$ and $\mathbf{C}$. In place of the orthonormality conditions (84), we require the *conjugacy* conditions

$$\mathbf{u}_i^T \mathbf{L}\mathbf{u}_j = \mathbf{v}_i^T \mathbf{C}\mathbf{v}_j = \delta_{ij}. \tag{146}$$

With these conditions, the generalized eigenvalue problem can be converted to the standard form of (79)–(80) using the transformations

$$\mathbf{M}' = \mathbf{L}^{-1/2}\mathbf{M}\mathbf{C}^{-1/2}, \tag{147}$$
$$\mathbf{u}' = \mathbf{L}^{1/2}\mathbf{u}, \tag{148}$$
$$\mathbf{v}' = \mathbf{C}^{1/2}\mathbf{v}. \tag{149}$$

We see that, by construction, the eigenvalues of $\mathbf{M}$ and $\mathbf{M}'$ are the same, but for different eigenvalue problems: (144)–(145) and

$$\mathbf{M}'\mathbf{v}' = \lambda\mathbf{u}', \tag{150}$$
$$\mathbf{M}'^{T}\mathbf{u}' = \lambda\mathbf{v}'. \tag{151}$$

Theorem 4.1 *The eigenvalues of* $\mathbf{M}'$ *lie in the interval [-1,1].*

Proof. Recall that the eigenvalues come in pairs: if $\lambda, \mathbf{u}', \mathbf{v}'$ solves the eigenvalue problem, then so does $-\lambda, \mathbf{u}', -\mathbf{v}'$. Then, we may (without loss of generality) restrict the discussion to eigenvalues satisfying $\lambda \geq 0$.

Let λ, $\mathbf{u}$, $\mathbf{v}$ be any solution to (144)–(145) with $\lambda > 0$. Then, in components,

$$\sum_j l_{ij} v_j = \lambda L_{ii} u_i, \tag{152}$$
$$\sum_i l_{ij} u_i = \lambda C_{jj} v_j. \tag{153}$$

Let $u_{\max}$ be the largest absolute component of $\mathbf{u}$, i.e., $u_{\max} = \max_i |u_i|$. Similarly, let $v_{\max} = \max_j |v_j|$. Since $l_{ij} \geq 0$, we can infer

$$v_{\max} \sum_j l_{ij} \geq \lambda L_{ii} |u_i|, \tag{154}$$
$$u_{\max} \sum_i l_{ij} \geq \lambda C_{jj} |v_j|. \tag{155}$$

Recalling the definitions of C_{jj} and L_{ii} given by (139) and (140), this implies

$$v_{\max} \geq \lambda |u_i|, \tag{156}$$
$$u_{\max} \geq \lambda |v_j|, \tag{157}$$

which must hold for all i and j; thus

$$v_{\max} \geq \lambda u_{\max}, \tag{158}$$
$$u_{\max} \geq \lambda v_{\max}. \tag{159}$$

Thus, we have $v_{\max} \geq \lambda^2 v_{\max}$, which implies $\lambda^2 \leq 1$ and therefore $-1 \leq \lambda \leq 1$. ∎

4.4 Mathematical Basis for Weighted Least-Squares

In weighted least-squares, a good weighting matrix to use is $\mathbf{L}^{-1}$, the inverse of the ray length matrix. In other words, we should set $w_i = L_{ii}^{-1}$. In an earlier lecture, we discussed the physical arguments for using such a weight matrix. Here we will show that mathematical arguments based on stability lead to the same choice of weight matrix.

There is an inherent arbitrariness to the choice of weight matrix in a least-squares minimization. Let $\mathbf{F}$ and $\mathbf{G}$ be two positive, diagonal weight matrices, $m \times m$ and $n \times n$ respectively. Then define the scaled inversion problem so that

$$\mathbf{M}' = \mathbf{F}^{-\frac{1}{2}}\mathbf{M}\mathbf{G}^{-\frac{1}{2}}, \quad \mathbf{s}' = \mathbf{G}^{\frac{1}{2}}\mathbf{s}, \quad \mathbf{t}' = \mathbf{F}^{-\frac{1}{2}}\mathbf{t}. \tag{160}$$

The (unweighted) damped least-squares minimization problem associated with (160) is to minimize the functional

$$\Psi'(\mathbf{s}') = (\mathbf{t}' - \mathbf{M}'\mathbf{s}')^T(\mathbf{t}' - \mathbf{M}'\mathbf{s}') + \mu(\mathbf{s}' - \mathbf{s}_0')^T(\mathbf{s}' - \mathbf{s}_0'), \tag{161}$$

with respect to $\mathbf{s}'$. The normal equations resulting from (161) are

$$(\mathbf{M}'^T\mathbf{M}' + \mu\mathbf{I})(\mathbf{s}' - \mathbf{s}_0') = \mathbf{M}'^T(\mathbf{t}' - \mathbf{M}'\mathbf{s}_0'). \tag{162}$$

The result for the untransformed $\mathbf{s}$ is exactly the same whether we use the functional (161) or the weighted least-squares functional

$$\Psi(\mathbf{s}) = (\mathbf{t} - \mathbf{M}\mathbf{s})^T\mathbf{F}^{-1}(\mathbf{t} - \mathbf{M}\mathbf{s}) + \mu(\mathbf{s} - \mathbf{s}_0)^T\mathbf{G}(\mathbf{s} - \mathbf{s}_0). \tag{163}$$

In either case, the result is

$$\mathbf{s} = \mathbf{s}_0 + (\mathbf{M}^T\mathbf{F}^{-1}\mathbf{M} + \mu\mathbf{G})^{-1}\mathbf{M}^T\mathbf{F}^{-1}(\mathbf{t} - \mathbf{M}\mathbf{s}_0). \tag{164}$$

In truth, every least-squares method is really a weighted least-squares method — some just have unit weights everywhere.

The minimum of (163) is achieved by the slowness model given in (164) as long as the matrix $\mathbf{M}^T\mathbf{F}^{-1}\mathbf{M} + \mu\mathbf{G}$ is invertible. Thus, we may relax the conditions placed on the weight matrix $\mathbf{G}$ somewhat if we so choose. One common choice is to make the regularization term correspond to minimizing the gradient or curvature of the model. Then, the matrix $\mathbf{G} = \mathbf{K}^T\mathbf{K}$, where $\mathbf{K}\mathbf{s}$ is either the gradient of the model or its Laplacian. Such a weight matrix is neither diagonal nor positive. In fact, a constant model vector lies in the null space of such a $\mathbf{G}$. The combined matrix $\mathbf{M}^T\mathbf{F}^{-1}\mathbf{M} + \mu\mathbf{G}$ may still be invertible however, since the null spaces of the two terms are generally orthogonal.

There are physical reasons for choosing particular weighting schemes and some of these reasons have been discussed in an earlier lecture. A sound mathematical reason for choosing a particular scheme might be "regularization." It may be difficult or impossible to compute the result (164) unless appropriate weight matrices are used. We saw in our discussion of *simple iteration* that this method will converge if the eigenvalues of the matrix $\mathbf{M}$ (or equivalently $\mathbf{M}'$ here) lie in the range $-2 \leq \lambda_i \leq 2$. So how can we choose the weight matrices to guarantee that the eigenvalues fall in the desired range?

For the sake of argument, suppose that

$$\mathbf{M}\mathbf{s} = \lambda \mathbf{F}\mathbf{r}, \tag{165}$$

$$\mathbf{M}^T\mathbf{r} = \lambda \mathbf{G}\mathbf{s}. \tag{166}$$

Then, again in components, we have

$$\sum_j l_{ij} s_j = \lambda F_{ii} r_i, \tag{167}$$

$$\sum_i l_{ij} r_j = \lambda G_{jj} s_i. \tag{168}$$

Letting $s_{\max}$ be the magnitude of the largest component of $\mathbf{s}$ and $r_{\max}$ the magnitude of the largest component of $\mathbf{r}$, we have

$$s_{\max} L_{ii} \geq \lambda F_{ii} |r_i|, \tag{169}$$

$$r_{\max} C_{jj} \geq \lambda G_{jj} |s_j|. \tag{170}$$

It follows that

$$s_{\max} \geq \lambda \frac{F_{ii}}{L_{ii}} r_{\max} \geq \lambda^2 \frac{F_{ii} G_{jj}}{L_{ii} C_{jj}} s_{\max}. \tag{171}$$

So, in general, we can guarantee that the eigenvalues λ will be bounded above by unity by requiring that

$$1 \geq \frac{L_{ii} C_{jj}}{F_{ii} G_{jj}}, \quad \text{for all} \quad i, j. \tag{172}$$

Many choices of $\mathbf{F}$ and $\mathbf{G}$ are permitted by (172), but perhaps the simplest choice is

$$\mathbf{F} = \mathbf{L} \quad \text{and} \quad \mathbf{G} = \mathbf{C}. \tag{173}$$

Thus, although the choice (173) is certainly not unique, it is nevertheless a good choice for the weight matrices in weighted least-squares, and guarantees that $\lambda^2 \leq 1$ as desired.

In a later lecture, we will find that another choice of weight matrices has the same constraining properties on the eigenvalues, yet has more useful properties in the nonlinear tomography algorithms.

5 Ghosts in Tomography

A ghost in seismic tomography is a model perturbation that does not affect the agreement between the predicted and measured first arrival traveltimes. For example, if

$$\mathbf{M}\mathbf{s} = \mathbf{t}, \quad \mathbf{M}(\mathbf{s} + \mathbf{g}) = \mathbf{t}, \tag{174}$$

then subtracting shows that

$$\mathbf{M}\mathbf{g} = 0, \tag{175}$$

so $\mathbf{g}$ lies in the null space of $\mathbf{M}$, *i.e.*, in the null space of the traveltime functional. A careful analysis of the ghosts shows that, while some are unavoidable due to the limited view angles used when the data were collected, others are caused by unfortunate choices made when discretizing the model. Thus, some of the ghosts may be eliminated by making unusual choices for the model parametrization.

It is important to realize from the outset that it may not be possible to eliminate all the ghosts. In fact, the normal solution to the least-squares problem cannot be found if $\mathbf{M}^T\mathbf{M}$ is not invertible. Lack of invertibility is caused by the presence of a right null space for $\mathbf{M}$ and the members of that null space we call ghosts. In some cases, simple tricks can be developed to eliminate the ghosts, but not always.

5.1 Types of Ghosts

We will now carry out an in-depth analysis of a few common ghosts that can occur in seismic tomography.

5.1.1 Single cell ghost

A single cell ghost occurs when no ray passes through a certain cell. That cell is uncovered, not illuminated, not hit by any of the rays in the data set (at least for the current choice of ray paths). Thus, the slowness of that cell is arbitrary, as it has no effect on determining any of the traveltimes in the data set.

The proper way to deal with such a cell is to assign it some arbitrary value, like the average slowness of all cells or the average of all contiguous cells.

5.1.2 Two cells with only one ray

When any two cells are covered by one and only one ray, a ghost arises because the increment of traveltime δt_i through these cells is invariant to a perturbation of the form

$$\mathbf{g}^T = (0, \ldots, 0, l_{ik}, 0, \ldots, 0, -l_{ij}, 0, \ldots, 0), \tag{176}$$

since

$$\delta t_i = l_{ij}s_j + l_{ik}s_k = l_{ij}(s_j + \alpha l_{ik}) + l_{ik}(s_k - \alpha l_{ij}), \tag{177}$$

where α is an almost arbitrary scalar. The one constraint on α is that the perturbed slowness vector

$$\mathbf{s}' = \mathbf{s} + \alpha\mathbf{g} \tag{178}$$

must be positive. Note that there is no ghost associated with a single cell having only one covering ray.

The proper way to deal with such pairs of cells (especially if they are contiguous) is to treat them as if they were combined into one larger cell, *i.e.*, assign the same value of slowness to both cells. This approach has the effect of eliminating the ghost while simultaneously reducing the size of the model space by one dimension.

If more than two cells are covered by one and only one ray, then there will be multiple ghosts (for p cells there will be $p-1$ ghosts). Again, one way to eliminate this problem is to treat all such cells as a single cell. This approach may not be the best one if the cells are not contiguous. Other approaches will be discussed in the section on eliminating ghosts.

5.1.3 Underdetermined cells in an overdetermined problem

The preceding discussion is a special case of a more general problem: underdetermined cells imbedded in an overdetermined inversion problem. By underdetermined we mean that we have fewer equations than unknowns. The example of two cells with only one ray is a common example of this effect. Others would be three cells with two rays, 20 cells with 15 rays, etc. The existence of underdetermined cells may be the result of poor experimental design, of physical limitations at the experimental site that reduce the possible range of view angles significantly, or they may be caused by severe ray bending effects when high contrasts in the slowness values are present. In the latter situation, we expect that rays will tend to avoid very slow regions (Fermat's principle says to take the fastest path, which may mean to go around the slow region). Since experiments will normally be planned to achieve the desired resolution assuming straight-ray coverage, the actual coverage in slow regions is smaller than planned and may be reduced by these ray bending effects to the extent of causing underdetermination.

This ghost problem can now be reduced to

$$\mathbf{M}'\mathbf{s}' = \delta\mathbf{t}', \tag{179}$$

where $\mathbf{M}'$ is an $m' \times n'$ matrix with $m' < n'$, $\mathbf{s}'$ is the subvector of the slowness model of length n', and $\delta\mathbf{t}'$ is the subvector of the traveltime increment of length m'. A particular solution of (179) is given by

$$\mathbf{s}' = \mathbf{M}'^T(\mathbf{M}'\mathbf{M}'^T)^{-1}\delta\mathbf{t}', \tag{180}$$

if the matrix $\mathbf{M}'\mathbf{M}'^T$ is invertible. But the general solution of (179) is any vector of the form

$$\mathbf{s}' = \mathbf{M}'^T(\mathbf{M}'\mathbf{M}'^T)^{-1}\delta\mathbf{t}' + \mathbf{g}', \tag{181}$$

where $\mathbf{g}'$ is any vector from the right null space of $\mathbf{M}'$. This null space must have dimension at least $n' - m'$.

The preferred solution to this problem is again to combine contiguous cells until the number of equations is at least equal to the number of unknowns. Then $n' - m' = 0$, and the null space is eliminated. Another method of dealing with the problem if the cells are not contiguous is to fix the slowness value of $n' - m'$ of those cells that have the least coverage, thus removing them from the inversion problem.

5.1.4 Stripes

One of the most common types of ghosts in borehole-to-borehole tomography is the vertical stripe. Stripes are ghosts caused by an unfortunate resonance of the model parametrization,

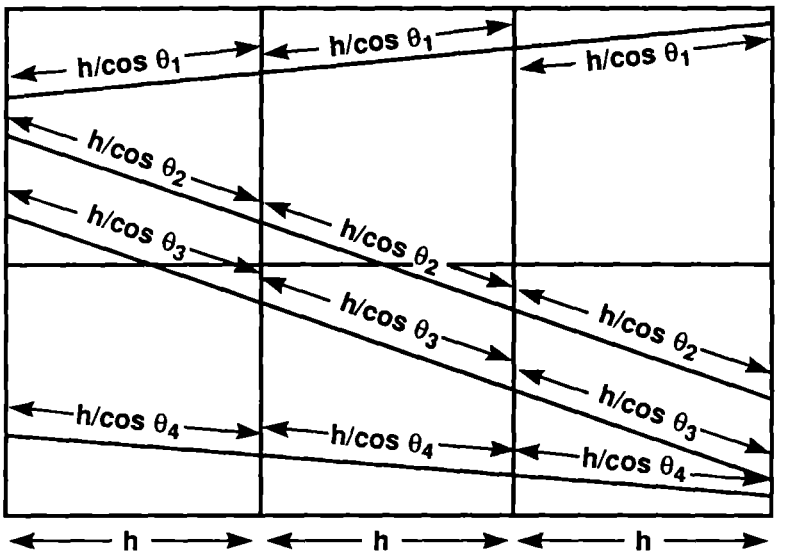

Figure 5: Stripes are caused by straight rays used in crosshole tomography.

the limited set of view angles possible in the crosshole geometry, and the use of straight rays in the reconstruction.

To see how the problem arises, consider the geometry of two vertical boreholes with square cells of dimension h in the image plane. For purposes of illustration, suppose that the borehole separation is just three cell widths and the borehole depth is two cell heights. To get from one borehole to the other, the rays must cross the lines forming the vertical boundaries between cells. Assuming straight rays, each ray is characterized by a total ray path length $L_i = 3h/\cos\theta_i$, where θ_i is the angle the ray makes with the horizontal. So the total path length in each vertical column is just $h/\cos\theta_i$. This part of the path length is shared among the cells in a column differently for each ray path, but that is not so important. What is important is that the sum is constant in each column for every ray.

The ray-path matrix takes the form

$$\mathbf{M} = \begin{pmatrix} \frac{d_{11}h}{\cos\theta_1} & \frac{d_{12}h}{\cos\theta_1} & \frac{e_{13}h}{\cos\theta_1} & \frac{e_{14}h}{\cos\theta_1} & \frac{f_{15}h}{\cos\theta_1} & \frac{f_{16}h}{\cos\theta_1} \\ \frac{d_{21}h}{\cos\theta_2} & \frac{d_{22}h}{\cos\theta_2} & \frac{e_{23}h}{\cos\theta_2} & \frac{e_{24}h}{\cos\theta_2} & \frac{f_{25}h}{\cos\theta_2} & \frac{f_{26}h}{\cos\theta_2} \\ \vdots & \vdots & \vdots & \vdots & \vdots & \vdots \\ \frac{d_{m1}h}{\cos\theta_m} & \frac{d_{m2}h}{\cos\theta_m} & \frac{e_{m3}h}{\cos\theta_m} & \frac{e_{m4}h}{\cos\theta_m} & \frac{f_{m5}h}{\cos\theta_m} & \frac{f_{m6}h}{\cos\theta_m} \end{pmatrix}, \tag{182}$$

where the ds, es, and fs are nonnegative fractions satisfying

$$\sum_{j=1}^{2} d_{ij} = \sum_{j=3}^{4} e_{ij} = \sum_{j=5}^{6} f_{ij} = 1, \tag{183}$$

for every ray path $1 \leq i \leq m$. The ds are associated with the cells in the first column; the es with the second column; and the fs with the third column. Then it is clear that these three vectors

$$\mathbf{g}_1 = \begin{pmatrix} 1 \\ 1 \\ -1 \\ -1 \\ 0 \\ 0 \end{pmatrix}, \quad \mathbf{g}_2 = \begin{pmatrix} 0 \\ 0 \\ 1 \\ 1 \\ -1 \\ -1 \end{pmatrix}, \quad \mathbf{g}_3 = \begin{pmatrix} 1 \\ 1 \\ 0 \\ 0 \\ -1 \\ -1 \end{pmatrix}, \tag{184}$$

are ghosts for this problem, since in each case we find that

$$\mathbf{Mg} = \begin{pmatrix} \frac{h}{\cos\theta_1} - \frac{h}{\cos\theta_1} \\ \frac{h}{\cos\theta_2} - \frac{h}{\cos\theta_2} \\ \vdots \\ \frac{h}{\cos\theta_m} - \frac{h}{\cos\theta_m} \end{pmatrix} = 0 \tag{185}$$

follows from (183).

These ghosts show up in the reconstructed slowness as vertical stripes — a constant slowness perturbation is subtracted from one column and added to any other column.

To eliminate these ghosts, we need to break the unfortunate symmetry that has caused this artifact to arise. These ghosts would not exist if the cells were not lined up perfectly with both of the vertical boreholes. So one solution is to use cells that are not square or rectangular, *i.e.*, odd shapes like hexagons, triangles, etc. Using a rectangular but staggered grid would also remove the degeneracy. Or, combining a few of the poorly covered cells near the top and bottom would also break the symmetry. A still simpler method of eliminating the problem (at least conceptually) is to use bent rays, rather than the artificially straight rays that are often incorrectly assumed to be adequate.

5.1.5 Linear dependence

Ghosts arise from the linear dependence of $\mathbf{M}$ or of submatrices such as $\mathbf{M}'$. The example of stripes arises from a gross linear dependence of all the rows of the full matrix $\mathbf{M}$. The examples of underdetermined group of cells arise because of poor coupling (or coverage) between the rays and the cells. Other, more subtle and complex, linear dependencies may also occur.

Indeed the defining equation for a ghost

$$\mathbf{Mg} = 0 \tag{186}$$

is a statement of linear dependence of the rows of $\mathbf{M}$. Equation (186) contains m equations for the n unknown components of $\mathbf{g}$, with $m > n$. Any n of these m equations are sufficient to determine $\mathbf{g}$ and the remaining $m-n$ equations can be determined from these n equations. An exception to this statement occurs when the ghost is caused by complete decoupling as in the case of the single cell ghost.

5.2 Eliminating Ghosts (Ghostbusting)

Ghosts may be removed by using a variety of techniques, some of which have already been described. Although ray bending can introduce ghosts in situations where very slow regions are avoided by most rays, it can also provide a simple solution to some of the problems created by the limited view angles available in crosshole measurements. Methods of improving the coupling between rays and cells include implementations using fat rays [Kak, 1984].

5.2.1 Fat rays

The fact that ray paths are stationary (*i.e.*, that small variations in the ray path have no effect on the traveltime to first order) means that each ray actually has a bundle of rays associated with it, all with virtually the same traveltime. We can improve the coupling between the rays and cells in the model by taking advantage of this fact. One possible approach is to use more than one ray between each source and receiver pair: for example, during the computation of the ray paths, we could save not only the ray we found with the least traveltime, but also save several other trial rays that were close to the best one. Then, in place of the single row of the ray-path matrix for the ith ray, we now insert multiple rows

$$\mathbf{M}_i = \begin{pmatrix} l_{11} & l_{12} & \cdots & l_{1n} \\ l_{21} & l_{22} & \cdots & l_{2n} \\ \vdots & \vdots & \ddots & \vdots \\ l_{\mu 1} & l_{\mu 2} & \cdots & l_{\mu n} \end{pmatrix}, \tag{187}$$

where μ is the multiplicity of the the ith ray path. This approach is relatively easy to implement either for bending methods or for shooting methods of ray tracing, and has the effect of multiplying the size of the data set by the number of rays (μ) saved per source/receiver pair. The disadvantage of using multiple ray paths per source/receiver pair is that the data storage problem also gets multiplied by the number of rays saved per pair.

Fat rays are an alternative method using the same underlying physics without increasing the size of our matrices. In this approach, we treat each ray as if it has a finite thickness. Then, instead of measuring the linear increment of the ray that has passed through a cell, in 2-D the ray now has an area associated with it and we measure the overlap of the ray area with the cell area. In three dimensions, these areas all become volumes. If the ray width in 2-D is Δw and the ray cross section in 3-D has area Δa, then the ray-path matrix becomes

$$\mathbf{M} = \frac{1}{\Delta w} \begin{pmatrix} a_{11} & a_{12} & \cdots & a_{1n} \\ a_{21} & a_{22} & \cdots & a_{2n} \\ \vdots & \vdots & \ddots & \vdots \\ a_{m1} & a_{m2} & \cdots & a_{mn} \end{pmatrix}, \tag{188}$$

with the a_{ij}s being overlap areas in two dimensions and

$$\mathbf{M} = \frac{1}{\Delta a} \begin{pmatrix} v_{11} & v_{12} & \cdots & v_{1n} \\ v_{21} & v_{22} & \cdots & v_{2n} \\ \vdots & \vdots & \ddots & \vdots \\ v_{m1} & v_{m2} & \cdots & v_{mn} \end{pmatrix}, \tag{189}$$

with the v_{ij}s being overlap volumes in three dimensions. For traveltime tomography, it is still important that the sums of the rows of $\mathbf{M}$ result in sensible ray path lengths, otherwise the reconstructed slowness values will not be meaningful. The disadvantage of the method just outlined is that the overlap areas and volumes are often tedious to compute.

Another method that has the advantages of both of the previous methods is first to obtain the set of near-ray-path lengths shown in (187) and then average them according to

$$\bar{l}_{ij} = \frac{1}{\mu} \sum_{i'=1}^{\mu} l_{i'j}. \tag{190}$$

With this approach, we end up with a single effective ray path and so do not increase the ray storage problem, but we have the advantage that the individual contributions $l_{i'j}$ leading to $\bar{l}_{ij}$ through (190) are comparatively easy to compute. The resulting ray-path matrix is

$$\mathbf{M} = \begin{pmatrix} \bar{l}_{11} & \bar{l}_{12} & \cdots & \bar{l}_{1n} \\ \bar{l}_{21} & \bar{l}_{22} & \cdots & \bar{l}_{2n} \\ \vdots & \vdots & \ddots & \vdots \\ \bar{l}_{m1} & \bar{l}_{m2} & \cdots & \bar{l}_{mn} \end{pmatrix}. \tag{191}$$

It is clear that fat rays will accomplish the goal of improving the coupling between the rays and cells. The matrices in (188) and (189) will certainly be significantly less sparse than the the usual $\mathbf{M}$ based on skinny rays. Whether this change will be sufficient to make a significant improvement in the reconstructions will, of course, depend on the particular application. In general, fat rays should be used in addition to (not instead of) the other methods of ghostbusting described in this section.

5.2.2 Summary

Methods of eliminating ghosts can be divided into two main categories: (*i*) experimental design and (*ii*) model design together with analytical tricks.

No amount of analysis can salvage a badly designed experiment. When designing a tomographic experiment, it is important to gather data from as many view angles as possible. It is also important to gather enough data so that the cells we can resolve from our data analysis are about the same size as the anomalies we want to detect. A rule of thumb is that the number of source/receiver pairs should be about *twice* the number of cells we want to resolve in our experiment. Another useful rule of thumb is to choose the average cell size to be about $3\lambda_{\max}$, where $\lambda_{\max} = 1/f_{\min} s_{\min}$ is the maximum expected wavelength associated with the minimum frequency $f_{\min}$ in the pulse propagation data and the minimum slowness $s_{\min}$ expected in the region to be imaged. This rule arises from extensive experience with the asymptotic analysis of wave propagation which we will not present here.

The analyst must design the model to take optimum advantage of the data gathered, while accounting for any prior knowledge of the medium to be imaged. The shapes and sizes of the model cells are ours to choose, and should be used to advantage to solve any problems that cannot be solved by good experimental design. We are always free to choose cells larger than the expected resolution of the traveltime data. We may eliminate some cells if they have poor ray coverage, or some contiguous cells with poor coverage may be combined into a single cell for purposes of reconstruction. Cells can be of any shape we choose; the choice of square or rectangular cells is often made for ease of display and for ease of computation of ray paths, but other considerations may drive us to use odd shapes for cells in some applications. Analytical tricks can be applied during the reconstruction process once we have the data at home. Smoothing and clipping the slowness model values can be done to force the reconstructed values to lie within reasonable limits. Fat rays are a last resort if the other methods are not sufficient to eliminate the ghosts.

5.3 Significance of Ghosts

It is important to recognize that elimination of all ghosts may be neither possible nor desirable. In our efforts to solve the inverse problem

$$\mathbf{Ms} = \mathbf{t} \tag{192}$$

for the slowness model $\mathbf{s}$, we should keep in mind that there are really three stages in the inversion process. The first stage is to find, if possible, a particular model $\mathbf{s}$ that satisfies the data. The second stage is to analyze the null space of the operator $\mathbf{M}$. We may use standard numerical techniques at this point in the analysis to perform the singular value decomposition of $\mathbf{M}$ and obtain a complete characterization of the null space. Having completed both of these steps, we can finally provide the complete solution to the inversion problem. In fact, it may be that we need perturbations from the null space to satisfy various physical or geological boundary conditions present at the site where the tomographic data were gathered. This process is completely analogous to the process of solving an ordinary differential equation by finding a particular solution, computing a set of homogeneous solutions, and finally producing a linear combination that satisfies the initial conditions.

6 Fast Ray Tracing Methods

The most expensive step in any traveltime inversion or tomography algorithm is the forward modeling step associated with ray tracing through the current best estimate of the wave speed model. It is therefore essential to make a good choice of ray tracing algorithm for the particular application under consideration. Prior to choosing a ray tracing method, a method of representing the model must be chosen. Three typical choices are: cells or blocks of constant slowness, a rectangular grid with slowness values assigned to the grid points and linearly interpolated values between grid points, or a sum over a set of basis functions whose coefficients then determine the model. The ray tracing method should be designed to produce optimum results for the particular model representation chosen.

We will consider three approaches to ray tracing:

1. Shooting methods.

2. Bending methods.

3. Full wave equation methods.

These three methods are based respectively on Snell's law, Fermat's principle, and Huygen's principle. We will find that shooting methods and wave equation methods should generally be used with smooth representations of the model such as linearly interpolated grids or spline function approximations, while bending methods are preferred for constant cell representations.

We will study each of these approaches in some detail in this lecture. But first we will try to answer a question that is commonly asked about the necessity of using bent rays in tomography.

6.1 Why Not Straight Rays?

Straight rays are used in x-ray tomography and the results obtained are very good, so why not use straight rays in seismic tomography? For x-rays traveling through the body, the index of refraction is essentially constant, so the ray paths are in fact nearly straight. Furthermore, the reconstruction in x-ray tomography is performed on the attenuation coefficient, not the wave speed, so the situation is not really comparable to that of seismic tomography. Reconstructions in seismic inversion and tomography are most often performed on the wave speed or wave slowness. Since the earth is not homogeneous, the speed of sound varies significantly and the effective index of refraction is far from being constant. Thus, the rays of seismic tomography really do bend significantly and this fact should be taken into account in the reconstruction.

Suppose that we use straight rays in our tomographic reconstruction when in truth the rays whose traveltimes have been measured were actually bent according to Fermat's principle or Snell's law. In a region where the wave speed is quite low, the true rays will tend to go around the region, but the straight rays go through anyway. So the backprojection along a straight ray will naturally focus the effects of a slow region into a *smaller region* than it should. Similarly, in a region where the wave speed is quite high, the true rays will tend to accumulate in the fast region, whereas the straight rays are completely resistant to this focusing effect. Thus, the backprojection along a straight ray will tend to defocus the effects of a fast region into a *larger region* than it should. If we could train our eyes to look for these effects in straight ray reconstructions, then it might not be essential to use bent rays. But until then, it is important to recognize that using straight rays has important effects on the resolution of the reconstruction. Regions of high wave speed will appear larger than true, so such regions are poorly resolved. Regions of low wave speed will appear smaller than true, so such regions are poorly defined.

Having said all this, nevertheless there are circumstances where I would recommend using straight rays in the reconstruction. First, if the region to be imaged contains very high contrasts so that some of the assumptions normally made to speed up the ray tracing codes are expected to be violated (*e.g.*, rays double back on themselves), then stable reconstructions with bent rays may be impossible while a straight ray reconstruction can still

give some useful information. Second, if the desired result is just a low resolution image showing whether or not an anomaly is present, then straight rays are entirely appropriate. Third, if a reconstruction for anisotropic wave speed is being attempted, then straight rays are recommended too, since the nonuniqueness expected in the reconstruction when bent rays are coupled with anisotropy in the model is so overwhelming that I think little can be done to overcome the problem at the present time.

Straight rays are always the fastest to compute since they depend only on the source and receiver locations. So if resolution is not an issue but speed of computation is, then of course straight rays can and probably should be used. However, using straight rays is limiting the reconstruction to be merely *linear tomography* and since *nonlinear tomography* is the subject of these lectures, we will not consider straight rays further.

6.2 The Ray Equations and Shooting Methods

Let the ray path P between two points A and B be represented by a trajectory $\vec{x}(u)$, where u is a scalar parameter that increases monotonically along the ray. We can then write the traveltime along the path as

$$t = \int_P s(\vec{x}(u))\, dl(u) \tag{193}$$

$$= \int_{u(A)}^{u(B)} f(\vec{x}, \dot{\vec{x}})\, du, \tag{194}$$

where $\dot{\vec{x}} = d\vec{x}/du$ and

$$f(\vec{x}, \dot{\vec{x}}) = s(\vec{x})|\dot{\vec{x}}|. \tag{195}$$

Fermat's principle implies that the stationary variation [Whitham, 1974]

$$\delta t = \int_{u(A)}^{u(B)} [\nabla_{\vec{x}} f \cdot \delta\vec{x} + \nabla_{\dot{\vec{x}}} f \cdot \delta\dot{\vec{x}}]\, du = 0. \tag{196}$$

Integrating by parts

$$\delta t = \int_{u(A)}^{u(B)} \left[\nabla_{\vec{x}} f - \frac{d}{du}\nabla_{\dot{\vec{x}}} f\right] \cdot \delta\vec{x} du = 0. \tag{197}$$

Since this must be true for all $\delta\vec{x}$, we can infer

$$\nabla_{\vec{x}} f - \frac{d}{du}\nabla_{\dot{\vec{x}}} f = 0. \tag{198}$$

Now we observe that

$$\nabla_{\vec{x}} f = |\dot{\vec{x}}|\nabla s, \tag{199}$$

$$\nabla_{\dot{\vec{x}}} f = s(\vec{x})\frac{\dot{\vec{x}}}{|\dot{\vec{x}}|}. \tag{200}$$

Further, we have that $dl = |\dot{\vec{x}}|du$, so stationarity of t implies

$$\nabla s = \frac{d}{dl}\left(s\frac{d}{dl}\vec{x}\right). \tag{201}$$

This is the *ray equation.*

In a 2-D application, we can rewrite the ray equation in terms of the angle θ of the ray from the x direction. First, note that

$$\frac{d}{dl}\vec{x} = \hat{\rho} = \cos\theta\hat{\mathbf{x}} + \sin\theta\hat{\mathbf{y}} \tag{202}$$

and

$$\frac{d}{dl}\hat{\rho} = \hat{\theta}\frac{d\theta}{dl} = (-\sin\theta\hat{\mathbf{x}} + \cos\theta\hat{\mathbf{y}})\frac{d\theta}{dl}, \tag{203}$$

so that

$$\nabla s = \frac{ds}{dl}\hat{\rho} + s\hat{\theta}\frac{d\theta}{dl}, \tag{204}$$

which implies

$$\hat{\theta}\cdot\nabla s = s\frac{d\theta}{dl}. \tag{205}$$

Finally, we get

$$\frac{d\theta}{dl} = \frac{1}{s}\left(\frac{\partial s}{\partial y}\cos\theta - \frac{\partial s}{\partial x}\sin\theta\right). \tag{206}$$

The ray equations form the basis for shooting methods of ray tracing. Starting at any source point, we initially choose a set of possible angles. An optimum initial span of angles can be determined if the range of wave-speed variation is known approximately. Then, we use the ray equations to trace the rays at each of these angles through the medium to the vicinity of the receiver of interest. Normally none of the initial angles turns out to be the correct one (*i.e.*, the one that produces a ray that hits the receiver), but often the receiver is bracketed by two of these rays. Then, by interpolation, we can find as accurate an approximation as we like: *i.e.*, choose a new set of angles between the pair that brackets the receiver, trace the rays for these angles, keep the two closest that bracket the receiver, and continue this process until some closeness objective has been achieved.

Shooting methods are very accurate, but also relatively expensive. We may have to shoot many rays to achieve the desired degree of accuracy. Furthermore, there can be pathological cases arising in inversion and tomography where it is difficult or impossible to trace a ray from the the source to receiver through the current best estimate of the slowness model. Such problems are most likely to occur for models containing regions with high contrasts. Then, there can exist shadow zones behind slow regions, where ray amplitude is small for first arrivals. Such problems can also arise due to poor choice of modelization. Shooting methods should normally be used with smooth models based on bilinear interpolation between grid points, or spline function approximations. If the desired modelization uses cells of constant slowness, shooting methods are not recommended.

6.3 The Eikonal Equation

Consider the wave equation for a field $\psi(\vec{x},t)$ in a medium with slowness $s(\vec{x})$:

$$\nabla^2\psi = s^2\frac{\partial^2\psi}{\partial t^2}. \tag{207}$$

Let us assume

$$\psi(\vec{x},t) = e^{i\omega(\phi(\vec{x})-t)}, \tag{208}$$

where $\phi(\vec{x})$ is a complex phase, the imaginary part of which determines the amplitude of ψ. Substituting into the wave equation, we get

$$(i\omega\nabla^2\phi - \omega^2\nabla\phi\cdot\nabla\phi + \omega^2 s^2)\psi = 0. \tag{209}$$

In the limit $\omega\to\infty$, ϕ becomes real, since (209) implies that[10]

$$\nabla\Re\phi\cdot\nabla\Re\phi - \nabla\Im\phi\cdot\nabla\Im\phi = s^2 \tag{210}$$

and

$$\nabla\Re\phi\cdot\nabla\Im\phi = 0, \tag{211}$$

and the wave equation reduces to the *eikonal equation*

$$|\nabla\phi| = s. \tag{212}$$

6.4 Vidale's Method

The method of Vidale (1988) uses a finite difference scheme to compute the traveltimes of waves in an arbitrary medium. The slowness of the medium is represented on the nodes of a rectilinear grid with bilinear (for 2-D media) interpolation assumed between nodes. The method approximates the wave field which propagates through a given element as a plane wave. This approximation is valid for the far field. (A different approach is used for the near field, but we will not cover this here.)

6.4.1 Algebraic derivation

Figure 6 shows one element of the grid. We number the nodes of the element in a counterclockwise manner, starting with the lower left node. Without loss of generality, we let the plane wave begin at node 0 with traveltime t_0, assumed known. The traveltime to the other nodes—t_1, t_2 and t_3—will then be greater than t_0 by an amount which depends on the direction of propagation and the grid element size h. In general we can write the Taylor series expansion

$$t_1 = t_0 + \frac{\partial t}{\partial x}h, \tag{213}$$

$$t_2 = t_0 + \frac{\partial t}{\partial y}h, \tag{214}$$

$$t_3 = t_0 + \left(\frac{\partial t}{\partial x} + \frac{\partial t}{\partial y}\right)h, \tag{215}$$

[10] $\Re\phi$ is the real part of ϕ, and $\Im\phi$ is the imaginary part of ϕ.

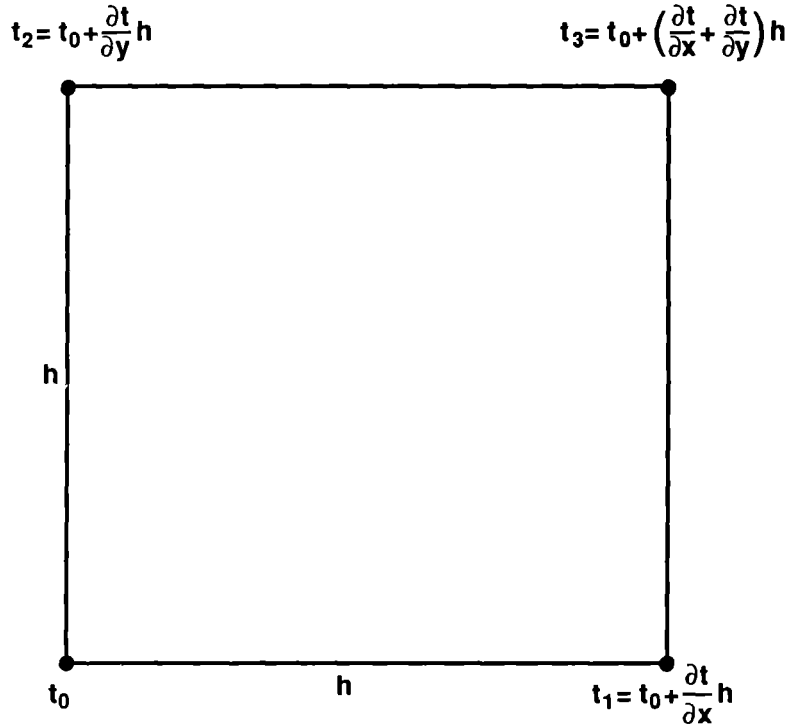

Figure 6: Diagram of a grid element used in Vidale's method.

valid to first order in h. We can solve these equations for the gradient of t, obtaining

$$2h\frac{\partial t}{\partial x} = t_3 + t_1 - t_2 - t_0, \tag{216}$$

$$2h\frac{\partial t}{\partial y} = t_3 + t_2 - t_1 - t_0. \tag{217}$$

The eikonal equation implies that $|\nabla t|^2 = s^2$. If we substitute from (216) and (217) for ∇t and an element average value of s, we get

$$(t_3 + t_1 - t_2 - t_0)^2 + (t_3 + t_2 - t_1 - t_0)^2 = 4\bar{s}^2 h^2, \tag{218}$$

where

$$\bar{s} = \frac{1}{4}(s_0 + s_1 + s_2 + s_3). \tag{219}$$

From (218), we find that the cross terms cancel so

$$(t_3 - t_0)^2 + (t_1 - t_2)^2 = 2\bar{s}^2 h^2. \tag{220}$$

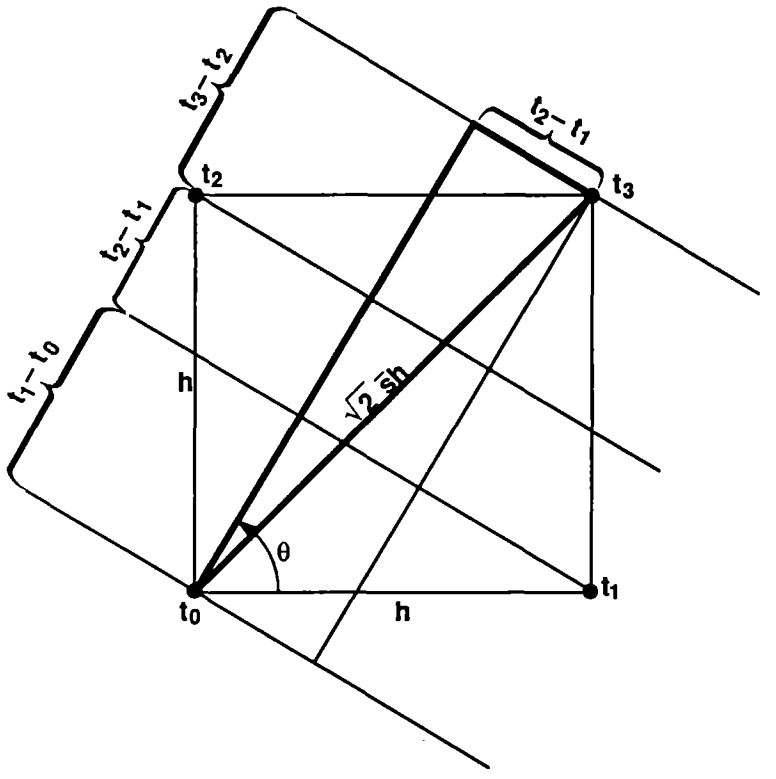

Figure 7: Geometry of plane wavefront incident on a grid element.

Solving for t_3, we get *Vidale's formula:*

$$t_3 = t_0 + \sqrt{2\bar{s}^2h^2 - (t_1 - t_2)^2}. \tag{221}$$

We can verify (221) for two limiting cases. First, for a wave traveling in the $+x$ direction, we must have $t_0 = t_2$ and, assuming s is constant, $t_1 = t_0 + \bar{s}h$. Substituting these into (221) then yields $t_3 = t_0 + \bar{s}h$, which is intuitively the correct answer. Similarly, Vidale's formula implies $t_3 = t_0 + \sqrt{2}\bar{s}h$ for a wave travel at 45 degrees to x, i.e., when $t_1 = t_2$.

6.4.2 Geometric derivation

We can gain more insight into the significance of Vidale's method by deriving the result another way. Now consider Fig. 7. We assume that to a first approximation it is satisfactory to treat the slowness in the cell as constant. The constant we choose is the average of the four grid slownesses at the corners of the cell $\bar{s} = 0.25(s_1 + s_2 + s_3 + s_4)$. If the planewave impinges on the cell from the lower left, making angle θ with the x-axis, then the simple geometrical construction in the figure shows that the following identities must hold:

$$t_1 - t_0 = \bar{s}h\cos\theta, \tag{222}$$

$$t_3 - t_2 = \bar{s}h\cos\theta, \tag{223}$$

$$t_2 - t_0 = \bar{s}h\sin\theta, \tag{224}$$

$$t_3 - t_1 = \bar{s}h\sin\theta. \tag{225}$$

We see directly from Fig. 7 that the right triangle whose hypotenuse is the diagonal of the cell and whose longest side is proportional to the time difference $t_3 - t_0$ has its short side proportional to $t_2 - t_1$. The Pythagorean theorem then tells us that

$$(t_3 - t_0)^2 + (t_2 - t_1)^2 = 2\bar{s}^2h^2, \tag{226}$$

in agreement with (220) and (221). Alternatively, we see that (222)–(225) show

$$(t_3 - t_0)^2 + (t_2 - t_1)^2 = \bar{s}^2h^2(\cos\theta + \sin\theta)^2 + \bar{s}^2h^2(\sin\theta - \cos\theta)^2 = 2\bar{s}^2h^2. \tag{227}$$

From our examination of the geometry for planewaves, we get a bonus. Now we can also find a simple estimate of the angle θ if we know the traveltimes. Clearly,

$$\tan\theta = \frac{t_2 - t_0}{t_1 - t_0} = \frac{t_3 - t_1}{t_3 - t_2} \tag{228}$$

follows from (222)–(225). It also follows from (216) and (217) that

$$\tan\theta = \frac{\partial t/\partial y}{\partial t/\partial x} = \frac{t_3 + t_2 - t_1 - t_0}{t_3 + t_1 - t_2 - t_0}, \tag{229}$$

a result that we may also infer from (222)–(225). Thus, it is possible to determine the angle θ to first order just by knowing the traveltimes at the corners of the cell. This fact suggests several alternatives for adding ray tracing to Vidale's finite difference traveltime computation, but we will not pursue that subject here.

Finally, note that (222)-(225) show that

$$t_3 = t_2 + t_1 - t_0. \tag{230}$$

Why is this *not* a useful identity for computing the traveltimes?

6.5 Bending Methods

Although in principle they can be, in practice bending methods are generally not as systematic or as accurate as shooting methods. However, they are also much less prone to convergence failures in the presence of pathological models with high relative contrasts (which can result in shadow zones occurring behind very slow regions). Bending methods start with some connected path between the source and receiver (generally a straight line for borehole-to-borehole tomography) and then use some method to reshape or bend that path to reduce and (we hope) minimize the overall traveltime along the path. Bending methods are conceptually based on Fermat's principle of least time; the minimization over paths in

(2) is being performed now essentially using trial and error. This method is just as legitimate as the others discussed previously and can be just as accurate if the search routine is sufficiently sophisticated. Also, bending methods are the only ones that I recommend using when the model is composed of cells of constant slowness. Other methods such as shooting take the cell boundaries in these models too seriously — trying to satisfy Snell's law exactly at these artificial boundaries while the approximate satisfaction of Snell's law achieved by the bending method using Fermat's principle is more consistent with the approximation to the physics embodied in the model.

6.5.1 The method of Prothero *et al.*

We will summarize the bending method of Prothero *et al.* (1988) for the case of 2-D ray paths.

Let (x_S, y_S) and (x_R, y_R) be the given endpoints of the ray. We seek the least time path between the two points, which we can describe with the function $y(x)$ or $x(y)$. (It is assumed that one of these functions is single valued.) Let us use $y(x)$ and, with no loss of generality, we take $x_S = 0$, $x_R = L$.

In ray bending, we begin with an initial ray $y_0(x)$ and seek a perturbation $\delta y(x)$ to the initial ray such that the traveltime along the perturbed ray is reduced. Typically the initial ray is taken to be a straight line:

$$y_0(x) = y_S(1 - \frac{x}{L}) + y_R\frac{x}{L}. \tag{231}$$

The perturbed ray is taken to be a harmonic series of the form

$$\delta y(x) = \sum_{k=1}^{K} a_k \sin\frac{k\pi x}{L}. \tag{232}$$

The order of the series is usually kept small (e.g., $K = 2$). Note that only sine, and not cosine, terms are used so that the endpoints of the ray remain unperturbed.

In terms of the $y(x)$, the traveltime is given by

$$t = \int_0^L s(x, y(x))\sqrt{1 + (dy/dx)^2}\, dx. \tag{233}$$

Prothero *et al.* (1988) use the Nelder-Mead search procedure to find coefficients a_k such that the traveltime is reduced. The Nelder-Mead approach may be used in any number of dimensions to seek the minimum of a complicated function, especially when local gradients of the function are difficult or expensive to compute. The main idea is to perform a sequence of operations on an n-dimensional simplex, so that the vertices of the simplex converge on the point where the function is minimum. In 2-D, the simplex is a triangle. The complicated function to be minimized in our problem is the traveltime functional. Using this approach, the traveltimes associated with three choices of the ordered pairs (a_1, a_2) are compared—for example, the origin $(0, 0)$ and two other points in the a_1a_2-plane. The point with the largest traveltime is then replaced with a new point found as the mirror reflection of the point about a line passing through the other two points.

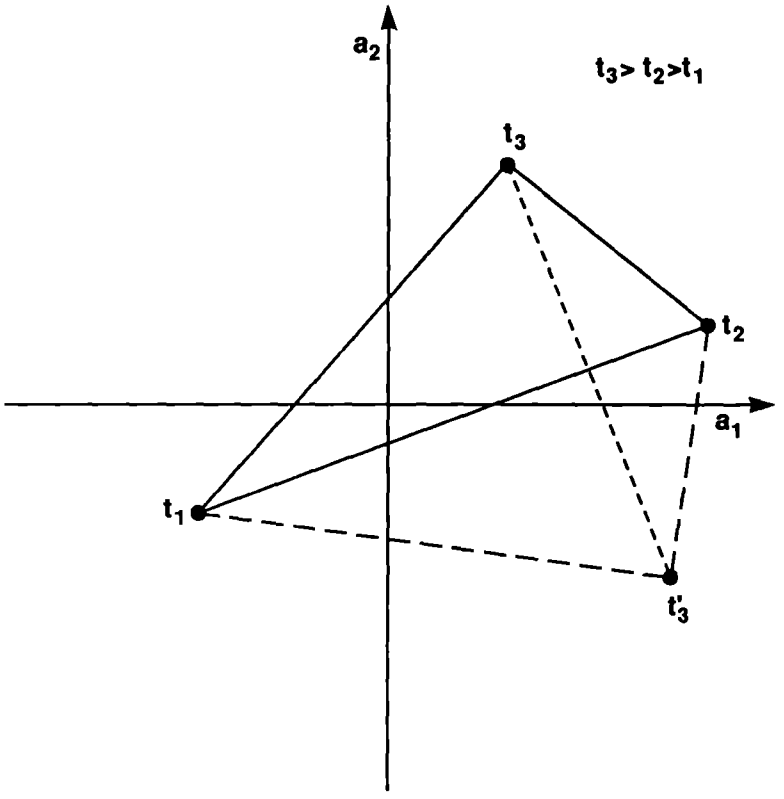

Figure 8: Illustration of the Nelder-Mead method.

Figure 8 illustrates the method. Starting with three points whose corresponding traveltimes are respectively $t_1 < t_2 < t_3$, the algorithm seeks to replace the point with the largest traveltime by a smaller traveltime t_3'. The figure shows the first attempt in such a process, which is usually reflection of the triangle across the line determined by the other two vertices of the triangle. If the traveltime associated with this point satisfies $t_3' < t_2$, then this point becomes a point of the new triangle. If $t_3' > t_2$, then other moves are made such as checking values between the original vertex and the reflected vertex or expansion/contraction of the triangle. When an improved (smaller traveltime) vertex is found, the vertices are relabelled and the process starts over for the new triangle. If no improvement (or improvement less than some preset threshold) is attained or some fixed number of iterations is exceeded, the process terminates for this ray path.

6.5.2 Getting started

One potential pitfall of this method occurs when attempting to choose a set of vertices for the starting triangle that avoids biasing the final results. Bias in this context means a tendency to choose rays that bow away from the straight path in the same direction. I

recommend always choosing the origin $(a_1, a_2) = (0,0)$ as one of the initial vertices, since this choice corresponds to a straight ray path and is clearly unbiased by definition. The straight path may be a good approximation to the true path whenever the wave speed constrasts in the model are low. Then, how should the other two vertices be chosen?

One rather obvious pairing can be excluded immediately: Suppose that we choose the point $(a_1, a_2) = (\alpha, \beta)$. Then the mirror image of the path across the source/receiver line is given by the point $(a_1, a_2) = (-\alpha, -\beta)$. However, rather than determining a triangle, these three points $(-\alpha, -\beta), (0,0), (\alpha, \beta)$ form a straight line in the $a_1 a_2$-plane. Thus, although pairing (α, β) with $(-\alpha, -\beta)$ is desirable from the point of view of minimizing bias, this pairing produces an undesirable degenerate version of the triangle needed in the Nelder-Mead algorithm. Therefore, we should exclude this possibility.

In general, we should expect the ray bending effect to be dominated by the coefficient a_1. Thus, although there clearly may be exceptions, we generally expect $|a_1| > |a_2|$ and very often $|a_1| >> |a_2|$. So we try to minimize the bias in the initial choice of vertices by pairing (α, β) with $(-\alpha, \beta)$, where $|\beta|$ is about an order of magnitude smaller than $|\alpha|$. This choice of pairing eliminates the major source of bias in the initial simplex while still producing a usable triangle for the Nelder-Mead algorithm. The precise value to be used for α depends on the expected range of variation (or contrast) in the wave speed in the region being imaged. In fact, the initial choice of α for this approach is closely related to the optimum choice of the maximum initial span of angles needed to start the shooting methods described earlier.

6.6 Comparison

On average, the method of Prothero *et al.* (1988) has been found to be as fast and as accurate as Vidale's method when 100 times fewer cells are used than in Vidale's modelization. So the bending method is considerably more accurate on a coarser grid, but also corresponding slower to compute. Vidale's method is not as accurate as the bending method for regions that are very slow compared to the background, due to limitations it has in or near shadow zones. The bending method is not quite as accurate as Vidale's method for regions of high wave speed relative to background and comparable computing time, apparently due to limitations of the ray parameterization embodied in (232). The hybrid approach of using the best (smallest) traveltimes found by either method as the "true" traveltime has been tested and gives better results than either method alone.

7 Nonlinear Seismic Tomography

The introduction of feasibility constraints into the traveltime tomography problem offers a unique opportunity to develop a variety of new reconstruction algorithms. A few of the ones that have been explored so far will be discussed here.

7.1 Linear and Nonlinear Programming

Linear tomography maps itself quite easily into linear programming, and nonlinear tomography into nonlinear programming [Strang, 1986; Fiacco and McCormick, 1990].

Recall that, if $\mathbf{u}^T = (1, \ldots, 1)$ is an m-vector of ones and $\mathbf{v}^T = (1, \ldots, 1)$ is an n-vector of ones, then

$$\mathbf{u}^T\mathbf{M} = \mathbf{v}^T\mathbf{C}, \tag{234}$$

where $\mathbf{C}$ is the coverage *matrix*, *i.e.*, the diagonal matrix whose diagonal elements are the column sums of the ray-path matrix. We will now define the coverage *vector* as

$$\mathbf{c} = \mathbf{C}\mathbf{v}. \tag{235}$$

7.1.1 Duality

The concept of duality in linear programming leads to some useful ideas both for linear and nonlinear traveltime tomography. (Actually it is even more useful for electrical impedance tomography as we will see later.) We will first define the following:

Definition 7.1 *The primal problem for traveltime tomography is to find the minimum of* $\mathbf{c}^T\mathbf{s}$ *subject to* $\mathbf{M}\mathbf{s} \geq \mathbf{t}$ *and* $\mathbf{s} \geq 0$.

Definition 7.2 *The dual problem associated with the primal is to maximize* $\mathbf{w}^T\mathbf{t}$ *subject to* $\mathbf{w}^T\mathbf{M} \leq \mathbf{c}^T$ *and* $\mathbf{w} \geq 0$.

The m-vector $\mathbf{w}$ has no physical significance, but plays the role of a nonnegative weight vector. One of the first consequences of this formulation is that, if we multiply the primal inequality on the right by $\mathbf{w}^T$ and the dual inequality on the left by $\mathbf{s}$ for feasible $\mathbf{s}$ and $\mathbf{w}$, then

$$\mathbf{c}^T\mathbf{s} \geq \mathbf{w}^T\mathbf{M}\mathbf{s} \geq \mathbf{w}^T\mathbf{t}. \tag{236}$$

We introduce a Lagrangian functional

$$\mathcal{L}(\mathbf{s}, \mathbf{w}) = \mathbf{c}^T\mathbf{s} + \mathbf{w}^T(\mathbf{t} - \mathbf{M}\mathbf{s}) \tag{237}$$

$$= (\mathbf{c}^T - \mathbf{w}^T\mathbf{M})\mathbf{s} + \mathbf{w}^T\mathbf{t}. \tag{238}$$

An admissible (feasible) weight vector is $\mathbf{w} = \mathbf{u}$. In fact, this is the only weight vector we need to consider because it saturates the dual inequality, producing equality in all components following (234) and (235). Thus, the dual problem in traveltime tomography is really trivial. We introduced it here because, despite its apparent triviality, there is one interesting feature.

In problems with nontrivial duality structure, it is possible to obtain interesting (nontrivial) bounds using the inequalities equivalent to (236). Here we are left with only the condition

$$\mathbf{c}^T\mathbf{s} \geq \mathbf{u}^T\mathbf{t} = T, \tag{239}$$

which we could have derived directly from the feasibility conditions $\mathbf{M}\mathbf{s} \geq \mathbf{t}$ for $\mathbf{s}$. Equation (239) is not trivial however, and can play an important role in linear and nonlinear programming algorithms for traveltime tomography.

7.1.2 Relaxed feasibility constraints

Given the set of observed traveltimes, t_i for $i = 1, \ldots, m$, we define two more types of feasibility sets.

Definition 7.3 (relaxed local feasibility set) *The relaxed local feasibility set with respect to a set of trial ray paths $\mathcal{P} = \{P_1, \ldots, P_m\}$ and observed traveltimes $t_1, \ldots, t_m$ is*

$$\mathcal{R}^{\mathcal{P}} = \{\mathbf{s} \mid \sum_{i=1}^{m} \tau_i^{P}(\mathbf{s}) \geq \sum_{i=1}^{m} t_i\}. \tag{240}$$

Definition 7.4 (relaxed global feasibility set) *The relaxed global feasibility set with respect to a set of observed traveltimes $t_1, \ldots, t_m$ is*

$$\mathcal{R}^{*} = \{\mathbf{s} \mid \sum_{i=1}^{m} \tau_i^{*}(\mathbf{s}) \geq \sum_{i=1}^{m} t_i\}. \tag{241}$$

Lemma 7.1 (sum of concave functions) *A (nonnegatively) weighted sum of concave functions is concave.*

Proof. Let $\tau_i(\mathbf{s})$ for $i = 1, \ldots, m$ be a set of concave functions and let w_i be a set of nonnegative weights. Then,

$$\sum_{i=1}^{m} w_i \tau_i(\lambda \mathbf{s}_1 + (1-\lambda)\mathbf{s}_2) \geq \sum_{i=1}^{m} w_i [\lambda \tau_i(\mathbf{s}_1) + (1-\lambda)\tau_i(\mathbf{s}_2)] \tag{242}$$

$$= \lambda \sum_{i=1}^{m} w_i \tau_i(\mathbf{s}_1) + (1-\lambda) \sum_{i=1}^{m} w_i \tau_i(\mathbf{s}_2), \tag{243}$$

so the weighted sum is concave. ∎

Theorem 7.1 *$\mathcal{R}^{\mathcal{P}}$ is a convex set.*

Theorem 7.2 *$\mathcal{R}^{*}$ is a convex set.*

Proof. Both theorems follow from the lemma and the fact that the unit-weighted sums in the definitions of the sets $\mathcal{R}^{\mathcal{P}}$ and $\mathcal{R}^{*}$ are respectively sums of the concave functions $\tau_i^{P}(\mathbf{s})$ and $\tau_i^{*}(\mathbf{s})$. ∎

Theorem 7.3 *Any point $\mathbf{s}^{*}$ that lies simultaneously on the boundary of both $\mathcal{F}^{\mathcal{P}}$ and $\mathcal{R}^{\mathcal{P}}$ solves the inversion problem.*

Theorem 7.4 *Any point $\mathbf{s}^{*}$ that lies simultaneously on the boundary of both $\mathcal{F}^{*}$ and $\mathcal{R}^{*}$ solves the inversion problem.*

Proof. The boundary of $\mathcal{R}^P$ is determined by the single equality constraint

$$\sum_{i=1}^{m} \tau_i^P(\mathbf{s}) = \sum_{i=1}^{m} t_i = T. \tag{244}$$

The boundary of $\mathcal{F}^P$ is determined by the set of inequality constraints

$$\tau_i^P(\mathbf{s}) \geq t_i, \quad \text{for all} \quad i = 1, \ldots, m, \tag{245}$$

with equality holding for at least one of the constraints. Summing (245) gives

$$\sum_{i=1}^{m} \tau_i^P(\mathbf{s}) \geq T, \tag{246}$$

where the equality applies if and only if $\tau_i^P(\mathbf{s}) = t_i$ for all i. Therefore, any model $\mathbf{s}^*$ that satisfies both (244) and (245) must solve the inversion problem.

The proof of the second theorem follows the proof of the first, with $\tau^*(\mathbf{s})$ replacing $\tau^P(\mathbf{s})$ everywhere. ∎

If we have found the correct ray-path matrix for the inversion problem and the data are noise free, then we expect that the hyperplane defined by $\mathbf{c}^T\mathbf{s} = T$ will intersect the feasibility boundary exactly at the point or points that solve the inversion problem. If we have not found the correct ray-path matrix or there is uncorrelated noise in our data $\mathbf{t}$, then there will be a *splitting* between the hyperplane of constant total traveltime and the feasible region. The point (or points) of closest approach between the convex feasible set and the hyperplane may then be defined as the set of points *solving* the the linear programming problem for fixed $\mathbf{M}$. An iterative nonlinear programming algorithm may then be constructed wherein the updated $\mathbf{M}$ is determined based on the solution of the last linear programming problem. This procedure converges if the degree of splitting (Euclidean distance) between the feasible set and the hyperplane of constant traveltime tends to zero from one iteration to the next.

7.2 More about Weighted Least-Squares

We learned in previous lectures that a good set of weights to use for weighted least-squares was $\mathbf{L}^{-1}$ for the traveltime errors and $\mathbf{C}$ for the smoothing or regularization term in a damped least-squares method. The arguments were based on assumptions of small deviations from a constant background or on the desire to precondition the ray-path matrix so its eigenvalues were normalized to the range $-1 \leq \lambda \leq 1$.

In a sense the methods used to choose weights previously were based on *linear tomography* ideas. We should now try to see if these ideas need to be modified for *nonlinear tomography*. Let $\mathbf{s}$ be the latest estimate of the slowness model vector in an iterative inversion scheme. Then, if $\mathbf{u}^T = (1, \ldots, 1)$ is an m-vector of ones and $\mathbf{v}^T = (1, \ldots, 1)$ is an n-vector of ones,

$$\mathbf{M}\mathbf{s} = \mathbf{T}\mathbf{u}, \tag{247}$$

$$\mathbf{M}^T\mathbf{u} = \mathbf{C}\mathbf{v} \equiv \mathbf{D}\mathbf{s}, \tag{248}$$

where $\mathbf{C}$ is the coverage matrix (diagonal matrix containing the column sums of $\mathbf{M}$) defined previously and the two new matrices ($\mathbf{T}$ and $\mathbf{D}$) are diagonal matrices whose diagonal elements are T_{ii}, the estimated traveltime for the ith ray path through the model $\mathbf{s}$,

$$T_{ii} = \sum_{j=1}^{n} l_{ij} s_j, \tag{249}$$

and D_{jj} where

$$D_{jj} \equiv C_{jj}/s_j = \sum_{i=1}^{m} l_{ij}/s_j. \tag{250}$$

For the sake of argument, let the diagonal traveltime matrix $\mathbf{T}$ be the weight matrix now, and compute the scaled least-squares point. The least-squares functional takes the form

$$\psi(\gamma) = (\mathbf{t} - \mathbf{M}\gamma\mathbf{s})^T \mathbf{T}^{-1} (\mathbf{t} - \mathbf{M}\gamma\mathbf{s}), \tag{251}$$

which has its minimum at

$$\gamma = \frac{\mathbf{s}^T \mathbf{M}^T \mathbf{T}^{-1} \mathbf{t}}{\mathbf{s}^T \mathbf{M}^T \mathbf{T}^{-1} \mathbf{M}\mathbf{s}}. \tag{252}$$

Equation (252) can be rewritten using (247) as

$$\gamma = \frac{\mathbf{u}^T \mathbf{t}}{\mathbf{u}^T \mathbf{T}\mathbf{u}}. \tag{253}$$

The factor γ that minimizes the least-squares error is therefore the one that either increases or decreases the total traveltime of the model $\mathbf{s}$ so it equals that of the data. If we assume that the measurement errors in the traveltime data $\mathbf{t}$ are unbiased, then it is very reasonable to choose models that have this property, because the total traveltime $\mathbf{u}^T\mathbf{t} = T$ will tend to have smaller error (by a factor of $m^{-\frac{1}{2}}$) than the individual measurements.

We see that requiring the models $\mathbf{s}$ to have the same total traveltime as the data is equivalent to requiring that the models all lie in the hyperplane defined by

$$\mathbf{u}^T \mathbf{M}\mathbf{s} = \mathbf{v}^T \mathbf{C}\mathbf{s} = \mathbf{c}^T \mathbf{s} = T. \tag{254}$$

But this is precisely the same hyperplane that arose naturally in the previous discussion of linear and nonlinear programming.

To carry this analysis one step further, now consider the weighted least-squares problem

$$\phi_\mu(\mathbf{s}) = (\mathbf{t} - \mathbf{M}\mathbf{s})^T \mathbf{T}^{-1} (\mathbf{t} - \mathbf{M}\mathbf{s}) + \mu(\mathbf{s} - \mathbf{s}_0)^T \mathbf{D}(\mathbf{s} - \mathbf{s}_0), \tag{255}$$

where we assume that the starting model $\mathbf{s}_0$ satisfies $\mathbf{c}^T\mathbf{s}_0 = T$. Then, the minimum of (255) occurs for $\mathbf{s}_\mu$ satisfying

$$(\mathbf{M}^T \mathbf{T}^{-1} \mathbf{M} + \mu\mathbf{D})(\mathbf{s}_\mu - \mathbf{s}_0) = \mathbf{M}^T \mathbf{T}^{-1} (\mathbf{t} - \mathbf{M}\mathbf{s}_0). \tag{256}$$

Multiplying (256) on the left by $\mathbf{s}_0^T$, we find that

$$(1+\mu)\mathbf{c}^T(\mathbf{s}_\mu - \mathbf{s}_0) = \mathbf{u}^T(\mathbf{t} - \mathbf{M}\mathbf{s}_0) = 0, \tag{257}$$

so the solution of the weighted least-squares problem (256) also has the property that its estimated total traveltime for all rays is equal to that of the data

$$\mathbf{c}^T\mathbf{s}_\mu = \mathbf{c}^T\mathbf{s}_0 = T. \tag{258}$$

Our conclusion is that the particular choice of weighted least-squares problem (256) has the ***unique*** property of holding the total estimated traveltime equal to the total of the measured traveltimes, *i.e.*, it constrains the least-squares solution to lie in the hyperplane $\mathbf{c}^T\mathbf{s} = T$. Assuming that the traveltime data are themselves unbiased (*i.e.*, $\mathbf{u}^T\Delta\mathbf{t} = 0$ where $\Delta\mathbf{t}$ is the measurement error vector), the result $\mathbf{s}$ is an unbiased estimator of the slowness. Moreover, this property is maintained for ***any*** value of the damping parameter μ. This result provides a connection between the linear programming approach and weighted linear least-squares. We can now use weighted least-squares and the formula (256) in a linear program if we like as a means of moving around in the hyperplane $\mathbf{c}^T\mathbf{s} = T$.

Now from our general analysis of the eigenvalue structure of weighted least-squares, recall that (171) shows, for $\mathbf{F} = \mathbf{T}$ and $\mathbf{G} = \mathbf{D}$, that we have

$$\frac{L_{ii}C_{jj}}{T_{ii}D_{jj}} \geq \lambda^2, \tag{259}$$

which must hold true for all values of i, j. From (250), we have $C_{jj}/D_{jj} = s_j$ so

$$\frac{L_{ii}s_j}{T_{ii}} \geq \frac{L_{ii}s_{\min}}{T_{ii}} \geq \lambda^2, \tag{260}$$

and from the definition of T_{ii} we have

$$T_{ii} = \sum_{j=1}^{n} l_{ij}s_j \geq L_{ii}s_{\min}. \tag{261}$$

We conclude that this choice of weight matrices also constrains the eigenvalues to be bounded by unity $1 \geq \lambda^2$.

If the matrix $\mathbf{M}$ is very large, it may be impractical to solve (256) by inverting the matrix $(\mathbf{M}^T\mathbf{T}^{-1}\mathbf{M} + \mu\mathbf{D})$. Instead, we may choose to use some version of the method we called "simple iteration" in an earlier lecture. For example, suppose that the kth iteration yields the model vector $\mathbf{s}_\mu^{(k)}$. Then, one choice of iteration scheme for finding the next iterate is

$$\mathbf{D}\mathbf{s}_\mu^{(k+1)} = \mathbf{D}\mathbf{s}_\mu^{(k)} + \mathbf{M}^T\mathbf{T}^{-1}(\mathbf{t} - \mathbf{M}\mathbf{s}_0) - (\mathbf{M}^T\mathbf{T}^{-1}\mathbf{M} + \mu\mathbf{D})(\mathbf{s}_\mu^{(k)} - \mathbf{s}_0). \tag{262}$$

It is not hard to show that this iteration scheme converges as long as the damping parameter is chosen so that $0 < \mu < 1$. [11] Furthermore, if we multiply (262) on the left by $\mathbf{s}_0^T$, we find that

$$\mathbf{c}^T(\mathbf{s}_\mu^{(k+1)} - \mathbf{s}_\mu^{(k)}) = (1+\mu)\mathbf{c}^T(\mathbf{s}_0 - \mathbf{s}_\mu^{(k)}). \tag{263}$$

[11] The reader may want to check this using the results of this subsection and the methods developed in the lecture on simple iteration.

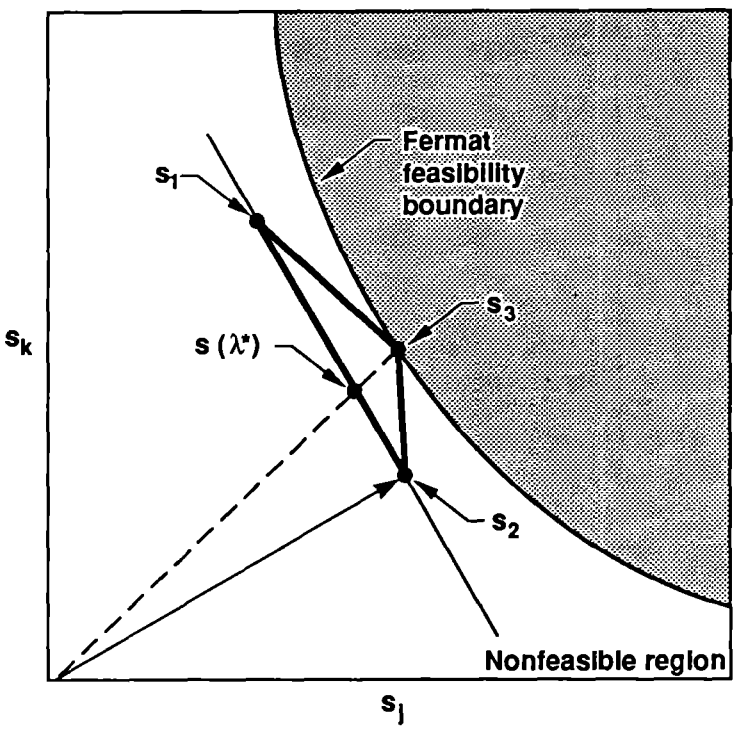

Figure 9: Snapshot of one iteration in a nonlinear tomography algorithm based on feasibility constraints.

It follows from (263) that, if $\mathbf{c}^T\mathbf{s}_0 = T$ and if $\mathbf{s}_\mu^{(0)} = \mathbf{s}_0$, then

$$\mathbf{c}^T\mathbf{s}_\mu^{(k)} = T \tag{264}$$

for all k. Thus, all the iterates stay in the hyperplane of constant traveltime. If we choose not to iterate to convergence, then this desirable feature of the exact solution $\mathbf{s}_\mu$ proven in (258) is still shared by every iterate $\mathbf{s}_\mu^{(k)}$ obtained using this scheme.

7.3 Stable Algorithm for Nonlinear Crosshole Tomography

Here we combine several ideas from the previous sections into an algorithm for nonlinear tomography. We recall that such algorithms are inherently iterative. In the general iterative algorithm posed earlier, the questionable step was how to update the current model $\hat{\mathbf{s}}$ to obtain a new model. Here we propose a method for this step [Berryman, 1989b; 1990].

Let $\mathbf{s}^{(k)}$ be the current model. An algorithm for generating the updated model $\mathbf{s}^{(k+1)}$ is as follows:

1. Set $\mathbf{s}_1$ to the scaled least-squares model:

$$\mathbf{s}_1 = \hat{\mathbf{s}}_{\mathrm{LS}[\mathbf{s}^{(k)}]}.$$

2. Set $\mathbf{s}_2$ to the damped least-squares model with respect to $\mathbf{s}_1$:

$$\mathbf{s}_2 = \hat{\mathbf{s}}_{\mathrm{LS}[\mathbf{s}_1,\mu]}.$$

3. Define the family of models

$$\mathbf{s}(\lambda) = (1-\lambda)\mathbf{s}_1 + \lambda\mathbf{s}_2,$$

where $\lambda \in [0,1]$.

4. Solve for λ^*, defined so that $\mathbf{s}(\lambda^*)$ yields the fewest number of feasibility violations. The number of feasibility violations is defined as the number of ray paths for which $t_i > \tau^*(\mathbf{s}(\lambda))$.

5. If λ^* is less than some preset threshold (say 0.05 or 0.1), reset it to the threshold value.

6. Set $\mathbf{s}^{(k+1)} = \mathbf{s}(\lambda^*)$.

The algorithm is illustrated in Fig. 9. The model labeled $\mathbf{s}_3$ is a scaled version of $\mathbf{s}(\lambda^*)$, scaled so that $\mathbf{s}_3$ is on the boundary of the feasible region ($\mathcal{F}^*$). The iteration is stopped when the perimeter of the triangle formed by $\mathbf{s}_1$, $\mathbf{s}_2$ and $\mathbf{s}_3$ drops below a prescribed threshold.

This algorithm has been tested on several problems both with real and with synthetic data and compared with a traditional damped least-squares algorithm (i.e., setting $\lambda^* = 1$ on each iteration). The new algorithm was found to be very stable and avoids the large oscillations in slowness often found in traditional least-squares methods.

7.4 Using Relative Traveltimes

When we do not have control over the seismic source location and timing as in the case of earthquakes, the absolute traveltimes are not known and it is important to understand how relative traveltimes may be used in seismic tomography [Aki, Christoffersson, and Husebye, 1977].

Rigorous application of the feasibility constraints $\mathbf{Ms} \geq \mathbf{t}$ requires knowledge of the absolute traveltimes. When such information is not available, we can use the information we have about the geology of the region to estimate the mean traveltime. Then we remove the meaningless mean of the data T/m and add back in the geological mean τ_0.

The *remove-the-mean operator* $\mathbf{R}$ for an m-dimensional vector space is defined as

$$\mathbf{R} = \mathbf{I} - \mathbf{u}\frac{1}{m}\mathbf{u}^T, \tag{265}$$

where $\mathbf{u} = (1,\ldots,1)$ is an m-vector of ones. Note that $\mathbf{RR} = \mathbf{R}$ so $\mathbf{R}$ is a projection operator. Then, we see that $\mathbf{R}$ applied to the traveltime vector $\mathbf{t}$ gives

$$\mathbf{Rt} = \mathbf{t} - \frac{T}{m}\mathbf{u}, \tag{266}$$

where $T/m = \mathbf{u}^T\mathbf{t}/m$ is the mean traveltime of the data set. Applying $\mathbf{R}$ to the ray-path matrix, we have

$$\mathbf{RM} = \mathbf{M} - \mathbf{u}\frac{T}{m}\mathbf{v}^T\mathbf{C} = \mathbf{M} - \mathbf{u}\frac{T}{m}\mathbf{c}^T. \tag{267}$$

The standard procedure for this problem is to solve the equation

$$\mathbf{M}'\mathbf{s} = \mathbf{t}', \tag{268}$$

where $\mathbf{M}' = \mathbf{RM}$ and $\mathbf{t}' = \mathbf{Rt}$. To apply the feasibility constraints, we must modify the problem to

$$\mathbf{Ms} \geq \mathbf{Rt} + \tau_0\mathbf{I}_m. \tag{269}$$

Hidden in this analysis is the fact that the earthquake sources are often far from the region to be imaged, so the "effective" source locations may be placed at the boundaries of the region to be imaged.

If we have predetermined the mean for the traveltime data, then it is clearly desirable to use an inversion procedure that preserves this mean, *i.e.*, choosing $\Delta\mathbf{s}$ so that

$$\frac{\mathbf{u}^T\mathbf{M}(\mathbf{s} + \Delta\mathbf{s})}{m} = \tau_0 \tag{270}$$

for all $\Delta\mathbf{s}$. Preserving the mean is equivalent to preserving the total traveltime along all ray paths, so

$$\mathbf{c}^T(\mathbf{s} + \Delta\mathbf{s}) = m\tau_0. \tag{271}$$

In other words, vary $\mathbf{s}$ so it stays in the hyperplane determined by (271). But we have studied just this problem using linear programming (239) and also using weighted least-squares (258). So we do not need to develop any new inversion methods for this special case.

7.5 Parallel Computation

Traveltime tomography algorithms tend to be parallelizable in a variety of ways. The use of the feasibility constraints only increases the degree of parallelism that is achievable by these algorithms.

First, the *forward modeling* may be parallelized. If the forward problem is solved using either shooting or bending methods, then it is straightforward to parallelize the code because each ray may be computed independently of the others, and therefore in parallel. If the forward problem is solved using a finite difference algorithm or a full wave equation method, then whether the algorithm is parallelizable or not depends on the details of the particular algorithm. For example, Vidale's method is not parallelizable, but a recent related method by von Trier and Symes [1991] is.

Second, the use of the feasibility constraints in inversion algorithms suggests that it might be advantageous to map out the feasibility boundary and then use the information

gained to search for improved agreement between the model and the data. Mapping the feasibility boundary can be done completely in parallel. Each model $\mathbf{s}$ may be treated in isolation, computing the best ray-path matrix for the model, and then finding the scaled model in the direction of $\mathbf{s}$ that intersects the feasibility boundary. The difficulty with this method is that it requires a figure of merit (in real problems) to help us determine whether one point on the feasibility is better than another. In ideal circumstances (no data error and infinite precision in our computers), the figure of merit would be the number of ray paths that achieve equality while satisfying the feasibility constraints

$$\mathbf{Ms} \geq \mathbf{t}. \tag{272}$$

When that number equals the number of ray paths, we have found an exact solution and, as the number increases towards this maximum value during an iterative procedure, the trial models $\mathbf{s}$ must be converging towards this solution. But in real problems, a figure of merit based on the number of equalities in (272) is not useful. In a series of numerical experiments, we have found that a useful figure of merit for real problems is the nonlinear least-squares functional

$$\Psi(\mathbf{s}) = \sum_{i=1}^{n} w_i [r_i^*(\mathbf{s}) - \mathbf{t}_i]^2. \tag{273}$$

If we have found an exact solution $\mathbf{s}^*$ to the inversion problem, (273) will vanish at that point on the feasibility boundary. As we approach this point, when we evaluate (273) at an arbitrary point on the feasibility boundary and compare the values at a variety of such points, we know from our analysis of convex programming that the points with the smallest values of (273) are clustered in a convex set. The smallest value we find may not be zero, in which case there is no exact solution to our inversion problem. This procedure has been implemented on a parallel processing machine, and the results obtained using this algorithm with the figure of merit (273) have been found to be comparable to those of the stable algorithm discussed earlier.

8 Other Nonlinear Inversion Problems

Although traveltime tomography has been the main thrust of these lectures, I want to make it clear that the ideas involving the feasibility constraints are very general. In fact, they apply to any inversion problem where the data are the minima of one of the variational problems of mathematical physics.

So in this final lecture, I will present two other inversion problems that lead to convex feasible sets and then show the general structure required to guarantee convex global feasibility. Finally, I will present another example that leads to a nonconvex feasibility set and will discuss the consequences of this difference for computing the solution of the inverse problem.

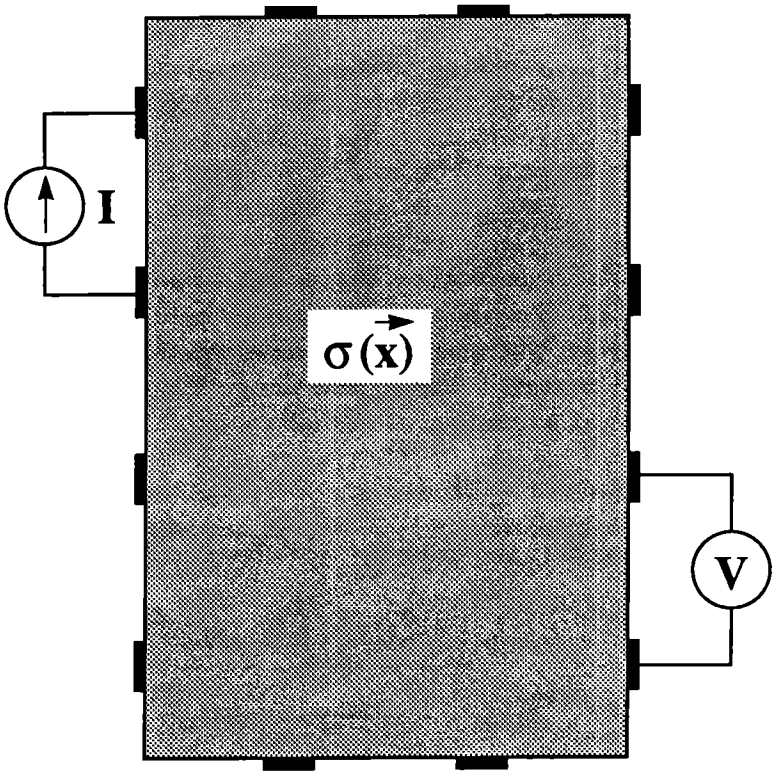

Figure 10: Experimental set up for electrical impedance tomography.

8.1 Electrical Impedance Tomography

Electrical impedance tomography [Dines and Lytle, 1981; Berryman and Kohn, 1990] attempts to image the electrical impedance (or just the conductivity) distribution inside a body using electrical measurements on its boundary. See Fig. 10. The method has been used successfully in both biomedical [Barber and Brown, 1986] and geophysical applications [Wexler, Fry, and Neuman, 1985; Daily, Lin, and Buscheck, 1987], but the analysis of optimal reconstruction algorithms is still progressing [Yorkey, Webster, and Tompkins, 1987; Kohn and McKenney, 1990]. The most common application is monitoring the influx or efflux of a conducting fluid (such as brine in a porous rock) through the body whose conductivity is being imaged. This method does not have high resolving power like radiological methods, but it is comparatively inexpensive and it therefore provides a valuable alternative when continuous monitoring is desired.

First, we will review some facts about this problem that play an important role in the analysis that follows. Recall that the power dissipated into heat is [Jackson, 1962]

$$P = \int \mathbf{J}(\mathbf{x}) \cdot \mathbf{E}(\mathbf{x})\, d^3x, \tag{274}$$

where

$$\mathbf{J}(\mathbf{x}) = \sigma(\mathbf{x})\mathbf{E}(\mathbf{x}), \tag{275}$$

$$\mathbf{E}(\mathbf{x}) = -\nabla\phi(\mathbf{x}), \tag{276}$$

and the current distribution satisfies

$$\nabla \cdot \mathbf{J}(\mathbf{x}) = 0 \tag{277}$$

away from all current sources. The quantities displayed are the current distribution $\mathbf{J}$, the isotropic conductivity σ, the electric field $\mathbf{E}$, and the potential ϕ. Substituting (275) and (276) into (277) gives Poisson's equation

$$\nabla \cdot (\sigma \nabla \phi) = 0. \tag{278}$$

Substituting (276) into (274) and using (277), we have

$$P = -\int \mathbf{J} \cdot \nabla\phi \, d^3x = -\int \nabla \cdot (\phi \mathbf{J}) \, d^3x. \tag{279}$$

Then, the divergence theorem shows that

$$P = -\int \phi \mathbf{J} \cdot \hat{n} \, da, \tag{280}$$

where $\hat{n}$ is a unit outward normal vector and da is the infinitesimal surface area on the boundary. If current is injected through metallic electrodes, the potential takes a constant value ϕ_k on the kth electrode of surface area a_k. If there are K electrodes, then (280) becomes

$$P = \sum_{k=1}^{K} \phi_k I_k, \tag{281}$$

where

$$I_k = -\int_{a_k} \mathbf{J} \cdot \hat{n} \, da \tag{282}$$

is the total current injected ($I_k > 0$) or withdrawn ($I_k < 0$) at the kth electrode. Since these are the only sources and sinks, we also have the sumrule

$$\sum_{k=1}^{K} I_k = 0. \tag{283}$$

If there are only two injection electrodes, then (281) reduces to

$$P = (\phi_1 - \phi_2) I_1 = \Delta\phi I, \tag{284}$$

so the power is the product of the measured potential difference $\Delta\phi$ across the injection electrodes and the injected current I.

The data for electrical impedance tomography have most often been gathered by injecting a measured current between two electrodes while simultaneously measuring the voltage differences between pairs of other electrodes placed around the boundary of the body being imaged. This process is then repeated, injecting current between all possible (generally adjacent) pairs of electrodes, and recording the set of voltage differences for each injection pair i. This data set has normally not included the voltage difference across the injection electrodes, because these voltages cannot be measured as reliably. A substantial contact impedance develops at the interface between the body and the injection electrodes when large currents are present. This problem can be reduced by using large electrodes or small currents. In this lecture, we will assume that voltage differences (and therefore the powers dissipated) across the injection electrodes are known, but it is not necessary that they be known to high accuracy.

Dirichlet's principle states that, given a conductivity distribution $\sigma(\mathbf{x})$ and a potential distribution $\phi(\mathbf{x})$, the power dissipation p_i realized for the ith current injection configuration is the one that minimizes the integral $\int \sigma|\nabla\phi|^2\, d^3x$ so that

$$p_i(\sigma) = \int \sigma(\mathbf{x})|\nabla\phi_i^*(\mathbf{x})|^2\, d^3x = \min_{\phi_i} \int \sigma(\mathbf{x})|\nabla\phi_i(\mathbf{x})|^2\, d^3x. \tag{285}$$

The trial potential field for the ith injection pair is $\phi_i(\mathbf{x})$, while the particular potential field that actually minimizes the the power is $\phi_i^*(\mathbf{x})$, and this one also satisfies Poisson's equation $\nabla\cdot(\sigma\nabla\phi_i^*) = 0$ within the body. Furthermore, if the effective power dissipation associated with the trial potential $\phi_i(\mathbf{x})$ is defined as

$$\bar{p}_i^{(\phi_i)}(\sigma) \equiv \int \sigma(\mathbf{x})|\nabla\phi_i(\mathbf{x})|^2\, d^3x, \tag{286}$$

then the measured powers P_i must satisfy

$$P_i = p_i(\sigma^*) \le \bar{p}_i^{(\phi_i)}(\sigma^*), \tag{287}$$

if $\sigma^*(\mathbf{x})$ is the true conductivity distribution. Note that if we vary the trial power dissipation (286) with respect to the trial potential, we find

$$2\int \sigma\nabla\phi\cdot\nabla\delta\phi\, d^3x = -2\int \nabla\cdot(\sigma\nabla\phi)\delta\phi\, d^3x = 0 \tag{288}$$

at a stationary point. We integrated once by parts to obtain (288). Since the volume variation $\delta\phi$ is arbitrary, its coefficient inside the integral must vanish, so we just recover Poisson's equation, as expected.

Now we begin to see the analogy developing between the seismic traveltime tomography problem and the electrical impedance tomography problem. If we consider the following set of correspondences:

$$s(\mathbf{x}) \to \sigma(\mathbf{x}),$$

$$t_i(s) \rightarrow p_i(\sigma),$$

$$\tau_i^P(s) \rightarrow \bar{p}_i^{(\phi_i)}(\sigma),$$

$$T_i \rightarrow P_i,$$

$$dl_i^P \rightarrow |\nabla \phi_i(\mathbf{x})|^2 \, d^3x,$$

$$dl_i^{P^*} \rightarrow |\nabla \phi_i^*(\mathbf{x})|^2 \, d^3x,$$

then we see that the analysis of convex functionals and feasibility sets presented for seismic traveltime tomography carries over directly to the electrical impedance tomography problem when it is formulated this way. For example, the scale invariance property holds for electrical impedance tomography, so multiplying σ by a scalar γ does not change the optimum potential distribution.

The feasibility constraints for electrical impedance tomography now take the form

$$\mathbf{K}\hat{\sigma} \geq \mathbf{p}, \tag{289}$$

where $\hat{\sigma}^T = (\sigma_1, \ldots, \sigma_n)$, $\mathbf{p}^T = (p_1, \ldots, p_m)$, and the E-squared matrix is given by

$$K_{ij} = \int_{\text{cell}_j} |\nabla \phi_i|^2 \, d^3x. \tag{290}$$

Least-squares methods may be applied to this problem in much the same fashion as in traveltime tomography [Kallman and Berryman, 1990].

A thorough analysis of the electrical impedance tomography problem would require another set of lectures. Lucky for you, I will not try to present them here. However, to excite your curiosity, I will mention another feature of the electrical impedance tomography problem not shared by the seismic tomography problem. So far we have discussed only Dirichlet's principle (285). In fact, there are two distinct variational principles for the conductivity problem: Dirichlet's principle and its dual, known as Thomson's principle. The second variational principle takes the form

$$P_i \leq \int |\mathbf{J}_i(\mathbf{x})|^2 / \sigma(\mathbf{x}) \, d^3x, \tag{291}$$

where $\mathbf{J}_i(\mathbf{x})$ is a trial current distribution vector for the ith current injection pair that satisfies the continuity equation $\nabla \cdot \mathbf{J}_i = 0$. The trial current distribution $\mathbf{J}_i(\mathbf{x})$ and the trial gradient of the potential $\nabla \phi_i(\mathbf{x})$ are generally unrelated except that, when the minimum of both variational functionals is attained, then $\mathbf{J}_i^*(\mathbf{x}) = -\sigma \nabla \phi_i^*(\mathbf{x})$. Then, of course, the current equals the conductivity times the electric field.

The existence of dual variational principles is a general property whenever the primal variational principle is a true minimum principle. Fermat's principle is only a stationary (not a minimum) principle, and so traveltime tomography does not possess this dual property.

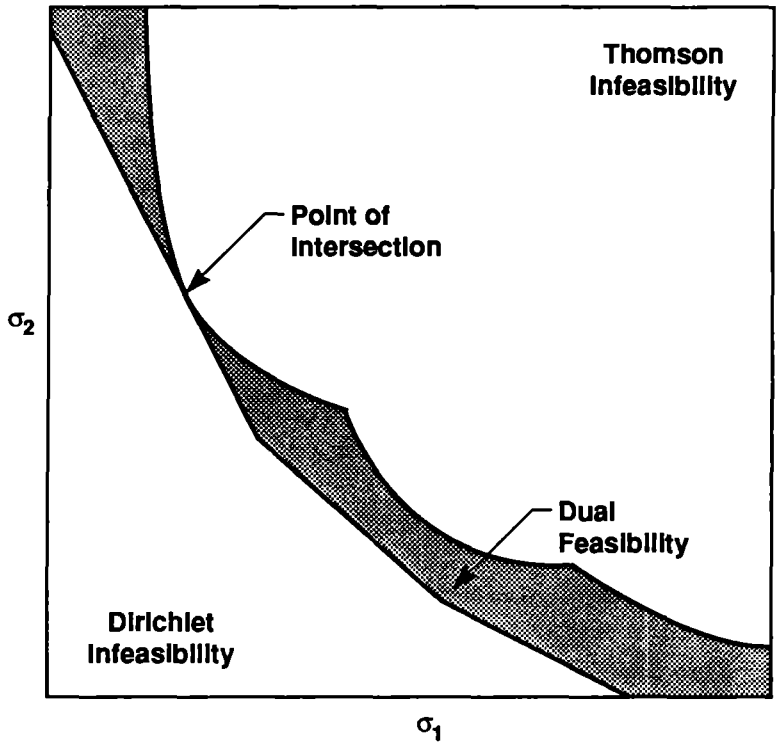

Figure 11: Dirichlet's principle and Thomson's principle provide upper and lower bounds on the dual feasibility region for electrical impedance tomography.

(If we attempt to formulate a dual for Fermat's principle as we did in the lecture on linear and nonlinear programming, we find the content of the dual results are essentially trivial.) The existence of the dual variational principles for electrical impedance tomography is important because it means that there are two independent sets of feasibility constraints for the conductivity model $\sigma(\mathbf{x})$. Furthermore, as illustrated in Fig. 11, these two sets of constraints allow us (in some sense) to obtain upper and lower bounds on the region of the conductivity model space that contains the solution to the inversion problem. See Berryman and Kohn [1990] for more discussion of this point.

8.2 Inverse Eigenvalue Problems

Inverse eigenvalue problems arise in the earth sciences during attempts to deduce earth structure from knowledge of the modes of vibration of the earth [Dahlen, 1968; Jordan and Anderson, 1974; Hald, 1980; Hald, 1983; Anderson and Dziewonski, 1984; McLaughlin, 1986; Dziewonski and Woodhouse, 1987; Lay, Ahrens, Olson, Smyth, and Loper, 1990].

Consider the typical forward problem associated with the inverse eigenvalue problem

$$-\nabla^2 u(\mathbf{x}) + q(\mathbf{x})u(\mathbf{x}) = \lambda u(\mathbf{x}) \tag{292}$$

on a finite domain with some boundary conditions on u. This is known as a Sturm-Liouville equation to mathematicians and as the Schroedinger equation to physicists. In quantum mechanics, the time-independent wave function is given by $u(\mathbf{x})$ and $q(\mathbf{x})$ is the potential. The eigenvalue is λ.

Now it is well-known that a Rayleigh-Ritz procedure may be used to approximate the eigenvalues λ [Courant and Hilbert, 1953]. In particular, the lowest eigenvalue is given generally by

$$\lambda_0 = \min_u \frac{\int (|\nabla u|^2 + qu^2)\, d^3x}{\int u^2\, d^3x}, \tag{293}$$

where admissible us satisfy the boundary conditions of (292) and have no other constraints, except being twice differentiable. The ratio on the right to be minimized is known as the Rayleigh quotient, and the denominator $\int u^2\, d^3x$ serves to normalize the wave function u.

Define the Rayleigh-quotient functional as

$$\Lambda(q, u_i) = \frac{\int (|\nabla u_i|^2 + qu_i^2)\, d^3x}{\int u_i^2\, d^3x}, \tag{294}$$

where u_i is a trial wave function subject to i constraints. Taking the variation of Λ with respect to u_i, we find that the stationary points of Λ satisfy

$$\frac{\int [-\nabla^2 u_i + qu_i - \Lambda(q, u_i)u_i]\delta u_i\, d^3x}{\int u_i^2\, d^3x} = 0. \tag{295}$$

We integrated once by parts to obtain (295) using the fact that the variations of δu vanish on the boundary. So, since the variations δu within the domain may be arbitrary, the term in brackets must vanish and the stationary points of the Rayleigh quotient therefore occur for u_is that satisfy (292) with $\lambda_i = \Lambda(q, u_i)$.

Clearly, we may define feasibility constraints for this problem in a manner analogous to that for the traveltime tomography problem and for the electrical impedance tomography problem. If the eigenvalues λ_i are our data, then for the correct potential q^* we must have

$$\lambda_i \equiv \Lambda(q^*, u_i^*[q^*]) \leq \Lambda(q^*, u_i), \tag{296}$$

where $u_i^*[q]$ is the eigenfunction associated with eigenvalue λ_i of the potential q. Thus, feasible qs satisfy

$$\lambda_i \leq \Lambda(q, u_i) \tag{297}$$

for all admissible u_is.

To show that this problem leads to a convex feasibility set, consider two potentials that satisfy the feasibility constraints for some fixed choice of u_i. Then,

$$\lambda_i \leq \Lambda(q_1, u_i) \quad \text{and} \quad \lambda_i \leq \Lambda(q_2, u_i) \tag{298}$$

and

$$\lambda_i \leq \epsilon\Lambda(q_1, u_i) + (1-\epsilon)\Lambda(q_2, u_i) \tag{299}$$

$$= \frac{\int (|\nabla u_i|^2 + [\epsilon q_1 + (1-\epsilon)q_2]u_i^2)\, d^3x}{\int u_i^2\, d^3x} \tag{300}$$

$$= \Lambda(q_\epsilon, u_i), \tag{301}$$

where the convex combination $q_\epsilon \equiv \epsilon q_1 + (1-\epsilon)q_2$. Thus, local (fixed u_is) feasibility follows simply from the linearity of the Rayleigh quotient (except for the shift at the origin) with respect to the potential q. Global feasibility follows from the variational properties of Λ with respect to u_i. (See the next subsection for the proof.)

Note that there is no scale invariance property for Λ similar to the one for the traveltime functional. However, it is true that wave functions are invariant to a constant shift in the potential, since it is easy to see that

$$\Lambda(q + \gamma, u) = \Lambda(q, u) + \gamma. \tag{302}$$

In our analysis, we can also make use of other members of the invariance group of (292) [Ames, 1972].

This inverse eigenvalue problem can be reformulated in terms of a different set of variational functionals. In particular, one such set of generalized Rayleigh-Ritz quotients has been constructed by Berryman [1988]; however, these functionals have a more complicated dependence on the potential q. Without linearity or shifted linearity in q, we cannot prove the convexity of the feasibility set and the structure of the inversion problem becomes less certain and possibly more complex.

8.3 General Structure for Convex Inversion Problems

The feasibility analysis presented in these lectures applies to a wide class of inverse problems that can be formulated so the data are minima of an appropriate variational problem. To see the general structure, consider a set of functionals $\Gamma_i(q, u)$ of two variables q and u. Then, if each functional is linear in one variable so that

$$\Gamma_i(aq_1 + bq_2, u) = a\Gamma_i(q_1, u) + b\Gamma_i(q_2, u), \tag{303}$$

and if the data γ_i bound $\Gamma_i(q_1, u)$ and $\Gamma_i(q_2, u)$ from below for any second argument u, then

$$\gamma_i \leq \Gamma_i(q_1, u) \quad \text{and} \quad \gamma_i \leq \Gamma_i(q_2, u) \quad \text{for all} \quad i = 1, \ldots, m, \tag{304}$$

and we have

$$\gamma_i \leq \lambda\Gamma_i(q_1, u) + (1-\lambda)\Gamma_i(q_2, u) = \Gamma_i(\lambda q_1 + (1-\lambda)q_2, u). \tag{305}$$

Therefore, Γ_i evaluated at the convex combination $q_\lambda = \lambda q_1 + (1-\lambda)q_2$ is also bounded below by the data. Thus, linearity for fixed u is sufficient to prove that feasible qs for the linear problem form a convex set. We call this the *local convex feasibility* property.

Then, when we consider variations of the second argument and assume that the data are minima of the variational functional over all possible us, we have

$$\gamma_i \equiv \Gamma_i(q^*, u^*[q^*]) \leq \Gamma_i(q^*, u), \tag{306}$$

where $u^*[q]$ is the particular function that minimizes the the functional Γ_i when q is the first argument. Then, we have

$$\gamma_i \leq \Gamma_i(q_1, u^*[q_1]) \leq \Gamma_i(q_1, u^*[\cdot]), \tag{307}$$

$$\gamma_i \leq \Gamma_i(q_2, u^*[q_2]) \leq \Gamma_i(q_2, u^*[\cdot]), \tag{308}$$

where $u^*[\cdot]$ is the correct (minimizing) u for some yet to be specified q. Combining (307) and (308) using the linearity property of Γ_i for its first argument, we have

$$\gamma_i \leq \lambda\Gamma_i(q_1, u^*[q_1]) + (1-\lambda)\Gamma_i(q_2, u^*[q_2]) \tag{309}$$

$$\leq \lambda\Gamma_i(q_1, u^*[\cdot]) + (1-\lambda)\Gamma_i(q_2, u^*[\cdot]) \tag{310}$$

$$= \Gamma_i(q_\lambda, u^*[\cdot]), \tag{311}$$

where $q_\lambda = \lambda q_1 + (1-\lambda)q_2$ is again the convex combination of q_1 and q_2. Now we are free to choose the $\cdot$ to be any permissible q, so we choose it for convenience to be q_λ. Then, we have the final result that

$$\gamma_i \leq \Gamma_i(q_\lambda, u^*[q_\lambda]). \tag{312}$$

The conclusion from (305) is that there are local convex feasibility sets and from (312) that there is a *global convex feasibility set* for the full nonlinear inversion problem, just as in the case for traveltime tomography.

The only properties we used were the linearity of the variational functional Γ_i for fixed u and the concavity of the functional that results from its variational nature.

The preceding proof is appropriate for Fermat's, Dirichlet's, and Thomson's principles. However, the proof must be modified for the inverse eigenvalue problem, because the Rayleigh quotient is a shifted linear functional of the potential q. We can fix this minor difficulty by considering

$$\Delta\Lambda(q, u_i) = \Lambda(q, u_i) - \Lambda(0, u_i) = \frac{\int q u^2 \, d^3x}{\int u^2 \, d^3x}, \tag{313}$$

which is linear in q. If

$$\lambda_i \leq \Lambda(0, u_i) + \Delta\Lambda(q_1, u_i), \tag{314}$$

$$\lambda_i \leq \Lambda(0, u_i) + \Delta\Lambda(q_2, u_i), \tag{315}$$

then we can carry through the analysis as before and conclude that

$$\lambda_i \leq \Lambda(0, u_i) + \Delta\Lambda(\epsilon q_1 + (1-\epsilon)q_2, u_i) = \Lambda(q_\epsilon, u_i). \tag{316}$$

This proves the *local convex feasibility* property for problems with variational functionals linear in the first argument except for a constant. The proof of *global convex feasibility* follows the proof already presented step by step and need not be repeated for this case.

8.4 Nonconvex Inversion Problems with Feasibility Constraints

Although we expect the idea of using feasibility constraints in inversion problems with variational structure to be a very general method, it may not always be the true that the variational functional is a concave functional of its arguments. If not, then the resulting nonlinear programming problem will not be convex.

As an example, consider the electrical impedance tomography problem again, but this time for complex (still isotropic) conductivity $\sigma = \sigma_R + i\sigma_I$. The dissipative part of σ is the real part σ_R, while the reactive part (proportional to the dielectric constant) is the imaginary part σ_I.

The current is proportional to the conductivity and the electric field, but now all quantities are complex so

$$\mathbf{J} = \sigma \mathbf{E} \tag{317}$$

becomes

$$\mathbf{j}_R + i\mathbf{j}_I = (\sigma_R + i\sigma_I)(\mathbf{e}_R + i\mathbf{e}_I). \tag{318}$$

The power dissipation for this problem is given by

$$P = \frac{1}{2}\int (\mathbf{J}\cdot\mathbf{E}^* + \mathbf{J}^*\cdot\mathbf{E})\, d^3x \tag{319}$$

$$= \int (\mathbf{j}_R\cdot\mathbf{e}_R + \mathbf{j}_I\cdot\mathbf{e}_I)\, d^3x \tag{320}$$

$$= \int \sigma_R(\mathbf{e}_R\cdot\mathbf{e}_R + \mathbf{e}_I\cdot\mathbf{e}_I)\, d^3x. \tag{321}$$

Rewriting (318) in matrix notation we have

$$\begin{pmatrix}\mathbf{j}_R\\ \mathbf{j}_I\end{pmatrix} = \begin{pmatrix}\sigma_R & -\sigma_I\\ \sigma_I & \sigma_R\end{pmatrix}\begin{pmatrix}\mathbf{e}_R\\ \mathbf{e}_I\end{pmatrix}. \tag{322}$$

Now we want to reformulate this problem as a variational principle in order to apply the ideas of feasibility constraints, but to do so we need a positive scalar functional. The power dissipation is a good choice again, but (322) is inconvenient for this purpose since the matrix is not positive definite [Milton, 1990]. Performing a Legendre transform on (322), we find that an alternative equation is

$$\begin{pmatrix}\mathbf{j}_R\\ \mathbf{e}_I\end{pmatrix} = \begin{pmatrix}\sigma_R + \frac{\sigma_I^2}{\sigma_R} & -\frac{\sigma_I}{\sigma_R}\\ -\frac{\sigma_I}{\sigma_R} & \frac{1}{\sigma_R}\end{pmatrix}\begin{pmatrix}\mathbf{e}_R\\ \mathbf{j}_I\end{pmatrix} \equiv \mathbf{\Sigma}\begin{pmatrix}\mathbf{e}_R\\ \mathbf{j}_I\end{pmatrix}. \tag{323}$$

Then, the matrix is positive definite (for $\sigma_R > 0$), since

$$\mathbf{\Sigma}\begin{pmatrix}\mathbf{e}_R\\ \mathbf{j}_I\end{pmatrix} = \lambda\begin{pmatrix}\sigma_R & 0\\ 0 & 1/\sigma_R\end{pmatrix}\begin{pmatrix}\mathbf{e}_R\\ \mathbf{j}_I\end{pmatrix} \tag{324}$$

implies that

$$\lambda + \frac{1}{\lambda} = 2 + \frac{\sigma_I^2}{\sigma_R^2}, \tag{325}$$

which guarantees that the eigenvalues λ and $1/\lambda$ are positive.

So now the power is given by

$$P = \int (\mathbf{j}_R \cdot \mathbf{e}_R + \mathbf{j}_I \cdot \mathbf{e}_I)\, d^3x \tag{326}$$

$$= \int (\mathbf{e}_R \quad \mathbf{j}_I)\, \Sigma \begin{pmatrix} \mathbf{e}_R \\ \mathbf{j}_I \end{pmatrix} d^3x \tag{327}$$

$$= \int [\sigma_R |\mathbf{e}_R|^2 + \frac{1}{\sigma_R} |\mathbf{j}_I - \sigma_I \mathbf{e}_R|^2]\, d^3x. \tag{328}$$

This is the final expression for the power. In this form, we have a valid variational principle. Also, note that the term $\mathbf{j}_I - \sigma_I \mathbf{e}_R = \sigma_R \mathbf{e}_I$ so the second term in the final expression for P is just $\sigma_R |\mathbf{e}_I|^2$.

To check the conditions for stationarity of this integral, we find that, if we vary with respect to $\mathbf{e}_R$, then

$$2 \int [\sigma_R \mathbf{e}_R - \frac{\sigma_I}{\sigma_R} (\mathbf{j}_I - \sigma_I \mathbf{e}_R)] \cdot \delta \mathbf{e}_R\, d^3x = 0. \tag{329}$$

If we vary with respect to $\mathbf{j}_I$, we find that

$$2 \int [\frac{1}{\sigma_R} (\mathbf{j}_I - \sigma_I \mathbf{e}_R)] \cdot \delta \mathbf{j}_I\, d^3x = 0. \tag{330}$$

Since the electric field is the gradient of a potential, (329) implies that

$$\nabla \cdot [\sigma_R \mathbf{e}_R - \frac{\sigma_I}{\sigma_R} (\mathbf{j}_I - \sigma_I \mathbf{e}_R)] = 0. \tag{331}$$

Similarly, since the current distribution is divergence free, (330) implies that

$$\frac{1}{\sigma_R} (\mathbf{j}_I - \sigma_I \mathbf{e}_R) = -\nabla \phi \tag{332}$$

for some scalar potential function ϕ. Thus, the expression in (332) acts like an electric field (in fact, it is $\mathbf{e}_I$) at the stationary point, while the quantity whose divergence is zero in (331) acts like a current distribution (in fact, it is $\mathbf{j}_R$). This completes the proof that (328) is a legitimate variational principle for the complex conductivity problem.

We can still talk about feasibility constraints for this problem, since

$$P_i \equiv \bar{p}_i(\sigma_R^*, \sigma_I^*, \mathbf{e}_R^*, \mathbf{j}_I^*) \leq \bar{p}_i(\sigma_R^*, \sigma_I^*, \mathbf{e}_R, \mathbf{j}_I) \tag{333}$$

with the trial power dissipation given by

$$\bar{p}_i(\sigma_R, \sigma_I, \mathbf{e}_R, \mathbf{j}_I) = \int [\sigma_R |\mathbf{e}_R|^2 + \frac{1}{\sigma_R} |\mathbf{j}_I - \sigma_I \mathbf{e}_R|^2]\, d^3x. \tag{334}$$

The starred quantities in (333) are the true ones for the experimental configuration. If we can find σs that violate the constraints implied by (333), then those σs are infeasible and the rest form the feasible set. However, $\bar{p}$ is not linear in its dependence on σ, so we cannot

prove that this functional is concave. [12] Therefore, we lack a proof of the convexity of the feasible set.

For fixed σ_I, $\mathbf{j}_I$, and $\mathbf{e}_R$, the minimum of (334) is achieved, for a model of constant conductivity cells, when the real conductivity in the jth cell is given by

$$\sigma_R^2 = \frac{\int_{\text{cell}_j} |\mathbf{j}_I - \sigma_I \mathbf{e}_R|^2 \, d^3x}{\int_{\text{cell}_j} |\mathbf{e}_R|^2 \, d^3x}. \tag{335}$$

This minimum value is

$$\min_{\sigma_R} \bar{p}_i = 2 \sum_{j=1}^{n} [\int_{\text{cell}_j} |\mathbf{e}_R|^2 \, d^3x \int_{\text{cell}_j} |\mathbf{j}_I - \sigma_I \mathbf{e}_R|^2 \, d^3x]^{\frac{1}{2}}. \tag{336}$$

Since the imaginary part of the conductivity may still be viewed as a variable, we can further minimize (336) by finding the minimum with respect to σ_I. This minimum occurs when

$$\sigma_I = \frac{\int_{\text{cell}_j} \mathbf{j}_I \cdot \mathbf{e}_R \, d^3x}{\int_{\text{cell}_j} \mathbf{e}_R \cdot \mathbf{e}_R \, d^3x} \tag{337}$$

for the imaginary part of the conductivity in the jth cell. Substituting into (336), we have the minimum power

$$\min_{\sigma_R, \sigma_I} \bar{p}_i = 2 \sum_{j=1}^{n} [\int_{\text{cell}_j} \mathbf{e}_R \cdot \mathbf{e}_R \, d^3x \int_{\text{cell}_j} \mathbf{j}_I \cdot \mathbf{j}_I \, d^3x - (\int_{\text{cell}_j} \mathbf{j}_I \cdot \mathbf{e}_R \, d^3x)^2]^{\frac{1}{2}}. \tag{338}$$

It follows from the Schwartz inequality for integrals that

$$(\int \mathbf{a} \cdot \mathbf{b} \, d^3x)^2 \leq \int \mathbf{a} \cdot \mathbf{a} \, d^3x \int \mathbf{b} \cdot \mathbf{b} \, d^3x \tag{339}$$

with equality applying *only* when $\mathbf{b}$ is proportional to $\mathbf{a}$, that each bracket in (338) is positive unless there is an exact solution such that

$$\mathbf{j}_I = \gamma \mathbf{e}_R, \tag{340}$$

for some scalar γ.

If the nonlinear programming problem is nonconvex but feasibility constraints are still applicable, what are the consequences for numerical solution of the inversion problem? For convex feasibility sets, the convex combination of any two points on the feasibility boundary is also feasible and therefore either lies in the interior or on the boundary of the feasible set. This property implies a certain degree of smoothness for the boundary itself. Clearly, if the

[12] Looking at (327) we see that the power is a linear functional of the matrix elements of Σ. However, this apparent linearity unfortunately does not help the analysis, because a physical constraint on the matrix elements is that $\det \Sigma \equiv 1$. It is not difficult to show that the convex combination of two matrices with unit determinant does not preserve this property. So the nonlinearity cannot be avoided by the trick of considering convex combinations of the matrix elements.

feasible set is nonconvex, then the convex combination of two points on the boundary may or may not lie in the feasible set; thus, the boundary itself may be jagged. Since the solution of the inversion problem still lies on the boundary (just as it did in the convex case), the lack of smoothness of the boundary may have important computational consequences: the boundary is still expected to be continuous, of course, but sharp local jumps could occur that might make convergence of an iterative method difficult to achieve.

As an iterative scheme progresses, the absolute minimum of the trial power (338) decreases towards zero. Thus, the feasibility constraints become *more* important for this problem as the scheme progresses to convergence.

9 Bibliography

9.1 Cited References

Aki, K., A. Christoffersson, and E. S. Husebye, 1976, Determination of the three-dimensional seismic structure of the lithosphere, *J. Geophys. Res.* **82**, 277–296.

Ames, W. F., 1972, *Nonlinear Partial Differential Equations in Engineering, Vol. II,* Academic Press, New York, Chapter 2, 87–145.

Anderson, D. L., and A. M. Dziewonski, 1984, Seismic tomography, *Scientific American* **251**, *number 10*, 60–68.

Barber, D. C., and B. H. Brown, 1986, Recent developments in applied potential tomography — APT, in *Information Processing in Medical Imaging*, S. L. Bascarach (ed.), Martinus Nijhoff, Dordrecht, 106–121.

Berryman, J. G., 1988, Bounds on decay constants for diffusion through inhomogeneous media, *J. Phys. A: Math. Gen.* **21**, 4423–4441.

Berryman, J. G., 1989a, Weighted least-squares criteria for seismic traveltime tomography, *IEEE Trans. Geosci. Remote Sensing* **27**, 302–309.

Berryman, J. G., 1989b, Fermat's principle and nonlinear traveltime tomography, *Phys. Rev. Lett.* **62**, 2953–2956.

Berryman, J. G., 1990, Stable iterative reconstruction algorithm for nonlinear traveltime tomography, *Inverse Problems* **6**, 21–42.

Berryman, J. G., 1991, Convexity properties of inverse problems with variational constraints, *J. Franklin Inst.*, to appear.

Berryman, J. G. and R. V. Kohn, 1990, Variational constraints for electrical impedance tomography, *Phys. Rev. Lett.* **65**, 325–328.

Burkhard, N. R., 1980, Resolution and error of the back projection technique algorithm for geophysical tomography, Lawrence Livermore National Laboratory preprint, UCRL-52984.

Courant, R., and D. Hilbert, 1953, *Methods of Mathematical Physics*, Vol. 1, Wiley, New York, 132–134.

Dahlen, F. A., 1968, The normal modes of a rotating elliptical earth, *Geophys. J. R. Astron. Soc.* **16**, 329–367.

Daily, W., W. Lin, and T. Buscheck, 1987, Hydrological properties of Topopah Spring tuff: Laboratory measurements, *J. Geophys. Res.* **92**, 7854–7864.

Devaney, A. J., 1984, Geophysical diffraction tomography, *IEEE Trans. Geosci. Remote Sensing* **22**, 3–13.

Dines, K. A., and R. J. Lytle, 1981, Analysis of electrical conductivity imaging, *Geophysics* **46**, 1025–1036.

Dziewonski, A. M., and J. H. Woodhouse, 1987, Global images of the earth's interior, *Science* **236**, 37–40.

Feynman, R. P., R. B. Leighton, and M. Sands, 1963, *The Feynman Lectures on Physics, Vol. I*, Addison-Wesley, Reading, Massachusetts, Chapter 26.

Fiacco, A. V. and G. P. McCormick, 1990, *Nonlinear Programming: Sequential Unconstrained Minimization Techniques*, SIAM, Philadelphia, Chapter 6, 86–112.

Frank, M., and C. A. Balanis, 1989, Methods for improving the stability of electromagnetic geophysical inversions, *IEEE Trans. Geosci. Remote Sens.* **27**, 339–343.

Hald, O. H., 1980, Inverse eigenvalue problems for the mantle, *Geophys. J. R. Astron. Soc.* **62**, 41–48.

Hald, O. H., 1983, Inverse eigenvalue problems for the mantle — II, *Geophys. J. R. Astron. Soc.* **72**, 139–164.

Hardy, G. H., J. E. Littlewood, and G. Pólya, 1934, *Inequalities*, Cambridge University Press, Cambridge, 70–101.

Herman, G. T., 1980, *Image Reconstruction from Projections - The Fundamentals of Computerized Tomography*, Academic, New York, Chapter 6, 100–107.

Hestenes, M. R., and E. Stiefel, 1952, Methods of conjugate gradients for solving linear systems, *J. Res. Nat. Bur. Stan.* **B 49**, 409–436.

Jackson, J. D., 1962, *Classical Electrodynamics*, Wiley, New York, 189–190.

Jeffrey, W., and R. Rosner, 1986a, On strategies for inverting remote sensing data, *Astrophys. J.* **310**, 463–472.

Jeffrey, W., and R. Rosner, 1986b, Optimization algorithms: Simulated annealing and neural network processing, *Astrophys. J.* **310**, 473–481.

Jordan, T. H., and D. L. Anderson, 1974, Earth structure from free oscillations and travel times, *Geophys. J. R. Astr. Soc.* **36**, 411–459.

Kallman, J. S., and J. G. Berryman, 1990, Weighted least-squares criteria for electrical impedance tomography, Lawrence Livermore National Laboratory, preprint, UCRL-JC-106000.

Kohn, R. V., and A. McKenney, 1990, Numerical implementation of a variational method for electrical impedance tomography, *Inverse Problems* **6**, 389–414.

Ladas, K. T., and A. J. Devaney, 1991, Generalized ART algorithm for diffraction tomography, *Inverse Problems*, submitted.

Lanczos, C., 1961, *Linear Differential Operators*, Van Nostrand, New York, Chapter 3, 100–162.

Lay, T., T. J. Ahrens, P. Olson, J. Smyth, and D. Loper, 1990, Studies of the earth's deep interior: Goals and trends, *Phys. Today* **43**, *number 10*, 44–52.

Lo, T.-W., G. L. Duckworth, and M. N. Toksöz, 1990, Minimum cross entropy seismic diffraction tomography, *J. Acoust. Soc. Am.* **87**, 748–756.

Lu, S.-Y., and J. G. Berryman, 1991, Inverse scattering, seismic traveltime tomography, and neural networks, *Intern. J. Imaging Sys. Tech.* **3**, to appear February, 1991.

Lytle, R. J., and K. A. Dines, 1980, Iterative ray tracing between boreholes for underground image reconstruction, *IEEE Trans. Geosci. Remote Sens.* **18**, 234–240.

McLaughlin, J. R., 1986, Analytical methods for recovering coefficients in differential equations from spectral data, *SIAM Rev.* **28**, 53–72.

Milton, G. W., 1990, On characterizing the set of possible effective tensors of composites: The variational method and the translation method, *Commun. Pure Appl. Math.* **43**, 63–125 (see Section 16).

Nelder, J. A., and R. Mead, 1965, A simplex method for function minimization, *Computer J.* **7**, 308–313.

Penrose, R., 1955a, A generalized inverse for matrices, *Proc. Cambridge Philos. Soc.* **51**, 406–413.

Penrose, R., 1955b, On best approximation solutions of linear matrix equations, *Proc. Cambridge Philos. Soc.* **52**, 17–19.

Prothero, W. A., W. J. Taylor, and J. A. Eickemeyer, 1988, A fast, two-point, three-dimensional raytracing algorithm using a simple step search method, *Bull. Seismol. Soc. Am.* **78**, 1190–1198.

Strang, G., 1986, *Introduction to Applied Mathematics*, Wellesley-Cambridge Press, Wellesley, MA, Chapter 8, 665–734.

Tabbara, W., B. Duchêne, Ch. Pichot, D. Lesselier, L. Chommeloux, and N. Joachimowicz, 1988, Diffraction tomography: Contribution to the analysis of some applications in microwaves and ultrasonics, *Inverse Problems* **4**, 305–331.

van Trier, J., and W. W. Symes, 1991, Upwind finite-difference calculation of traveltimes, *Geophysics*, submitted.

Vidale, J. E., 1988, Finite-difference calculation of travel time, *Bull. Seismol. Soc. Am.* **78**, 2062–2076.

Vidale, J. E., 1990, Finite-difference calculation of travel time in 3-D, *Geophysics* **55**, 521–526.

Wexler, A., B. Fry, and M. R. Neuman, 1985, Impedance-computed tomography algorithm and system, *Appl. Opt.* **24**, 3985–3992.

Whitham, G. B., 1974, *Linear and Nolinear Waves,* Wiley, New York, Chapters 7, 11 and 14.

Wu, R. S., and M. N. Toksöz, 1987, Diffraction tomography and multi-source holography applied to seismic imaging, *Geophysics* **52**, 11–25.

Yorkey, T. J., J. G. Webster, and W. J. Tompkins, 1987, Comparing reconstruction algorithms for electrical impedance tomography, *IEEE Trans. Biomed. Engng.* **34**, 843–852.

9.2 General References

Aki, K., and P. G. Richards, *Quantitative Seismology: Theory and Methods,* Vol. II, Freeman, New York, Chapter 12.

Ammon, C. J., G. E. Randall, and G. Zandt, 1990, On the nonuniqueness of receiver function inversions, *J. Geophys. Res.* **95**, 15303–15318.

Beylkin, G., 1984, The inversion problem and applications of the generalized Radon transform, *Commun. Pure Appl. Math.* **37**, 579–599.

Bois, P., M. La Porte, M. Lavergne, and G. Thomas, 1972, Well-to-well seismic measurements, *Geophysics* **37**, 471–480.

Chen, S. T., L. J. Zimmerman, and J. K. Tugnait, 1990, Subsurface imaging using reversed vertical seismic profiling and crosshole tomographic methods, *Geophysics* **55**, 1478–1487.

Colton, D., R. Ewing, and W. Rundell (eds.), 1990, *Inverse Problems in Partial Differential Equations*, SIAM, Philadelphia.

Cottle, R. W., and C. E. Lemke (eds.), 1976, *Nonlinear Programming*, SIAM-AMS Proceedings, Volume IX, Am. Math. Soc., Providence, RI.

Daudt, C. R., L. W. Braile, R. L. Nowack, and C. S. Chiang, 1989, A comparison of finite-difference and Fourier method calculation of synthetic seismograms, *Bull. Seismol. Soc. Am.* **79**, 1210–1230.

Evans, J. R., and J. J. Zucca, 1988, Active high-resolution seismic tomography of compressional wave velocity and attenuation structure at Medicine Lake Volcano, Northern California Cascade Range, *J. Geophys. Res.* **93**, 15016–15036.

Ewing, W. M., W. S. Jardetzky, and F. Press, 1957, *Elastic Waves in Layered Media,* McGraw-Hill, New York.

Gisser, D. G., D. Isaacson, and J. C. Newell, 1988, Theory and performance of an adaptive current tomography system, *Clin. Phys. Physiol. Meas.* **9A**, 35–41.

Grünbaum, F. A., 1980, A study of Fourier space methods for "limited angle" image reconstruction, *Numer. Funct. Anal. Optimiz.* **2**, 31-42.

Henderson, R. P., and J. G. Webster, 1978, An impedance camera for spatially specific measurements of the thorax, *IEEE Trans. Biomed. Engng.* **25**, 250–254.

Ivansson, S., 1983, Remark on an earlier proposed iterative tomographic algorithm, *Geophys. J. R. Astron. Soc.* **75**, 855–860.

Jackson, D. D., 1972, Interpretation of inaccurate, insufficient and inconsistent data, *Geophys. J. R. Astr. Soc.* **28**, 97–109.

Jordan, T. H., and J. N. Franklin, 1971, Optimal solutions to a linear inverse problem in geophysics, *Proc. Nat. Acad. Sci.* **68**, 291–293.

Justice, J. H., A. A. Vassiliou, S. Singh, J. D. Logel, P. A. Hansen, B. R. Hall, P. R. Hutt, and J. J. Solanski, 1989, Tomographic imaging in hydrocarbon reservoirs, *J. Imaging Sys. Tech.* **1**, 62–72.

Kak, A. C., 1984, Image reconstruction from projections, in *Digital Image Processing Techniques*, M. P. Ekstrom (ed.), Academic, New York, Chapter 4, 111–170.

Louis, A. K., 1981, Ghosts in tomography — The null space of the Radon transform, *Math. Meth. Appl. Sci.* **3**, 1-10.

Luenberger, D. G., 1969, *Optimization by Vector Space Methods*, Wiley, New York, Chapters 6 and 10, 160–168, 283–297.

Luenberger, D. G., 1973, *Introduction to Linear and Nonlinear Programming*, Addison-Wesley, Reading Massachusetts, Chapters 7 and 8, 148–155, 168–186.

McMechan, G. A., J. M. Harris, and L. M. Anderson, 1987, Crosshole tomography for strongly variable media with applications to scale model data, *Bull. Seismol. Soc. Am.* **77**, 1945–1960.

Natterer, F., 1986, *The Mathematics of Computerized Tomography*, Wiley, New York.

Nelson, G. D., and J. E. Vidale, 1990, Earthquake locations by 3-D finite-difference travel times, *Bull. Seismol. Soc. Am.* **80**, 395–410.

Nolet, G. (ed.), 1987, *Seismic Tomography: With Applications in Global Seismology and Exploration Geophysics,* Reidel, Dordrecht.

Scales, J. A., A. Gersztenkorn, and S. Treitel, 1988, Fast l_p solution of large, sparse, linear systems: Application to seismic travel time tomography, *J. Comput. Phys.* **75**, 314–333.

Smith, K. T., D. C. Solmon, and S. L. Wagner, 1977, Practical and mathematical aspects of the problem of reconstructing objects from radiographs, *Bull. Am. Math. Soc.* **83**, 1227–1270.

Tarantola, A., and A. Nercessian, 1984, Three-dimensional inversion without blocks, *Geophys. J. R. Astron. Soc.* **76**, 299–306.

Tarantola, A., and B. Valette, 1982, Generalized nonlinear inverse problems solved using the least squares criterion, *Rev. Geophys. Space Phys.* **20**, 219–232.

Vidale, J. E., and H. Houston, 1990, Rapid calculation of seismic amplitudes, *Geophysics* **55**, 1504–1507.

Witten, A. J., and E. Long, 1986, Shallow applications of geophysical diffraction tomography, *IEEE Trans. Geosci. Remote Sens.* **24**, 654–662.

Zandt, G., 1981, Seismic images of the deep structure of the San Andreas fault system, Central Coast Ranges, California, *J. Geophys. Res.* **86**, 5039–5052.

Zucca, J. J., G. S. Fuis, B. Milkereit, W. D. Mooney, and R. D. Catchings, 1986, Crustal structure of Northeastern California, *J. Geophys. Res.* **91**, 7359–7382.